Development of three dimensional and *in vivo* modelling systems for the overexpression of Active-β-catenin in osteosarcoma

by

Kristin Hinton

A thesis submitted in partial fulfillment of the requirements for the degree of

Master of Science

Department of Surgery
University of Alberta

ABSTRACT

Introduction:

Osteosarcoma (OS) is a primary bone malignancy most commonly found in children and adolescents. The 5-year survival rate for OS is 60%, which decreases to 27% when distant metastases are present. Currently no tests are available to identify those patients at risk of metastatic spread at the time of diagnosis. The canonical Wnt/β-catenin signalling pathway has been implicated in many cancers including OS, and overexpression of β-catenin has been shown to correlate with metastasis in OS. Recently, active β-catenin (ABC)—the transcriptionally active form of β-catenin—has specifically been found to be elevated in the metastatic cell lines SaOS2-LM7 (LM7) and HOS-143B (143B) compared to their non-metastatic parent cell lines, SaOS2 and HOS. The present study was undertaken to develop three-dimensional (3D) cell culture and *in vivo* models to observe the effects of over-expression of both ABC and β-catenin in OS with the hypothesis that increased expression of ABC but not β-catenin would result in more aggressive cellular features in three-dimensional (3D) cell culture.

Methods:

OS cell lines SaOS2 and HOS underwent liposomal transfection with pEGFP-C2-ABC (SaOS2-ABC, HOS-ABC), pEGFP-C2-β-catenin (SaOS2-βcat, HOS-βcat), and an empty vector negative control (SaOS2-GFP, HOS-GFP). For each transfected cell line, untransfected parent cell line, and the metastatic daughter cell lines LM7 and 143B, 3D cell cultures (spheroids) were established in a scaffold with differing proportions of an extracellular protein-rich basement membrane matrix (BMM) and collagen and maintained for 7-14 days. Prior to fixation, low resolution images were taken of the live cells to observe the spheroid morphology and interactions. These images were

analyzed to measure the invasion area (IA) and spheroid area (SA), which were used to calculate invasion length. To investigate the effects of the overexpression of ABC on OS *in vivo*, an orthotopic murine xenograft model was developed. The proximal tibial metaphysis of NOD/SCID mice was injected with a cell suspension containing either SaOS2, SaOS2-ABC, SaOS2-βcat, SaOS2-GFP, or LM7 cells. Mice were euthanized after 28 days, and the tibias and lungs were examined for primary and metastatic tumors.

Results

3D cultures conditions were optimized for the growth of all untransfected cells and for transiently transfected HOS spheroids. Stably transfected HOS cells formed smaller spheroids with smaller invasion areas ($p<0.05$). Transfected SaOS2 cells did not readily for spheroids in the 3D culture conditions. Intraosseous injection of SaOS2 and LM7 cells into the proximal tibial metaphysis did not result in primary or metastatic tumors for any cell line.

Conclusions:

We developed a 3D cell culture protocol to study the effects of ABC overexpression on OS, particularly in HOS cells. We anticipate this will allow us to further explore whether ABC plays a role in aggressive and metastatic OS that is distinct from β-catenin, which has been suggested by previous findings from our lab. Evaluating ABC levels at the time of diagnostic biopsy may be beneficial to identify patients at risk for metastasis. Additional pharmacologic and clinical investigations would confirm the viability of ABC as a prognostic marker and therapeutic target.

PREFACE

This thesis is an original work by Kristin Hinton. The research project, of which this thesis is a part, received research ethics approval from the University of Alberta Research Ethics Board, Project Name "Osteosarcoma Progression: Role of beta-catenin/active beta-catenin", No. AUP00004041, October 20, 2022.

The histopathologic examinations of the animal specimens in this project were performed by Dr. Nick Nation, a board-certified veterinary pathologist.

Chapter 2 of this thesis has been published as K. Hinton, A. Kirk, P. Paul, and S. Persad "Regulation of the Epithelial to Mesenchymal Transition in Osteosarcoma" Biomolecules, vol. 13, issue 2, 398. I was responsible for the literature review as well as the manuscript composition. A. Kirk assisted with the data collection and contributed to manuscript edits. P. Paul and S. Persad were involved with concept formation and manuscript composition. S. Persad was the supervisory author.

DEDICATION

A dedication to my husband, Andrew Kirk, without whose support I would be completely adrift.

ACKNOWLEDGEMENTS

I would like to thank my graduate supervisor Dr. Sujata Persad for all of her guidance, reassurance, and inspiration. Thanks also to my co-supervisor Dr. Paulose Paul for his invaluable mentorship, teaching, and clinical support. I'm grateful to Dr. Fred Berry on my supervisory committee not only for his individual support and feedback with respect to this project but also for helping navigate completing my degree in the Department of Surgery.

Thank you to Jocelyn Bischof who provided day to day guidance in the lab and who was instrumental in planning and performing the animal experiments. I'm also thankful for the guidance and assistance of Elizabeth Garcia who provided training in many lab techniques and helped to finish some final experiments towards the end of the project. Thank you to Carrie Soltys who helped guide me through periods of transition in the lab, provided advice whenever I needed it, and gave me a space to vent.

I'm grateful for the guidance of Dr. Kristi Baker and John Githaka from Dr. Swie Goping's lab in 3D culture techniques and invasion assays, and to Dr. Mary Hitt and Dr. Nick Nation for providing invaluable resources and feedback with respect to the design of our animal experiments. I am particularly thankful for Dr. Baker providing me daily mentorship and lab space to learn the 3D culturing techniques and for being a sounding board for troubleshooting our protocol.

Thank you to Tak Landry for his initial mentorship and teaching of many lab techniques, and to Tak and Noureen Ali for their previous work on this project.

Table of Contents

List of Tables

List of Figures

1 Introduction

1.1 Overview of osteosarcoma

Osteosarcoma (OS) has an annual incidence of 2-5 per million[1,2]. It has a slight male preponderance[3,4], a peak incidence between ages 10-19 and a second peak in adults over age 60[1,2,5]. The 5-year overall survival in OS is 60% and this drops to 27% if there are distant metastases[6]. Nearly 1 in 5 people with OS have metastases at the time of diagnosis[7] and a further 28% will develop metastases within 5 years of diagnosis[8].

OS most commonly affects the metaphysis of long bones. The most common sites of disease are the distal femur, proximal tibia, and proximal humerus[9]. It results in pain and decreased mobility of the affected limb and can present with a palpable mass or a pathologic fracture[10,11]. Initial investigations include radiographic and magnetic resonance imaging (MRI), and the diagnosis is ultimately made with a tissue biopsy[12]. After diagnosis, local and systemic staging is classified by either the American Joint Committee on Cancer (AJCC)[13] or Enneking[14] systems. The AJCC system is described in Tables 1.1 and 1.2.

Table 1.1 AJCC Osteosarcoma Staging Manual 7th Edition[13]

Anatomic Stage/Prognostic Groups				
Stage	**T**	**N**	**M**	**Grade**
IA	T1	N0	M0	Low grade (G1, G2), GX
IB	T2	N0	M0	Low grade (G1, G2), GX
	T3	N0	M0	Low grade (G1, G2), GX
IIA	T1	N0	M0	High grade (G3, G4)
IIB	T2	N0	M0	High grade (G3, G4)
III	T3	N0	M0	High grade (G3, G4)
IVA	Any T	N0	M1a	Any G
IVB	Any T	N1	Any M	Any G
	Any T	Any N	M1b	Any G

Table 1.2 Definitions of the TMN AJCC Staging Components

Primary Tumor (T)		**Regional Lymph Nodes (N)**	
TX	Primary tumor cannot be assessed	NX	Regional lymph nodes cannot be assessed
T0	No evidence of primary tumor	N0	No regional lymph node metastasis
T1	Tumor 8cm or less in greatest dimension	N1	Regional lymph node metastasis
T2	Tumor more than 8cm in greatest dimension		
T3	Discontinuous tumors in the primary bone site		
Distant Metastasis (M)		**Histologic Grade (G)**	
M0	No distant metastasis	GX	Grade cannot be assessed
M1	Distant metastasis	G1	Well-differentiated - low grade
M1a	Lung	G2	Moderately differentiated - low grade
M1b	Other distant sites	G3	Poorly differentiated
		G4	Undifferentiated

After diagnosis, treatment is initiated and generally involves a combination of neoadjuvant chemotherapy, surgery, and adjuvant chemotherapy[12]. Despite this, disease survival has not increased in several decades[15].

1.2 Osteosarcoma cell biology

Like all sarcomas, OS originates from mesenchymal cells. However, the exact precursor cell type is unknown, and hypothesized to be either osteoblast or mesenchymal stem cells prior to differentiation[16]. Regardless of the exact precursor, the resulting malignant transformation to OS is accompanied by any of a number of different genetic mutations, most commonly in the p53 protein, which is a regulator of the cell cycle[17]. The majority of OS cases are sporadic, but a proportion have been linked to hereditary conditions such as Li-Fraumeni Syndrome, Werner Syndrome, Rothmund-Thompson Syndrome, Bloom Syndrome, Hereditary Retinoblastoma and Paget's disease[18,19]. The majority of these conditions are systemic syndromes resulting from mutations affecting cell cycle regulation or DNA replication and repair[17].

The abnormal cells resulting from the malignant transformation form a mass that typically begins in the metaphysis of the bone, which can then spread locally into the surrounding tissues and metastasize either within the affected bone ("skip lesion") or to a distant site of spread[9]. By far the most common site for distant spread is the lung, which is a site of metastasis in over 85%

of metastatic disease, followed by skeletal metastases in 21.3%. Fewer than 10% of patients with metastases had tumors located in any other site[9].

Osteosarcoma metastasis occurs in three stages: dissemination from the primary tumor, transit within the circulator system, and colonization and establishment of distant metastases[20]. In the first stage, OS cells invade into surrounding tissues, a process that requires dissociation from the basement and degradation the extracellular matrix (ECM) in the tumor microenvironment. The ECM in OS is comprised of a number of proteins from the collagen, fibronectin, laminin, and proteoglycan families[21]. The degradation of the ECM in OS metastasis is facilitated by the matrix metalloproteinase (MMP) family[20,21], and both MMP-2 and MMP-9 have been linked to invasive OS phenotype[22]. While separation from the basement membrane and ECM typically triggers a form of apoptosis termed anoikis[23], OS cells evade this fate via a complex process of anchorage-independent growth[24].

The next step in the metastatic process is to invade into the vascular system. This is accomplished through cell-cell interactions of tumor and endothelial cells, which is mediated by runt-related transcription factor 2 (RUNX2), osteopontin, urokinase-type plasminogen activator (uPAR), and formyl peptide receptor type 1 (FPR1)[20]. Once in the systemic circulation, tumor cells then localize to the site of distant metastasis, most commonly lung[9], and extravasate from the vessel. The mechanism of this is not fully understood but may involve mechanical restriction of the lung vessels and/or exosomes released by OS cells that preferentially interact with lung cells, promoting the attraction and recruitment of OS cells to the metastatic site[20].

1.3 Biomarkers for predicting osteosarcoma prognosis

There are currently few reliable biomarkers to predict OS prognosis despite investigations into many candidates. Prognostic factors detectable on a routine blood draw would be an ideal tool for clinicians as they are minimally invasive and can be repeated at regular intervals to monitor for any change. Many potential serum biomarkers have been investigated though few have become routinely used in clinical practice. However, clinical practice guidelines recommend monitoring both serum alkaline phosphatase (ALP) and serum lactate dehydrogenase (LDH)[12]. ALP has a significant positive correlation with tumor volume, metastases, and decreased overall survival[25–29]. LDH has similarly been associated with tumor volume and poor survival[25,26,30]. Other serum markers with potential prognostic value include hemoglobin[31], red cell distribution width

(RDW)[32], and leukocyte ratios[33]. However, these general indicators of poor survival do not necessarily provide a clear direction for change in the approach to monitoring or treating a patient with OS.

Many recent investigations into potential biomarkers examine cell composition or cellular proteins within the tumor micro-environment or cancer cells themselves from the biopsy sample. With respect to cell types in the tumor micro-environment, there is a growing prognostic interest in the presence and relative abundance of immune cells such as tumor-associated macrophages[34] and tumor infiltrating lymphocytes[35–37]. There have also been recent correlations between overall survival and tumor vascular invasion[38,39].

Recently, dozens of proteins and non-coding ribonucleic acids (ncRNAs) have been identified as candidates for prognostic biomarkers in OS. The advantage of these markers as opposed to something such as a blood test is that they provide not only diagnostic information but also avenues for investigating the exact mechanism of local spread and distant metastasis as well as potential therapeutic targets.

1.4 The role of Active β-catenin in osteosarcoma

One possible biomarker to identify patients at risk of metastasis is Active β-catenin (ABC). The regulation of β-catenin by the canonical *wnt* pathway and its role in the epithelial to mesenchymal transition (EMT) is described in detail in Chapter 2. The *wnt* signalling pathway is highly conserved and crucial for the regulation of many cell processes. In the absence of *wnt*, β-catenin is sequestered in the cytoplasm by a degradation complex consisting of Adenomatous Polyposis Coli (APC), Axin, Glycogen Synthase Kinase 3β (GSK3β) and Casein Kinase 1 (CK1). Phosphorylated β-catenin is then ubiquitinated and targeted for proteasomal degradation[40]. In the presence of wnt, the protein binds to the Frizzled receptor and initiates the *wnt* signalling cascade, resulting in the dephosphorylation of β-catenin. This can then localize to the nucleus and act as a transcription factor. This nuclear form of β-catenin is ABC, which is partially dephosphorylated at the N-terminal residues serine (S) 37 and threonine (T) 41 by protein phosphatase 2A (PP2A) via the phosphoinositide 3-kinase (PI3K) pathway[41]. The different phosphorylation states of β-catenin are shown in Figure 1.1. Once in the nucleus, ABC acts as a transcription factor for many target genes involved in cell proliferation, stem cell differentiation, cell survival, migration, and angiogenesis[40], all key features of tumorigenesis, local invasion, and metastasis. β-catenin has a

well-established oncogenic potential, which can only occur if the protein is translocated to the nucleus[42]. Thus, ABC is both the active for of β-catenin as well as the potential oncogene.

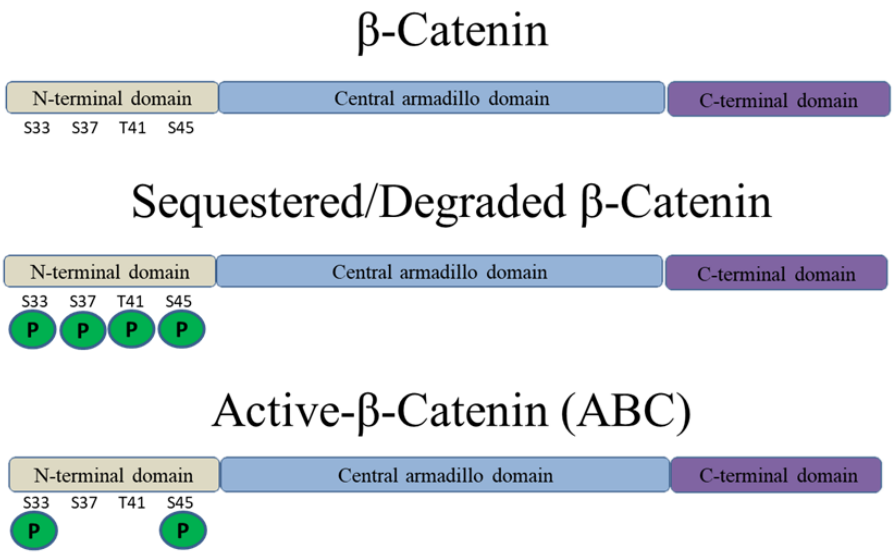

Figure 1.1 Phosphorylation states of β-catenin

Specific to OS, Haydon *et al.* identified β-catenin accumulation in over 70% of OS tumor samples but unfortunately did not differentiate between cytoplasmic and nuclear subcellular location[43]. Similarly, non-specified cytoplasmic and/or nuclear accumulation was identified in xenograft OS tumors developed in an *in vivo* murine model[44]. Ali *et al.* identified a strong correlation between nuclear ABC levels and known metastatic cell lines *in vitro* as well as a correlation between nuclear ABC and OS tumor stage on a tissue microarray analysis[45], and Fang *et al*. found ABC levels were increased in multiple OS cell lines compared to non-cancerous osteoblast cells, and that inhibition of the *wnt* pathway reduced OS cell migration and invasion *in vitro*[46].

1.5 Models to study osteosarcoma *in vitro* and *in vivo*

Thus far, the investigations into the role of ABC in OS have largely been performed in traditional two-dimensional (2D) cell culture[45,46]. While these methods are well-established, relatively simple, and possible to perform in most laboratories, they fail to capture the complex cell-cell interactions that occur in nature. This may be especially relevant for mesenchymal cells such as OS as they have a particularly complex three-dimensional structure compared to epithelial cells, the origin cells of carcinomas. As a result, there is a growing interest in the study of OS in a

three-dimensional (3D) *in vitro* model[47–49]. 3D cell-culture refers to the development of spheroids via a variety of methods such as allowing the cells to grow and aggregate on low binding plates or by cell suspension in a supportive matrix such as collagen, alginate, or solubilized basement membrane protein solution[48].

Once results have been established in cell culture, the next step of investigation is often an *in vivo* model. OS is frequently investigated in a murine model, which may be either ectopic, orthotopic, or intravenous cellular injections. While ectopic subcutaneous implantation of cells is technically less challenging than an orthotopic model, it may not accurately represent the conditions of the tumors in nature given the separate tissue location. Intravenous cellular injection provides direct access of tumor cells to the vascular system, which offers a convenient model for metastases that would be established following tumor invasion into the vascular system. Orthotopic models of OS involve the implantation of cells directly into the bone and allows both the study of primary tumorigenesis as well as metastasis[50].

1.6 Hypothesis

ABC plays a role in an invasive and metastatic OS phenotype *in vitro* and *in vivo*.

1.7 Objectives

- Establish OS cell lines that overexpress ABC and endogenous β-catenin.
- Develop a scaffold-based 3D culture protocol to study the effects of ABC overexpression on OS invasion.
- Develop an orthotopic murine model to study the effects of ABC overexpression on tumorigenesis and metastasis *in vivo*.

2 Regulation of the epithelial to mesenchymal transition in osteosarcoma. Biomolecules 2023, 13(2), 398

Review

Regulation of the Epithelial to Mesenchymal Transition in Osteosarcoma

Kristin Hinton [1], Andrew Kirk [2], Paulose Paul [1] and Sujata Persad [3,*]

[1] Division of Orthopaedic Surgery, Department of Surgery, University of Alberta, Edmonton, AB T6G 2B7, Canada; hinton@ualberta.ca (K.H.); paulose.paul@albertahealthsevices.ca (P.P.)

[2] Faculty of Medicine and Dentistry, University of Alberta, Edmonton, AB T6G 2R7, Canada; arkirk@ualberta.ca

[3] Department of Pediatrics, University of Alberta, Edmonton, AB T6G 2R3, Canada

* Correspondence: sujata.persad@ualberta.ca

Abstract: The epithelial to mesenchymal transition (EMT) is a cellular process that has been linked to the promotion of aggressive cellular features in many cancer types. It is characterized by the loss of the epithelial cell phenotype and a shift to a more mesenchymal phenotype and is accompanied by an associated change in cell markers. EMT is highly complex and regulated via multiple signaling pathways. While the importance of EMT is classically described for carcinomas—cancers of epithelial origin—it has also been clearly demonstrated in non-epithelial cancers, including osteosarcoma (OS), a primary bone cancer predominantly affecting children and young adults. Recent studies examining EMT in OS have highlighted regulatory roles for multiple proteins, non-coding nucleic acids, and components of the tumor micro-environment. This review serves to summarize these experimental findings, identify key families of regulatory molecules, and identify potential therapeutic targets specific to the EMT process in OS.

Keywords: osteosarcoma; epithelial-mesenchymal transition; transcriptional regulation; long non-coding RNAs; circular RNAs; microRNAs; tumor microenvironment; cancer therapeutics

2.1 Introduction

Osteosarcoma (OS) is a primary bone malignancy with an annual incidence of 2–4 per million[2]. It typically affects children, teens, and young adults[5], with a peak incidence from ages 10–19[2], a second peak in adults over 60[5], and a slight male preponderance[4]. The overall 5-year

survival rate for OS is 60% but decreases to 27% in the presence of distant metastases[51]; the rate of metastases at diagnosis is 18%[7].

The origin of OS is poorly understood. As a sarcoma, it arises from mesenchymal cells, but it is not currently known whether the precursor cells are osteoblasts or mesenchymal stem cells[16]. Although the etiology of OS is largely a mystery, multiple risk factors have been identified. These include medical conditions such as hereditary retinoblastoma, Li-Fraumeni syndrome, Werner syndrome, Rothmund-Thompson syndrome, Bloom syndrome, and Paget's disease[4]. Other risk factors include exposure to ionizing radiation and alkylating agents, both of which may have been used in the treatment of a prior malignancy[4].

The mainstay of treatment for osteosarcoma is surgical resection and frequently involves both neoadjuvant and adjuvant chemotherapy for higher grade tumors[12]. While advances in surgical techniques and chemotherapeutic regimens were associated with an initial improvement in outcomes, overall survival in OS has not significantly changed in several decades[52]. As medicine becomes more personalized, there is a growing interest in the identification of novel targeted therapies. A key component in developing targeted therapy is identifying specific pathways, proteins, or other molecules essential to cancer cell function. One of the cellular features often associated with aggressive cancers is the epithelial to mesenchymal transition (EMT).

2.2 EMT in Cancer

EMT is depicted in Figure 2.1. It is a process by which cells exhibiting an epithelial phenotype adopt a mesenchymal phenotype, which facilitates migration, invasion, and metastasis[53]. It exists in equilibrium with a reverse and complementary process, the mesenchymal to epithelial transition (MET), wherein cells revert back to an epithelial phenotype. Primary epithelial tumors exhibit epithelial cell markers such as E-cadherin. These cells demonstrate apical polarity, adhesion to a basement membrane, and tight cellular junctions[54]. For many cancers, EMT is critical in the early transition from normal to malignant cells. It is characterized by downregulation of epithelial cell markers, destabilization and loss of cell–cell junctions, loss of adherence to basement membrane and apical polarity, and cytoskeletal reorganization[53]. The result of these changes is a cell with mesenchymal morphology and characteristics.

Given the migratory potential of mesenchymal cells compared to epithelial cells, EMT has long been linked to cancer metastasis. However, inhibition of EMT has not been shown to affect the establishment of cancer metastases in vivo[55,56], and the cells found within metastatic tumors

are more likely to exhibit an epithelial phenotype[56,57]. Despite this, tumor cells that have undergone EMT appear to drive local invasion and angiogenesis of the primary tumor[57]. These results suggest that EMT is critical for tumor invasion into the local vascular system, allowing cells to migrate to distant organs where secondary tumors are established largely by cells with an epithelial phenotype, which have a greater propensity for proliferation[53]. These may be either cells that have undergone EMT and subsequently MET or primary tumor cells that did not undergo EMT[57].

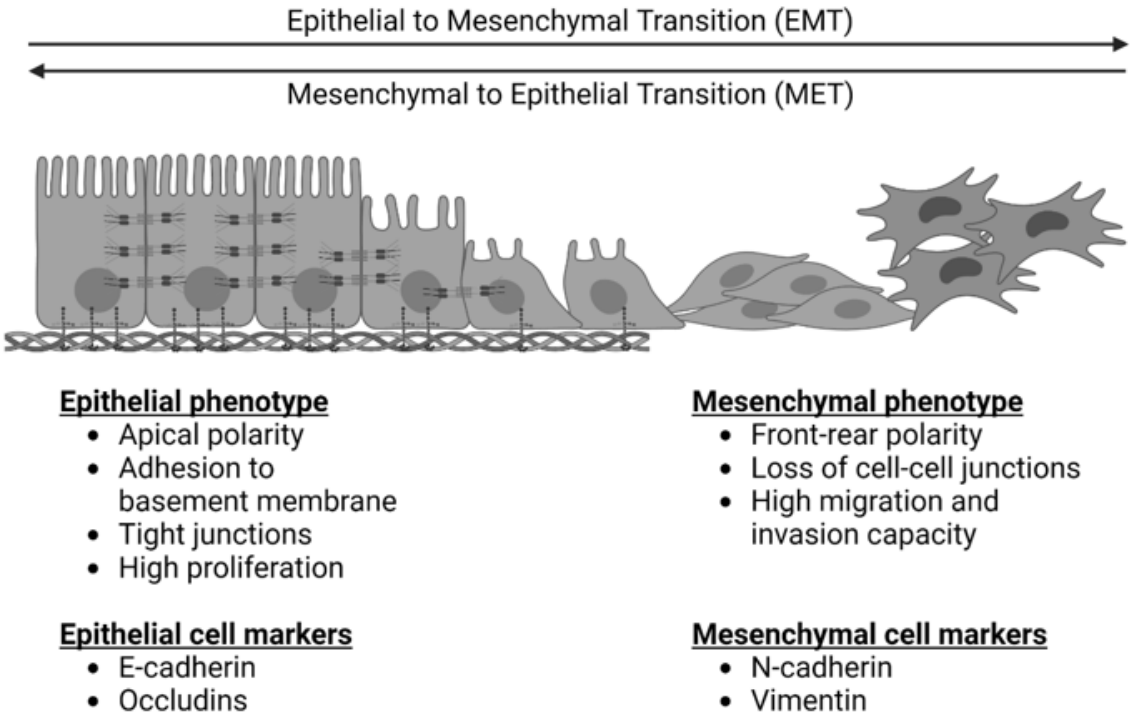

Figure 2.1 The epithelial to mesenchymal transition (EMT) and the reverse process of the mesenchymal to epithelial transition (MET). EMT is characterized by a loss of epithelial cell markers, an increase in mesenchymal cell markers, a loss of apical cell polarity, a loss of tight cell junctions, and an increased capacity for cell migration and invasion. MET is characterized by a loss of mesenchymal cell markers, an increase in epithelial cell markers, increased apical cell polarity, tight junctions, adherence to a basement membrane, and increased cell proliferation.

The molecular pathways associated with EMT are summarized in Figure 2.2. Zinc-finger E-box binding homeobox (ZEB), snail family transcriptional repressor 1 (SNAIL), snail family transcriptional repressor 2 (SLUG), and twist-related protein (TWIST) are well-known EMT transcription factors that are established downstream targets of multiple signaling pathways, including the canonical *wnt*/β-catenin pathway, the neurogenic locus notch homolog protein (Notch) pathway, the Transforming Growth Factor β/Suppressor of Mothers Against Decapentaplegic (TGFβ/SMAD) pathway, the phosphoinositide 3-kinase (PI3K)/Akt pathway, the

mitogen-activated protein kinase (MAPK) pathway, the Ras/Raf/Mitogen-activated protein kinase/ERK kinase/extracellular-signal-regulated kinase (RAS/RAF/MEK/ERK) axis, and the Janus kinase-Signal Transducer and Activator of Transcription JAK/STAT pathway[54]. These signaling cascades often interact, share many intermediaries, and impact the regulation of one another. This presents a challenge for studying and targeting EMT, as the individual pathways are difficult to isolate.

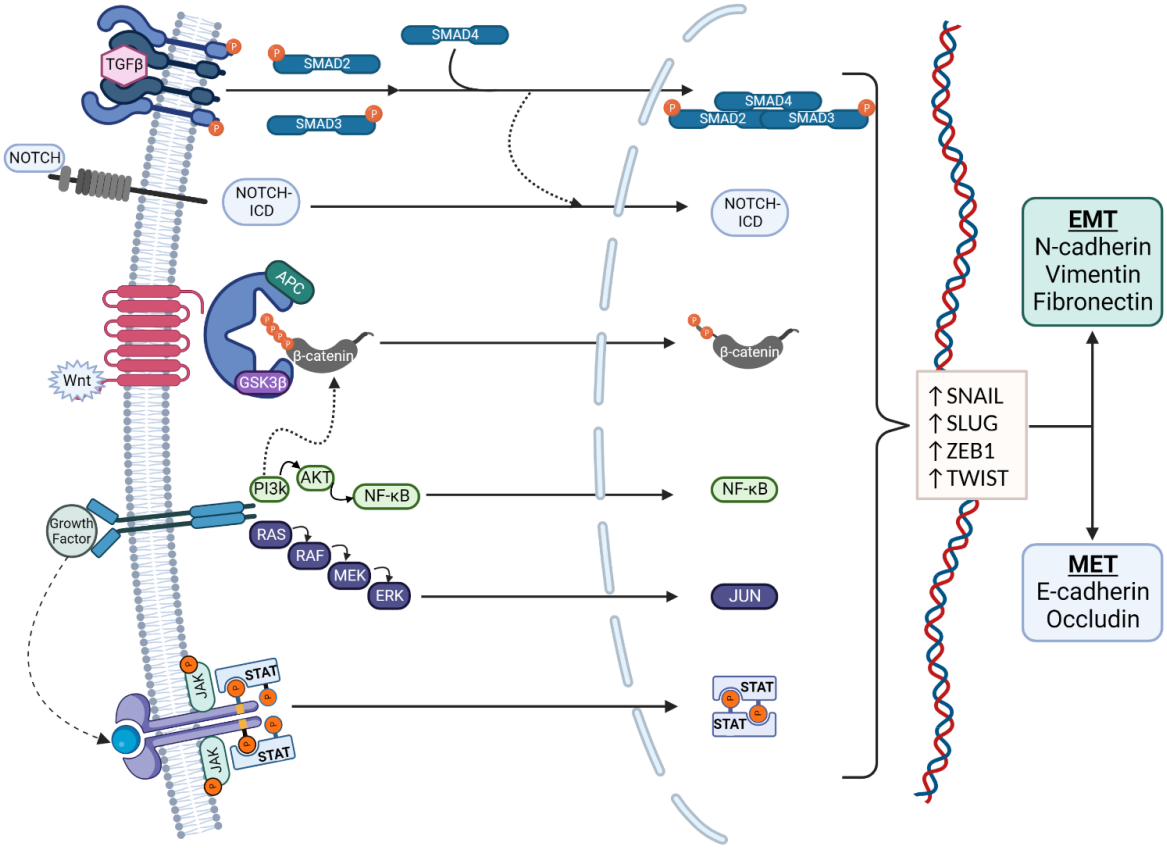

Figure 2.2 Signaling pathways in EMT. EMT regulation is complex and affected by multiple pathways, which also interact with each other. Regulation is typically via the Transforming Growth Factor β (TGFβ)/SMAD, Notch, canonical wnt, phosphoinositide 3-kinase (PI3K)/Akt, RAS/RAF, and JAK/STAT pathways. The transcription factors that mediate EMT are primarily Snail, Slug, ZEB1, and TWIST. EMT is characterized by an increased production of

N-cadherin, vimentin, and fi-bronectin, and MET is characterized by an increased production of E-cadherin and Occludin.

2.3 EMT Signaling Pathways

2.3.1 TGFβ/SMAD Pathway

The TGFβ family of proteins includes three TGFβ isoforms, activins, and bone morphogenic proteins (BMPs)[58]. In EMT, TGFβs bind to TGFβ receptors (1/2), which initiate a signaling cascade, leading to the increased transcription of genes involved in EMT. Binding of TGFβ to its receptors (1/2) leads to phosphorylation of SMAD2 and SMAD3, which then form a complex with SMAD4. BMPs also bind TGFβ receptors, activating SMAD1 and SMAD5 and then forming a complex with SMAD4. These trimeric complexes migrate to the nucleus to act as transcription factors.

SMAD complexes activate the mesenchymal genes vimentin and fibronectin, as well as the EMT transcription factors Snail, Slug, Zinc finger E-box-binding homeobox 1 (ZEB1) and Twist. These, in turn, repress E-cadherin and can upregulate the expression of TGFβ ligands, establishing a positive feedback loop to maintain EMT[53,59,60].

2.3.2 Canonical wnt Pathway

The canonical *wnt* pathway is considered to be a key activator of EMT[53]. Signaling is initiated by a group of *wnt* ligands that bind to Frizzled receptors and trigger a cascade of events, leading to the nuclear translocation of β-catenin. β-catenin is constitutively produced in the cell and stored in cytosolic pools. In the absence of *wnt* signaling, phosphorylated β-catenin is associated with a destruction complex, ubiquitinated, and degraded by proteasomes. Following activation of the canonical *wnt* pathway, β-catenin is dephosphorylated and translocates to the nucleus, where it acts as a transcriptional co-factor to induce the expression of genes involved in cell differentiation, proliferation, and tumorigenesis[61,62].

This pathway has been directly implicated in EMT via the expression of Twist, Slug, N-cadherin, and the repression of E-cadherin[63]. The known EMT transcription factor Snail has been shown to positively regulate *wnt* signaling[64]. The inhibition of Secreted Frizzled Related Protein 1 (SFRP), a negative regulator of *wnt* ligands, has also been shown to have EMT-like effects in breast carcinoma cells in vitro, while sensitizing them to TGFβ-induced EMT[65].

β-catenin is also located at the cell membrane as part of an E-cadherin-containing multi-component adherens junction complex, which is a component of cell–cell interaction junctions. β-catenin contributes to anchoring E-cadherin, a transmembrane cell–cell adhesion protein at the cell surface to the intracellular actin cytoskeleton. β-catenin is released from the adherens complex upon disruption of these adherens junctions between cells. Once available in the cytosol, it enters the pathway described above and is either phosphorylated and degraded or, if the *wnt* pathway is active, dephosphorylated and translocated to the nucleus to function as a transcription factor for EMT-genes[66]. E-cadherin can therefore act as a negative regulator of the canonical *wnt* pathway by sequestering most of the β-catenin in the epithelial cell membrane.

2.3.3 Notch Pathway

The Notch pathway has been implicated in inducing EMT in both normal and neoplastic tissues, and is involved in controlling cell fate, differentiation, and proliferation. Four isoforms (Notch1 through Notch4) are known to bind Delta-like or Jagged family ligands. This interaction triggers a series of proteolytic events leading to the active fragment Notch Intracellular Domain (Notch ICD), which then acts in the nucleus, where it associates with binding partners and transcriptional activators[67]. Several components of the Notch pathway are highly expressed at the invasive margins of tumors, which express EMT markers such as vimentin, suggesting an important role for the Notch pathway in the regulation of EMT[68]. Notch acts via transcriptional regulation of ZEB, Snail, and Slug, which repress expression of E-cadherin and induce expression of vimentin and fibronectin[67–69].

There is crosstalk between the Notch and TGFβ pathway that occurs via SMADs. As described above, the SMAD family of proteins are integral to TGFβ signaling. They have also been shown to associate with Notch-ICD. This affects the expression of genes downstream of both Notch and TGFβ that are required for mesenchymal differentiation, a key component in EMT[70]. Silencing components of the Notch pathway have also been shown to prevent TGFβ-induced EMT[71].

2.3.4 Tyrosine Kinase Pathways

Mitogenic growth factors also play a role in the regulation of EMT. The binding of these growth factors causes their receptors to dimerize and induces the activation of both receptor and non-receptor tyrosine kinases (TKs). This enables the activation of several pathways—including the MAPK, JAK-STAT, and phosphatidylinositol 3-kinase-Akt (PI3-Akt) pathways. All of these

have been implicated in EMT, and are involved in cell growth, proliferation, and migration [72]. PI3K/Akt has also been shown to play an important role in the regulation of transcriptionally active β-catenin, a key molecule in the previously discussed *wnt* signaling pathway[41]. Inhibition of TKs is a growing field of study in cancer therapeutics, with multiple inhibitors currently under investigation[73].

Inhibition of fibroblast growth factor (FGF), a mitogenic growth factor that participates in the induction of EMT via activation of the MAPK, induces the reverse process MET in vitro and delays tumor growth in vivo[74]. One isoform, FGF2, has been associated with reduced overall survival in several carcinoma types if overexpressed[74].

The binding of epidermal growth factor (EGF) to its receptor leads to activation of MAPK pathway and decreased expression of E-cadherin[75]. EGF also activates the JAK2-STAT3 pathway, which leads to EMT activation via Twist[76]. Additionally, EGF has been shown to induce EMT via TGFβ signaling and regulation of Snail[77] and phosphorylation of SMAD2/SMAD3[78].

The activation of Akt, or Protein Kinase B, has been shown to upregulate the phosphorylation of Twist1 and inhibit apoptosis[79], and the inhibition of Akt has been shown to induce MET[80]. For example, hepatocyte growth factor (HGF) has been shown to activate EMT[81], which can be reversed via inhibition of the PI3K/Akt pathway. HGF was found to enhance tumor progression and metastasis of hepatocellular carcinoma in association with the c-MET receptor tyrosine kinase[82], a known activator of PI3K/Akt.

2.4 EMT in OS

As a mesenchymal cancer, the importance of EMT in OS has been disputed[83,84]. In fact, an early investigation including 4 clinical osteosarcoma samples by Sato et al. found there was no detectable E-cadherin expression in these cells[85], suggesting that the repression/downregulation of E-cadherin—a classically described step in EMT—would not be possible. In contrast, Yin et al. found that 20.6% of OS tissue samples expressed E-cadherin and those that did were less likely to metastasize, whereas the expression of Twist was significantly related to metastases and poorer overall survival[86]. The promotion of EMT in OS characterized by increased migration and invasion in vitro has been shown to be mediated via upregulation of Snail[87–100], Slug[101,102], Twist[103–106], and ZEB[107–110].

The following sections give an overview of studies that have examined the roles of different EMT regulatory molecules in OS. All of these were found to affect the expression of

EMT-related cell-markers and are correlated closely with EMT-associated cellular features such as increased migration and invasion. Many also showed a link between their proposed EMT-regulatory molecule and OS metastases in vivo in animal models. Taken together, these results suggest that EMT does play a role in osteosarcoma and is associated with a more aggressive tumor phenotype. However, the term "transition" is not ideally suited to sarcoma cancers, and EMT may be better thought of as a set of pathways utilized to maintain and promote the existing mesenchymal phenotype.

Sannino et al. posited a possible hybrid phenotype in sarcoma tumors cells, utilizing the EMT and MET pathways to acquire both mesenchymal and epithelial characteristics that favor the initiation and establishment of distant metastases[83].

The highlighted pathways important in EMT regulation have all been shown to have a role in OS. TGFβs promote EMT and metastases in OS[111], and TGFβ inhibition has been shown to decrease EMT in OS[101,112–117]. Chen et al. also identified that estrogen-related receptor α (ERRα) upregulates TGF-β-mediated EMT in two OS cell lines[93]. Others have highlighted roles for MAPK[106,118–120] and JAK/STAT[95,121–125].

Notch signaling promotes proliferation, migration, and invasion of OS cells, and Notch overexpression increased tumor growth in vivo[126–129]. Notch inhibition reduced chemo-resistance in OS in vitro[130]. *Wnt* signaling has also been shown to mediate EMT in OS[92,131–146]. It has been proposed that *wnt* signaling is particularly important in the pathogenesis of OS cancer stem cells[147].

TKs are of particular interest in OS, and multiple different TK proteins have been associated with aggressive cellular phenotypes. Many studies have demonstrated a regulatory role in OS for the downstream TK pathways PI3K/Akt[148–156] and RAS/RAF/MEK/ERK[104,157–160]. Multiple TK inhibitors have been a part of recently completed or ongoing clinical trials in the treatment of OS, including Apatinib, Axitinib, Cabozantinib, Cediranib, Crizotinib, Dasatinib, Imatinib, Pazopanib, Regorafenib, Sorafenib, and Sunitinib[161,162].

2.5 Regulation of EMT in OS—Proteins

As a complex and multi-faceted process, several proteins have been implicated in EMT regulation in OS[87,91,92,96–98,104,105,107,121,131,135,136,139,142,148–151,154–156,158,163–193] and these are summarized in Tables 2.1 and 2.2. These proteins were found to either promote[87,91,96,97,104,107,121,131,135,136,139,142,148–151,154–156,158,163–188] or inhibit[92,98,105,133,189–193] EMT in vitro, and the majority were found to be correspondingly upregulated or downregulated in clinical

OS tissue samples and/or established cell lines compared to normal controls. Each group of authors found a significant correlation between the studied protein and the levels of EMT-related proteins, such as E-cadherin, N-cadherin, and vimentin. They also reported a significant effect on aggressive cellular characteristics, such as migration and invasion ability in vitro. Where noted, the results were confirmed in vivo with mouse xenograft experiments.

A detailed review of the individual proteins investigated for their regulatory role in EMT of OS cells is outside of the scope of this review. Generally, their endogenous functions can be grouped into the following families: cell cycle regulation, immunity/inflammatory, cell signaling, cell structure, and metabolism. Each of these categories has a logical impact on EMT and/or cancer cell behavior.

Changes to cell differentiation and cell cycle regulation are recognized mechanisms by which normal cells can become cancerous. We identified 22 proteins with a regulatory role in EMT in OS whose endogenous functions impact these processes[96,97,105,107,121,133,139,142,154,158,168,172,173,181–188,193]. This group can be represented by several ubiquitin ligases[139,185] and deubiquitinases[137,187,188] that are known to target proteins critical for cell growth, proliferation, and differentiation. These were all found to be upregulated in clinical samples of osteosarcoma, and the overexpression or inhibition of these proteins was found to correlate with markers for EMT and OS cell proliferation.

The importance of immunity and inflammation on cancer progression is widely recognized[194], and these systems have also been implicated in the regulation of EMT[195]. Twelve of the EMT regulatory proteins described in Tables 2.1 and 2.2 function as part of immunity and inflammation[87,91,149,151,156,165,166,169,174,177,179,192], many of which can be designated as "pro-inflammatory" proteins[149,156,165,166], and others that function as part of the development and activation of immune cells[87,91,151,169,179]. For example, the Programmed Death Ligand 2 (PD-L2) protein is a ligand for the Programmed Death 1 (PD-1) receptor, which is protective against T cell-mediated death in conjunction with tumor-associated macrophages[196]. Ren et al. found that PD-L2 knockdown decreased EMT and inhibited migration, invasion, and colony formation of OS cells in vitro, and reduced OS metastases in vivo in a mouse model[179].

Table 2.1 Effects of highly expressed proteins on EMT in OS

Protein	Increased Levels in Clinical Sample	Promoted EMT	Promoted Cell Migration/Invasion	Promoted In Vivo Tumor Growth	Promoted In Vivo metastasis	Endogenous Function
ACTL6A[163]	■	■	■		■	Structure
AIM2[156]		■	■			Immune
BMP-2[135]		■	■	■		Cell Signaling
Calponin 3[164]	■	■	■	■	■	Structure
Cathepsin E[165]	■	■	■	■	■	Immune
COPS3[158]	■	■	■	ns	■	Cell Cycle Regulation
COX2[149]		■	■			Inflammation
CPE-ΔN[136]		■	■			Cell Signaling
$cPLA_2a$[166]	■	■	■			Inflammation
CPXM2[167]	■	■	■			Cell Signaling
Cul4A[168]	■	■	■			Inflammation
CXCR6[169]	■	■	■			Immune
Cyr61[104,170]		■	■		■	Cell Signaling
E2F1[121]	■	■	■			Cell Cycle Regulation
EPB41L3[171]	■	↓	↓			Structure
Fibulin-3[131]	■	■	■	■		Structure
Fibulin-4[148]	■	■	■	■		Structure
HOXB7[172]	■	■	■			Cell Cycle Regulation
HuR[173]	■	■	■			Cell Cycle Regulation
ICSBP[87]	■	■	■			Immune
IL-33[151]		■	■			Inflammation
MAGL[174]	■	■	■	■		Inflammation
Metadherin[175]		■	■			Cell Signaling
NETO2[155]	■	■	■			Cell Signaling
OLR1[176]	■	■	■	■	■	Cell Signaling
P2X7[150]	■	■	■	■	■	Cell Signaling
PADI4[177]	■	■	■			Inflammation
PDGFRβ[154]		■	■			Cell Cycle Regulation

PD-L2[179]	■	■	■	■	■	Inflammation
PGI[178]		■	■	■		Metabolism
RIPK4[142]	■	■	■			Cell Cycle Regulation
SenP1[180]		■	■			Cell Signaling
SENP3[181]	■	■	■			Cell Cycle Regulation
SIRT1[107]	■	■	■			Cell Cycle Regulation
SOX3[96]	■	■	■		■	Cell Cycle Regulation
SOX5[97]	■	■	■			Cell Cycle Regulation
ST6Gal-1[182]		■	■			Cell Cycle Regulation
TANK1[183]		■	■			Cell Cycle Regulation
Tim-3[91]	■	■	■			Immune
TRIM29[184]	■	■	■			Cell Cycle Regulation
TRIM66[185]	■	■	■	■		Cell Cycle Regulation
UHRF1[186]		■	■			Cell Cycle Regulation
USP7[139]	■	■	■			Cell Cycle Regulation
USP17[187]	■	■	■			Cell Cycle Regulation
USP22[188]	■	■	■	■	■	Cell Cycle Regulation

■ YES/Significant association; ns: No significant association; ↓ Inverse association; Not studied/reported.

Table 2.2 Effects of poorly expressed proteins in OS.

Protein	Decreased Levels in Clinical Sample	Inhibited EMT	Inhibited Cell Migration/Invasion	Inhibited In Vivo Tumor Growth	Inhibited In Vivo Metastasis	Endogenous Function
ARID1a[189]	■	■	■			Cell Signaling
Ezrin[190]		■	■	■	■	Structure
FTL[191]	■	■	■			Metabolism
GPER[98]	■	■	■			Cell Signaling
LAIR-1[192]	■	■	■			Immune
RASSF4[133]	■	■	■			Cell Cycle Regulation
SOX6[105]	■	■	■			Cell Cycle Regulation
TSSC3[92]	■	■	■		■	Cell Cycle Regulation
WWOX[193]	■	■	■			Cell Cycle Regulation

■ YES/Significant association; Not studied/reported.

Many of the described proteins are implicated in cell signaling[98,135,136,150,155,168,176–178,181,190]. In addition to cell–cell interactions, this broad grouping includes the regulation of multiple cell processes that affect multiple other pathways and functions, including but not limited to cell cycle regulation, inflammation, immunity, and metabolism.

Finally, a subset of the proteins associated with EMT in OS are either structural proteins or regulate cell structure via interaction with the cytoskeleton[131,148,163,164,171,190]. This is perhaps the simplest and most logical grouping given the key morphological changes that take place during the EMT transformation, as depicted in Figure 2.1. Interestingly, Yuan et al. found that Erythrocyte Membrane Protein Band 4.1-like 3 (EPB41L3)—a cytoskeletal protein involved in cytoskeletal rearrange-ment, intracellular transport, and signal transduction—was increased in OS tissues and cell lines but was associated with an inhibition of EMT, migration, invasion, and cell viability in OS cell culture[171]. This pattern of expression was opposite to all of the other proteins impacting EMT in OS identified in this review.

When reported, the EMT pathways most implicated in these studies were wnt and PI3K/Akt. The nuclear localization and, therefore, transcriptional activity of the wnt/β-catenin pathway has also been shown to be regulated by PI3K[73], suggesting overlap in these EMT control mechanisms. The most frequently identified downstream target was Snail, which is known to promote EMT by suppressing E-cadherin expression[197], and further upregulates wnt signaling and EMT[64].

2.6 Regulation of EMT in OS—Non-Coding Ribonucleic Acids

Another key group of regulatory factors of EMT/MET in OS are non-coding ribonucleic acids (ncRNAs). These molecules have many forms and functions[198], one of which is gene regulation. Typically identified through queries to the Gene Expression Omnibus (GEO), the differential expression of multiple separate long non-coding RNAs (lncRNAs)[199], microRNAs (miRNAs)[200], circular RNAs (circRNAs)[201,202], and pseudogenes[203] have been found to relate to OS prognosis[204]. Tables 2.3 and 2.4 summarize ncRNAs implicated in OS EMT regulation. Again, they were found to have a role in either promoting[100,106,109,119,128,129,132,137,140,141,143,145,151,205–238] or inhibiting[90,92,94,108,120,134,138,144,146,153,239–266] EMT and invasive cellular behaviors of OS cells in vitro, and there was significant overlap in the affected pathways and ultimate downstream targets. Very frequently there are multiple non-coding RNAs involved in the same pathway as they can also regulate other nucleic acids.

Table 2.3 Effects of highly expressed non-coding ribonucleic acids.

Ribonucleic Acid	Increased Levels in Clinical Sample	Promoted EMT	Promoted Cell Migration/ Invasion	Promoted In Vivo Tumor Growth	Promoted In Vivo Metastasis	Associated Pathways/Targets
circ-FOXM1[145]		■	■	■		miR-320a, *wnt*
circ-PRKAR1B[205]		■	■	■	■	miR-361-3p, FZD4
LINC00319[206]	■	■	■			miR-455-3p, NFIB
LINC00324[207]	■	■	■			WDR66, HuR
LINC00460[208]		■	■			miR-1224-5p, FADS1
LINC02381[209]	■	■	■	■		miR-503-5p, CDCA4
lncRNA AFAP1-AS1[106]	■	■	■	■		Rho, ROCK, p38
lncRNA BCRT1[210]	■	■				miR-1303, FGF7
lncRNA CASC15[143]	■	■	■	■	■	*wnt*/β-catenin
lncRNA CCAT2[211]	■	■	■			LATS2, c-Myc
lncRNA CRNDE[128,140]	■	■	■	■		Notch1, SP1, *wnt*/β-catenin
lncRNA DDX11-AS1[212]		■	■	■		miR-873-5p, IGF2BP2
lncRNA FAL1[213]	■	■	■			GSK-3β
lncRNA GHET1[141,214]	■	■	■	■		Ki67, *wnt*/β-catenin
lncRNA HCP5[215]		■	■			SP1
lncRNA HNF1A-AS1[216]	■	■	■			
lncRNA HIF1A-AS2[217]	■	■	■	■		miR-33b-5p, SIRT6
lncRNA HOXA-AS2[218]	■	■	■			miR-502c-3p
lncRNA LMCD1-AS1[219]	■	■	■			miR-106b-5p, SP1
lncRNA miR210HG[220]	■	■	■	■		miR-503
lncRNA MNX1-AS1[221]	■	■	■			Snail
lncRNA MSC-AS1[222]	■	■	■	■		miR-142, CDK6, PI3K/Akt
lncRNA NEAT1[223]	■	■	■	■		miR-186-5p, HIF-1α
lncRNA PGM5-AS1[224]	■	■	■	■	■	miR-140-5p, FBN1
lncRNA PVT1[267]	■	■	■			

lncRNA RUSC1-AS1[226]	■	■	■	■		miR-340-5p, PI3K/Akt
lncRNA SNHG1[227]	■	■	■			miRNA-101-3p, ROCK1, PI3K/Akt
lncRNA SNHG4[228]	■	■	■	■		miR-377-3p
lncRNA SNHG7[129]	■	■	■	■		MiR-34a, Notch-1, BCL-2, CDK6, SMAD4
lncRNA SNHG20[229]	■	■	■			
lncRNA SPRY4-IT1[90,109]		■	■	■		miR-101
lncRNA TUG1[132,230]	■	■	■	■	■	miR-144-3p, miR-143-5p, EZH2, HIF-1α, *wnt*
lncRNA XIST[100]	■	■	■			miR-153, SNAI1
miR-17-5p[231]	■	■	■			SRCIN1
miR-19[119]	■	■	■			SPRED2, ERK/MAPK
miR-31-5p[137]	■	■	■	■		AXIN1, *wnt*/β-catenin
miR-93[232]	■	■	■			TIMP2
miR-130a[233]	■	■	■			PTEN
miR-135b[234]		■	■			TAZ
miR-155[235]		■	■			TNFa, TP53INP1
miR-196a[236]	■	■	■			HOXA5
miR-199b-5p[237]	■	■	■			HER2
miR-210-5p[152]	■	■	■	■	■	PIK3R5, Akt
Pseudogene MSTO2P[238]	■	■	■	■		PD-L1

■ YES/Significant association; Not studied/reported.

Table 2.4 Effects of poorly expressed non-coding ribonucleic acids.

Ribonucleic Acid	Decreased Levels in Clinical Samples	Inhibited EMT	Inhibited Cell Migration/ Invasion	Inhibited In Vivo Tumor Growth	Inhibited In Vivo Metastasis	Associated Pathways/Targets
lncRNA FER1L4[239,240]	■	■	■			miR-18a-5p, PI3K/Akt
lncRNA GAS5[268]	■	■	■	■		miR-221, ARHI

lncRNA MEG3[241]	■	■	■			miR-361-5p, FoxM1
lncRNA NKILA[242]	■	↑	■			NFκB, Snail
lncRNA TUSC8[243]	■	■	■			miR-197-3p, EHD2
miR-7[244]	■	■	■	■		IGF1R
miR-16[245]	■	■	■			RAB23
miR-25[246]	■	■	■	■		SOX4
miR-29a[247]	■	■	■			SOCS1/NFκB, DNMT3B
miR-107[134]	■	■	■			*wnt*/β-catenin
miR-125a-5p[248]	■	■	■			MMP11
miR-128[249]	■	■	■			Integrin A2
miR-132[250]		■	■			SOX4
miR-139-5p[251]	■	■	■	■		DNMT1
miR-140-3p[252]	■	■	■			TRAF6, TGFB
miR-145[94]	■	■	■			Snail
miR-181c[253]	■	■	■	■		SMAD7, TGFB
miR-203[254]	■	■	■			RAB22A
miR-331-3p[146]	■	■	■			MGAT1, Bcl/Bax, *wnt*/β-catenin
miR-342-5p[138]	■	■	■			*wnt*/β-catenin
miR-363[255,256]	■	■	■	■		PDZD2, NOB1
miR-377-3p[228]	■	■	■	■		CuL1, *wnt*/β-catenin
miR-382[257]	■	■	■		■	YB-1
miR-384[258]	■	■	■			MECP2, IGFBP3
miR-449a[153]	■	■	■			EZH2, PI3K/Akt
miR-486[259]	■	■	■			PIM1
miR-488[260]	■	■	■			AQP3
miR-489[261]	■	■	■	■		NAA10
miR-499a[262]	■	■	■	■		TGFβ, EGFR, Akt, SHKBP1
miR-503[263]		■	■			c-myc

miR-506-3p[264]		■	■			SPHK1, LC3II/I
miR-708-5p[108]		■	■			ZEB1
miR-761[265]	■	■	■	■		ALDH1B1, TGFB
miR-765[159]	■	■	■			MTUS, ERK
miR-CT3[120]	■	■	■			p38/MAPK
miR-let-7d[266]		■	↑			CCND2, E2F2

■ YES/Significant association; ↑ Inverse association; Not studied/reported.

Unlike the pattern observed in the majority of these findings, Yuan et al. found that although erythrocyte membrane protein band 4.1-like 3 (EPB41L3) was upregulated in OS cell lines and clinical tissue samples, knockdown of EPB41L3 significantly increased the migration and invasion capacity of the investigated cell lines despite decreased cell viability[172]. The findings were similarly mixed for lncRNA NKILA[145] and miR-let-7d[266]. These studies highlight the complexity of EMT regulation in OS and suggest that it is only one possible factor relating to tumor behavior and prognosis.

2.7 Regulation of EMT in OS—The Tumor Microenvironment

There has been increased recognition of the importance of the tumor microenvironment on various cellular functions and characteristics. This is the three-dimensional structure surrounding tumor cells and comprises immune cells, vascular network, and extra-cellular matrix (ECM), among other components. The tumor microenvironment is unique not only for different cancer types but also for individual patients, and it is influenced by multiple factors, including patient sex and presence of metastases[269]. A better understanding of the interactions within the tumor micro-environment is expected to lead to the development of personalized treatments targeted at individual patients' tumors.

Han et al. found that the presence of tumor-associated macrophages (TAMS) and the expression of the inflammatory marker cyclo-oxygenase 2 (COX2) correlated with OS metastases in clinical samples[123]. They also found co-culture of OS cells with TAMS promoted EMT and aggressive cellular features in vitro, which was reversible by COX2 inhibition. Additionally, COX2 inhibition reduced pulmonary metastases in vivo in a murine model[123]. Ling et al. found that Von Willebrand Factor (VWF)—which is secreted by the endothelial cells lining blood vessels—promoted EMT in vitro following OS and endothelial cell co-culture, as well as tumor growth and metastasis in vivo in a mouse model[270].

In addition to the cellular and biochemical makeup of the tumor microenvironment, the biomechanical properties of the ECM may also play a role in regulating EMT. Dai et al. developed a three-dimensional cell culture model with varying degrees of ECM stiffness[271]. This may be of particular relevance when evaluating OS tumors that exist in the bone—a relatively rigid environment—but eventually expand into the surrounding soft tissues, which are substantially less rigid. It may also account for some of the differences in OS metastatic patterns as more than 85% of metastatic OS occurs in the lungs, a soft tissue, compared to only 21% that occurs in the bone[9].

2.8 Targeting EMT in Osteosarcoma

Given its close association with aggressive and metastatic OS, EMT is a natural target for OS treatment. Treatments targeting EMT in OS include known medications, hormones, novel small molecules, and herbal medicines. The currently recommended chemotherapy regimen for OS includes doxorubicin, cisplatin, and high-dose methotrexate. At low doses, cisplatin has been shown to promote EMT, migration, invasion, and in vivo tumor growth[130]. However, these findings were reversible with inhibition of the EMT-related Notch pathway. EMT is recognized as an important factor contributing to chemotherapy resistance in multiple cancers[272], which was shown in OS by Ding et al., who found that OS cells induced to be resistant to methotrexate exhibited higher levels of EMT proteins and greater migration and invasion[273].

Other drugs that have not traditionally been used to treat osteosarcoma clinically but have been shown to inhibit EMT in OS in vitro include the cholesterol medication lovastatin[274] and zolendronate, a bisphosphonate medication used in the treatment of osteoporosis and other metabolic bone disorders[275,276]. In addition to the suppression of EMT, migration, and invasion, Kim et al. showed that OS cells and orthotopic tumors in mice had increased radiation-sensitivity following treatment with zolendronate, and this combination therapy was more effective than either treatment on its own[276].

Several hormone therapies have also been investigated for their effect on EMT in OS. These include estrogen, which inhibited EMT and promoted apoptosis of OS cells at high doses[277]. Treatment with irisin, a hormone derived from skeletal muscle, also suppressed OS EMT, cell proliferation, migration, and invasion[95]. Melatonin, a sleep-related hormone that is widely commercially available, has been shown to inhibit EMT[99,278,279] and OS cell migration and invasion in vitro, with additional results in vivo showing reduced metastasis in mice[279]. In contrast, treatment of OS cells with visfatin[88], a metabolic peptide first identified in visceral fat, induced

EMT and increased cell migration and invasion. While these results do not suggest a direct role for visfatin in treatment of OS, further studies could examine the potential therapeutic effects of visfatin regulation.

Newer therapies with peptides and other small molecules allow for targeting more specific biologic functions, often associated with receptor inhibition. Inhibition of CXCR4 with Peptide R inhibited EMT, cell migration, and invasion in OS cells, and was thought to have the potential for less toxicity than existing CXCR4 inhibitors[280]. Similar suppression of EMT, inhibition of cell migration/invasion, and reduced tumorigenesis in vivo was observed with inhibition of vascular endothelial growth factor receptor-2 (VEGFR2) by Apatinib[281], Krüppel-like factor 5 (KFL5), and early growth response gene 1 (EGR1) by ML264[124], and TGF-β by RepSox[113]. The 4′-aminochalcones D14 and D15 were found to inhibit EMT, cell migration, and invasion through upregulation of p53[282].

The investigation of traditional and herbal medicines and their derivatives (both natural and synthetic) is a growing area of interest. The effect on EMT in OS has been studied for a number of these compounds[89,101,112,114–118,125,157,160,283–291], with results summarized in Table 2.5. While the majority of these inhibited both EMT and aggressive cellular characteristics, such as migration and invasion, Jiang et al. found that triptolide, a compound found in the vine *Tripterygium wilfordii*, increased EMT in OS cells in vitro but inhibited proliferation and invasion[291].

Table 2.5 Traditional and herbal medicine effects on EMT in OS.

Compound	Inhibits EMT	Inhibits Cell Migration/Invasion	Inhibits In Vivo Tumor Growth	Inhibits In Vivo Metastasis	Associated Pathways/Targets
3'hydroxyflavone[157]	■	■	■	■	MEK/ERK
Baicalin[117,160]	■	■	■		ERK, TGF-β
Berberine[283,284]	■	■			EZH2, Rad51
Chimaphilin[116]	■	■			PI3K/Akt, ERK, TGF-β
Cinnamomum cassia extract[112]	■	■	■		TGF-β
Dehydroandrogranpholide[285]	■	■			SATB2
Delphinidin[118]	■	■			ERK, MAPK
Gamabufotalin[114]	■	■		■	PI3K/Akt, TGF-β
Glaucocalyxin A[115]	■	■		■	TGF-β, Smad

Magnoflorine[286]	■	■			miR-410-3p, HMGB1, NF-κB
Nitidine Chloride[89]	■	■			Akt, GSK-3β, Snail
Oridonin[101]	■	■		■	TGF-β, Smad, Snail
Piperlongumine[125]	■	■	■		miR-30d-5p, SOCS3, JAK2/STAT3
Polyphillin I[292]	■	■			NF-κB, c-Myc
Rosmarinic acid[288]	■	■			DJ-1, PI3K/Akt
Salvia clandestina extract[289]	■	■			Akt/PKB
Sauchinone[290]	■	■			Sonic hedgehog
Triptolide[291]	↑	■			miR-181a, PTEN

■ Significant association; ↑ Inverse association; Not studied/reported.

A non-pharmacological treatment targeting EMT in OS was also reported. Tumor-treating electrical field (TTEF) was reported to suppress EMT, cell migration, invasion, and angiogenesis of OS cells in culture via potential effects on VEGF and matrix metalloproteinase 2 (MMP2)[293].

1.1 Conclusions

EMT has significant implications in OS, despite its mesenchymal origin. Multiple studies have correlated changes in EMT with a more aggressive OS phenotype, both in vitro and in vivo. More than 100 proteins and non-coding nucleic acids have been identified as having a potential regulatory role in the OS EMT/MET pathways, and these may prove to be viable therapeutic targets and/or prognostic factors. These results should be interpreted with caution. While many of the studies discussed in this review confirmed the presence of their specific molecule of interest in clinical samples, most of the cell culture and animal studies were performed with only a handful of established cell lines. The majority of OS samples do not exhibit any E-cadherin and would therefore not experience a significant change secondary to E-cadherin suppression, a key process in EMT. It is possible that the cell lines most frequently utilized for these investigations are in the minority that do express E-cadherin and therefore exaggerate the EMT effect. Unfortunately, as OS is a rare cancer, any findings such as these are difficult to generalize. However, a role for EMT/MET has clearly been shown in cell culture and may well be a viable therapeutic target. Further work in additional cell lines or primary cell culture would help to confirm the findings outlined in this review.

Author Contributions: Conceptualization S.P. and K.H.; methodology, S.P., K.H., and A.K.; data curation, K.H. and A.K.; writing—original draft preparation K.H.; writing—review and editing, K.H., A.K., S.P., and P.P.; visualization, K.H.; supervision, S.P. and P.P. All authors have read and agreed to the published version of the manuscript.

Funding: This research received no external funding.

Institutional Review Board Statement: Not applicable.

Informed Consent Statement: Not applicable.

Data Availability Statement: Not applicable.

Conflicts of Interest: The authors declare no conflicts of interest.

3 Materials and Methods

3.1 Cell lines and culture conditions

Experiments were performed with four OS cell lines: HOS, 143B, SaOS2, and SaOS2-LM7 (LM7). HOS, 143B, and SaOS2 cells were purchased from ATCC (catalog nos. CRL-1543, CRL-8303, and HTB-85, respectively). LM7 cells were a generous gift from Dr. Eugenie Kleinerman of The University of Texas M.D. Anderson Cancer Center, Houston, Texas, USA.

HOS cells were initially derived from a 13-year-old female patient in 1971. 143B cells were formed from an oncogenic transformation of HOS via transfection with the ki-ras oncogene[294]. SaOS2 cells were derived from an 11-year-old female patient in 1972. LM7 was developed via multiple passages through a mouse model, selecting for metastatic cells[295].

All cell lines were maintained in Complete Media (CM), which was Minimal Essential Medium (MEM, Gibco, 10320-021) supplemented with 10% fetal bovine serum (FBS, Gibco, 12483-020), 1% penicillin-streptomycin (Gibco, 15140-122), 1mM sodium pyruvate (Gibco, 11360-070), and 2mM L-Glutamine (Gibco, 25030-081). Cells were cultured at 37°C, 5% CO_2. Cells were passaged by incubating flask with 0.05% Trypsin (Gibco, 25300-054) for 5 minutes at 37°C and 5% CO_2. Trypsin activity was then inhibited by the addition of CM, and the resulting cell suspension was centrifuged for 5 minutes at 1300 rpm. Supernatant was discarded and the pellet was resuspended in CM and seeded in a new flask.

3.2 Transfection

3.2.1 Plasmid construct design

Plasmids for the overexpression of ABC and β-catenin were constructed using a pEGFP-C2 backbone (Clontech, 6083-1). The backbone has the following components: a CMV promoter sequence, a GFP reporter gene, a resistance gene for neomycin/kanamycin for bacterial and mammalian selection, and a resistance gene for geneticin for mammalian selection. For ABC, to mimic constitutive phosphorylation of the S33 and S45 residues of ABC, these were substituted in the endogenous β-catenin sequence with aspartic acid (D). To prevent phosphorylation of the S37 and T41 residues that might ultimately result in sequestration and degradation of the protein, these residues were substituted by alanine (A). The ABC and β-catenin sequences were inserted downstream of the GFP reporter resulting in final proteins that were fused with GFP. The final

ABC and β-catenin plasmid constructs were created by GeneArt, Thermo Scientific and are pictured in Figure 3.1.

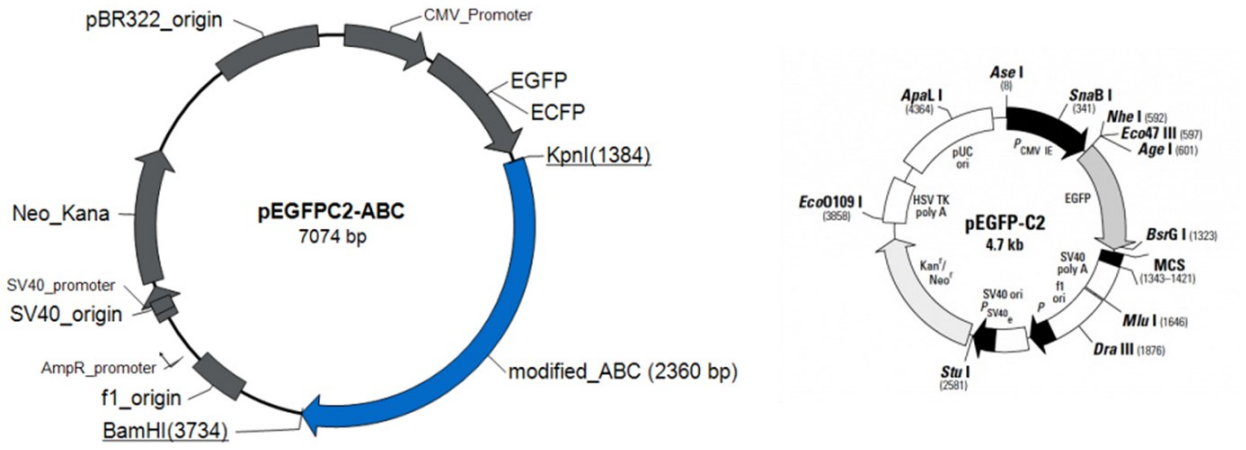

Figure 3.1 pEFFPC2-ABC construct design and pEGFP-C2 backbone

3.2.2 Liposome-based transfection

The overexpression of ABC, β-catenin, and GFP was achieved via liposomal transfection with the ABC-pEGFP-C2, βcat-pEGFP-C2, and empty vector pEGFP-C2 plasmids, respectively. HOS and SaOS2 cells were seeded in 6-well plates and transfected once they reached 70-90% confluence. GenJet *in vitro* DNA Transfection Reagent (SignaGen, SL100488) was used according to the manufacturer's recommended protocol with 1 µg of DNA and 6 µL of transfection reagent per well. The cells were incubated with the transfection reagent and DNA for 18-24 hours and then media was replaced with CM. Cells were maintained for an additional 24 hours, transfection efficiency was then determined with fluorescence microscopy and cells were utilized for additional investigations such as 3D culture and Western Blot. Transfected cell lines with ABC, β-catenin, and empty vector are hereafter denoted with the suffixes -ABC, -βcat, and -GFP, respectively.

3.2.3 Stably transfected cell lines

HOS and SaOS2 cells were transfected as described above with either ABC, β-catenin, or the GFP empty vector plasmid. After growing for 48 hours, CM was changed for Stable Media (SM), which was CM supplemented with 1mg/mL Geneticin to select for stably transfected cells. Media was changed every 2-3 days for 10 days. Following this, cells were imaged with a fluorescent microscope and colonies of fluorescing cells were isolated, scraped off of the plate, resuspended in SM, and added to a new plate. This process was repeated until all the cells on the

plate exhibited a uniform pattern of fluorescence. Stable cells were characterized by determining that the GFP-ABC and GFP-βcat had the same subcellular localization pattern as the endogenous proteins. Cells continued to be maintained in SM. These stable cell lines were then used for three-dimensional culture and animal experiments as described below.

3.3 Three-dimensional cell culture

3.3.1 Establishment and maintenance of 3D cultures

3D cultures were established in scaffolds containing different proportions of basement membrane matrix (BMM, Corning Matrigel®, 354234) and neutralized collagen. At the time of creating the cultures, the appropriate volume of collagen (Collagen I 3mg/mL Gibco, A10483-01) was mixed with 1mM sodium hydroxide (NaOH) and CM in the following proportions: 1,000µL neutralized collagen = 64µL NaOH + 100µL CM + 868µL collagen. This was then mixed with BMM (Corning Matrigel®, 354234) and kept on ice. Table 3.1 shows the different proportions of BMM and collagen that were trialled for growing spheroids of HOS, 143B, SaOS2, and LM7. Meanwhile, 8-chamber slides (Nunc™ Lab-Tek II Chambered Coverglass, Thermo Scientific, 155409) and 24-well plates (Nunc™ Cell-Culture Treated Multidishes, Thermo Scientific, 142485) were pre-warmed to 37°C.

Table 3.1 Mixtures of basement membrane matrix (BMM) and neutralized collagen investigated for suitability in supporting spheroids of HOS, 143B, SaOS2, and LM7

Scaffold Mixture	Proportion BMM	Proportion Neutralized Collagen	% collagen
1	1	0	0%
2	9	1	10%
3	4	1	20%
4	2	1	33%
5	1	1	50%
6	0	1	100%

3D cultures were established with all cell lines including 143-B, HOS, HOS-ABC, HOS-βcat, HOS-GFP, LM7, SaOS-ABC, SaOS-βcat, and SaOS-GFP. 143-B and LM7 served as positive controls while the untransfected cell lines and the -GFP cell lines were negative controls. Cells were grown to 70-90% confluence and then lifted from the plates with the application of 0.05%

trypsin for 5 minutes at 37°C and 5% CO_2, trypsin activity was stopped with the addition of CM or SM depending on the maintenance media for the culture. The cell suspension was then centrifuged at 1300 rpm for 5 minutes. The supernatant was discarded, and the pellet was resuspended in CM or SM. Cells were then counted using a Countess II FL automated cell counter.

The appropriate volume of the cell suspension was then added to and very gently mixed with the gel matrix and did not exceed 20% of the final volume. The final concentration of 143-B, HOS and HOS transfectants was 50 cells/µL and the final concentration of LM-7, SaOS2, and SaOS2 transfectants was 100 cells/µL. 3D cultures intended for microscopy were plated in 8-chamber slides and 3D cultures intended for Western Blot were plated in 24-well plates. 50 µL of the BMM-collagen cell-suspension was plated in each chamber/well with care not to touch the walls. The plates and slides were then carefully transferred to the incubator at 37°C and 5% CO_2 for 20-30 minutes to allow the gels to set. Each well was then supplemented with CM or SM warmed to 37°C depending on the cells. Media was changed every 2-3 days.

3.3.2 Measuring invasion area, spheroid area, and invasion length

After 10-14 days, live spheroids were imaged with an EVOS microscope at 4x magnification. The spheroid area (SA) and invasion area (IA) were calculated by the ImageJ software as indicated by the example in Figure 3.2. Spheroid radius (SR) and invasion radius (IR) were then calculated according to the following formula: $radius = \sqrt{(\frac{area}{\pi})}$. These values were used to calculate invasion length (IL) according to the following equation: IL = IR – SR[296].

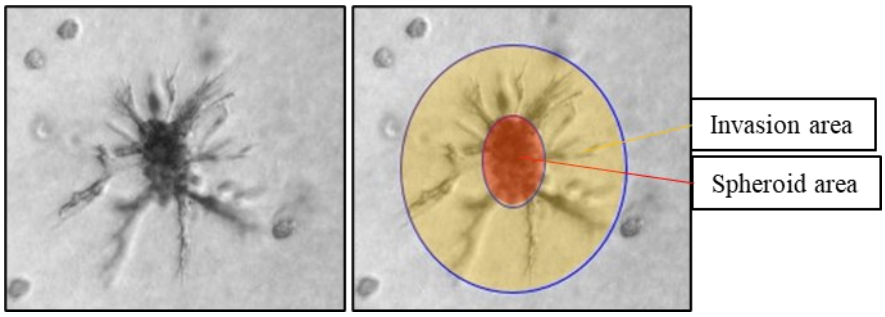

Figure 3.2 Spheroid area (SA) and invasion area (IA) were calculated by the ImageJ software based on circular figures drawn around the spheroid body and the ends of the longest projections, respectively. These values were used to

approximate spheroid radius and invasion radius, which were in turn used to calculate invasion length (IL) by the formula IL = IR – SR.

3.3.3 Confocal microscopy

The spheroids were imaged after 7 days for 143-B, HOS, and HOS-transfectants, and after 10 days for LM7, SaOS2, and SaOS2 transfectants. Spheroids were fixed with 2% paraformaldehyde for 15 minutes, washed with phosphate-buffered saline (PBS), quenched with NH_4Cl for 30 minutes, washed 3 times with PBS, permeabilized for 30 minutes with 0.5% Triton X-100 (Fisher, BP151-500) in PBS, blocked for 30 minutes with blocking buffer (3% bovine serum albumin (BSA) and 0.05% Triton X-100 in PBS), then incubated for 30 minutes with 1 µg/mL 4',6'-diamidino-2-phenylindole (DAPI, Sigma-Aldrich, D9542) in blocking buffer, washed 3 times with PBS, then incubated for 30 minutes with phalloidin (Invitrogen, A22287) mixed 1:1000 in PBS. A think layer of antifade mounting agent (ProLong™ Gold Antifade Mountant, Invitrogen, P36934) was then applied to each chamber and allowed to cure overnight. Slides were stored at 4°C and protected from light.

Fixed and stained spheroids were then imaged at 20x magnification with a spinning disk confocal microscope. A representative sample of spheroids from each chamber was imaged and analysed for qualitative morphologic characteristics.

3.3.4 Preparation of spheroid lysate

Spheroids were grown until the gel matrices started to become unstable (about 10-14 days) and then collected and lysed for Western blot. Media was removed and each well was washed with cold PBS, dislodging the collagen/BMM gel matrix. PBS and matrices were transferred from the well to a 15 mL conical tube – up to 5 wells containing spheroids of the same cell line were combined into a single tube. PBS/gel suspension was centrifuged at 4°C and 1000 rpm for 5 minutes resulting in a fluid-fluid layer. The supernatant was carefully aspirated to the fluid-fluid meniscus, and the pellet was resuspended with 1mL of 0.05% trypsin then incubated in a 37°C water bath for 5 minutes. Trypsin activity was inhibited by the addition of 2mL of CM and the suspension was pipetted to mix. This was then centrifuged at 4°C and 1500 rpm for 5 minutes forming a solid pellet. The supernatant was aspirated, and the pellet was resuspended in 1mL of PBS to remove any residual media. It was then centrifuged at 1300 rpm for 5 minutes. The supernatant was discarded, and the pellet was resuspended in 100µL of lysis buffer (RIPA buffer, Sigma, R0278 with Protease Inhibitor Cocktail Tablet, Roche, 04693159001). This suspension was

then sonicated at 4°C for two 5 second pulses then centrifuged at 4°C and 7000 rpm for 10 minutes. Protein concentration of the supernatant was determined with Pierce™ bicinchoninic acid (BCA) protein assay kit (Thermo Scientific, 23227).

3.4 Western Blot

Whole cell lysate containing 20 µg of protein was diluted to a final volume of 40 µL containing 1x loading buffer. Samples were boiled in a water bath for 5 minutes then immediately cooled on ice. Samples were loaded into the wells of a 7.5% polyacrylamide gel, and sodium dodecyl sulfate-polyacrylamide gel electrophoresis (SDS-PAGE) was performed. The proteins were then transferred to a polyvinylidene fluoride (PVDF) membrane (Bio-Rad, 1620177) at 100 V and 4°C for 90 minutes. Membranes were blocked for 1 hour in 5% milk in Tris-buffered saline (TBS) containing 0.1% tween-20 (TBST) followed by incubation with primary antibody diluted in the milk-TBST solution at 4°C overnight. Membranes were then washed with TBST and then incubated with secondary antibody linked to horseradish peroxidase (HRP) at room temperature for 1 hour and then washed with TBST. The HRP-secondary antibody signal was detected using the Western Lightning Plus ECL (Perkin Elmer, NEL 104001) detector reagent and the bands were visualized with a Bio-Rad ChemiDoc™ Imaging System. Primary and secondary antibodies are listed in Table 3.2.

Table 3.2 Primary and secondary antibodies for Western blots

Primary Antibody Target	**Animal Source**	**Product Number**	**Dilution**
β-catenin (amino-terminal antigen)	Rabbit	Cell Signalling 9581S	1:1000
Active-β-catenin (anti ABC), clone 8E7	Mouse	Millipore 05-665	1:250
EGFP	Mouse	Abcam AB184601	1:1000
β-actin	Mouse	Santa Cruz Biotechnology sc-69879	1:10,000
Secondary Antibody Target	**Animal Source**	**Product Number**	**Dilution**
Rabbit Immunoglobulin	Goat	Bio-Rad 1706515	1:1000
Mouse Immunoglobulin	Goat	PerkinElmer NEF822001	1:1000

3.5 Orthotopic murine model

An overview of the murine model is provided in Figure 3.3.

3.5.1 Mice

Research ethics approval was obtained for a pilot study to examine the effects of ABC overexpression on osteosarcoma *in vivo* (AUP 00004041). Fifteen nonobese diabetic/severe combined immunodeficiency (NOD SCID) mice (Charles River strain 394) were transferred to the animal facility at age 4.5 weeks. They were maintained on a standard diet of 4.5% rodent chow, which was freely available. The mice were given 5 days to acclimatize to the facility and personnel.

3.5.2 Preparation of cells for injection

At 5 weeks, the orthotopic xenograft implantation was performed. The mice were divided into 5 groups of 3 to be injected with the following cells: SaOS2, SaOS2-GFP, SaOS2-βcat, SaOS2-ABC, and LM7. On the morning of the procedure, the cells, which had been grown to 70-90% confluence, were lifted from the flasks with the application of 0.05% trypsin for 5 minutes at 37°C and 5% CO_2, trypsin activity was stopped with the addition of CM. The cell suspension was then centrifuged at 1300 rpm for 5 minutes. The supernatant was discarded, and the pellet was resuspended in PBS. Cells were then counted using a Countess II FL automated cell counter and diluted to a concentration of 10^5 cells/µL. These suspensions were stored on ice until the time of injection.

3.5.3 Orthotopic xenograft implantation procedure

The mice were anesthetized with inhaled isoflurane until they reached a deep surgical plane and closely monitored for respiratory rate, cyanosis, and pedal reflexes throughout the procedure. Pre-operative analgesia was provided with 5mg/kg meloxicam and 0.5 mg/kg slow-release buprenorphine. The hair was removed from the left hind limb with a depilatory cream (Nair™). The limb was then washed with iodine followed by chlorhexidine surgical scrub solutions. Once dry, the limb was held fully flexed and a small 3-5mm incision was made overlying the patellar tendon, which was incised in line with the skin to expose the tibial plateau. A sharp bevelled 18-gauge needle was introduced through the tibial plateau into the tibial metaphysis. This needle was then removed and replaced with a second 18-gauge bevelled needle fitted with 10µL syringe containing a cell suspension of 10^6 cells in 10µL of PBS. The incision was then sutured closed

with a single 4-0 vicryl suture. Anesthetic gas was then stopped, and the mouse was monitored until regaining consciousness.

3.5.4 Post-operative monitoring

The mice received nutritional support with a gel boost diet supplement for the week following the procedure and post-procedure infection prophylaxis sulfamethoxazole-trimethoprim (Novotrimel®) for 2 days prior to procedure and 7 days afterward. Mice were observed for signs of wound complications, infection, and general distress daily according to the checklist outlined in Table 3.3. Each animal was weighed prior to the procedure, daily for three days afterward, and then once every three days. If weight loss greater than 5% was observed, they continued to be weighed daily until they were back within 5% of their pre-procedure weight then resumed the usual schedule. Tumors were to be measured with calipers once palpable. If a mouse had a score of 3 in the respiration or responsiveness category, it was euthanized within an hour. If a mouse had a score of 3 in the body weight or gait category or had a total score of 12 or more, it was euthanized by the end of the day. If a mouse had a total score of 6-11 then it was given a dose of 0.05 mg/kg subcutaneous buprenorphine and reassessed in 2-3 hours. If no improvement in score, the mouse was euthanized.

Table 3.3 Daily Mouse Observation Scoring Checklist

Body Weight	
0	0-5% body weight loss
1	6-12% body weight loss
2	13-19% body weight loss
3	≥20% body weight loss
Responsiveness	
0	Bright, alert and responsive
1	Quiet and responds to movement
2	Lethargic, does not respond to movement, responds to touch
3	Moribund and non-responsive **(requires euthanasia)**
Respiration	
0	Normal rate (<170 breaths/minute) and effort
1	Mild increase (170-200 breaths/minute) and increased effort visible on chest
2	Moderate elevation in rate (200-240/minute) or increased effort obvious on chest
3	Sever, open-mouth breathing or holding elbows out from chest **(requires euthanasia)**

Posture	
0	Normal (back extended, moves freely)
1	Hunched (a hunched or arched back)
Gait	
0	Normal movement and mobility
1	Abnormal (tremors, ataxia, paresis)
2	Lameness on 1 limb, still weight bearing
3	Non-weight bearing, unable to use one or more limbs **(requires euthanasia)**
Hair Coat	
0	Normal (smooth, groomed, glossy)
1	Abnormal (rough, un-groomed, dull-appearing, dry, or pilo-erection)
Nest Building	
0	Standard quality nest
1	Poor quality of nest
Vocalization	
0	No vocalization when handled/restrained or while mobing around the cage
1	Vocalization when handled/restrained or while moving around the cage
Skin Incision	
0	Healthy incision
1	Incision open <0.5 cm with granulation tissue present
1	Incision open >0.5cm with no granulation tissue present **(incision must be resutured)**
1	Mild-moderate swelling, discharge or redness
1	Severe swelling, discharge or redness **(Contact HSLAS)**
Tumor	
0	Tumor <16mmx16mm
4	Tumor ≥16mmx16mm
4	Any tumor dimension >20mm
4	Ulceration of tumor

3.5.5 Euthanasia, necropsy, and pathology

The mice were euthanized 28 days following the procedure. Each mouse was anesthetized to a deep surgical plane with inhaled isoflurane. Once they were unresponsive, a cervical dislocation was performed. After death was confirmed by the absence of pulse and respiration, necropsy was performed. The left hind limb was carefully dissected to remove muscle and tendon

and preserve as much of the femur, tibia, and knee joint (with intact capsule) as possible. The lungs and liver were also carefully removed. All samples were placed in 10% neutral buffered formalin for fixation for several days. Following fixation, limbs were demineralized and then each was placed in a cassette in preparation for processing. The liver and all lung lobes were also fixed in 10% neutral buffered formalin and following fixation were sectioned to a thickness of 2 mm and placed into cassettes for processing. All tissues in cassettes were processed and embedded into paraffin blocks using routine techniques. A five micron thick section was made of each paraffin embedded tissue, placed on a glass slide, stained with hematoxylin and eosin and cover slipped. Stained slides were then examined microscopically by a board-certified veterinary pathologist for microscopic anatomic abnormalities including, but not limited to location of experimental injection sites, presence/ absence of tissue reactions to injected material, presence/absence of tumor engraftment in bone and presence/absence of tumor metastasis to lung and liver. All abnormalities were documented and assessed as to significance in terms of the experimental procedure.

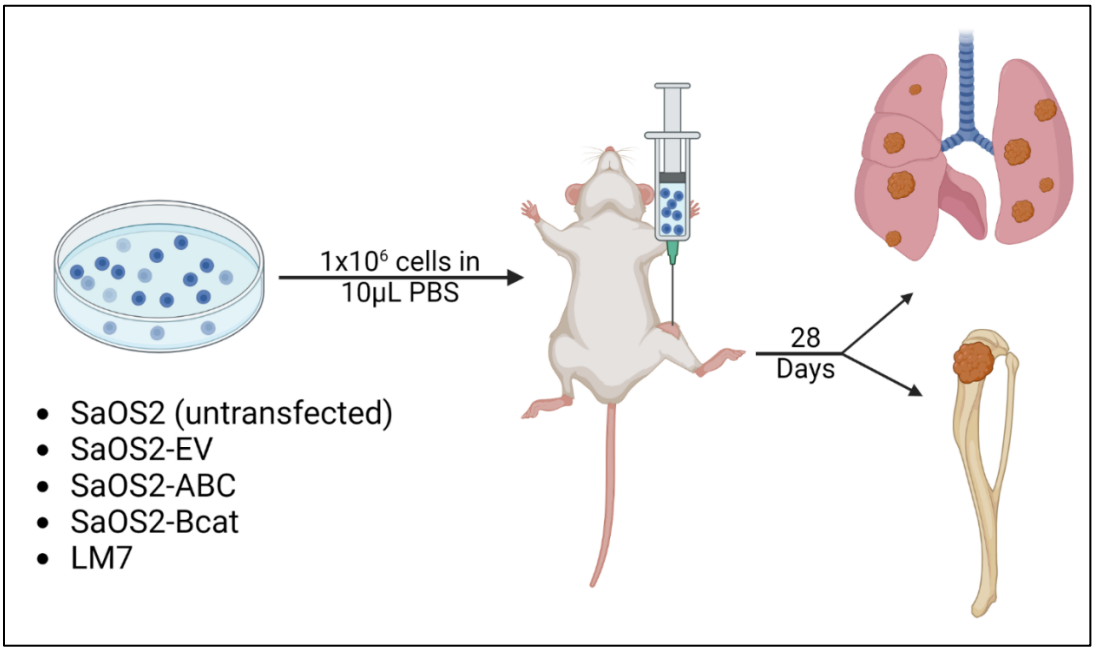

Figure 3.3 Overview of orthotopic murine model of OS

3.6 Statistical analysis

Statistical tests were performed with Microsoft Excel and Stata (StataBE 17). Two-tailed t-tests were used to compare invasion area, spheroid area, and invasion length between transient and

stable transfections. One-way ANOVA was used to analyse differences in invasive length between cell lines in the two respective families (HOS family: HOS/HOS-GFP/HOS-βcat/HOS-ABC/143-B; SaOS2 family: SaOS2/SaOS2-GFP/SaOS2-βcat/SaOS2-ABC/LM7). Where ANOVA indicated a significant difference, a Bonferroni test was done to determine which means were significantly different. Results were considered statistically significant at $p<0.05$.

4 Results

4.1 HOS and SaOS2 cells were successfully transfected with ABC and β-catenin

Figures 4.1 and 4.2 show representative brightfield and fluorescent microscope images demonstrating successful transfection of the GFP-fused ABC and β-catenin as well as the GFP empty vector into the HOS and SaOS2 cell lines. The resulting transfectants were termed HOS-ABC, HOS-βcat, HOS-GFP, SaOS2-ABC, SaOS2-βcat, and SaOS2-GFP. Transfection efficiency was improved with the empty vector plasmid as well as in the SaOS2 cells though greater cytotoxicity was observed in the SaOS2 cells.

Stably transfected cell lines were established through selection with geneticin. Figures 4.3 and 4.4 show the fluorescence pattern of the stably transfected cells. The resulting transfectants were termed HOS-ABC_s, HOS-$βcat_s$, HOS-GFP_s, SaOS2-ABC_s, SaOS2-$βcat_s$, and SaOS2-GFP_s. Intracellular location of the fluorescence was confirmed to be the same as the transient transfections at 10x magnification (not shown). Western blot and immunofluorescence experiments completed by a previous student confirmed production of the fused GFP-ABC and GFP-β-catenin proteins and the colocalization of the fluorescent proteins with their endogenous counterparts [297]. The overall fluorescence of the stably transfected cells became less bright through the selection process.

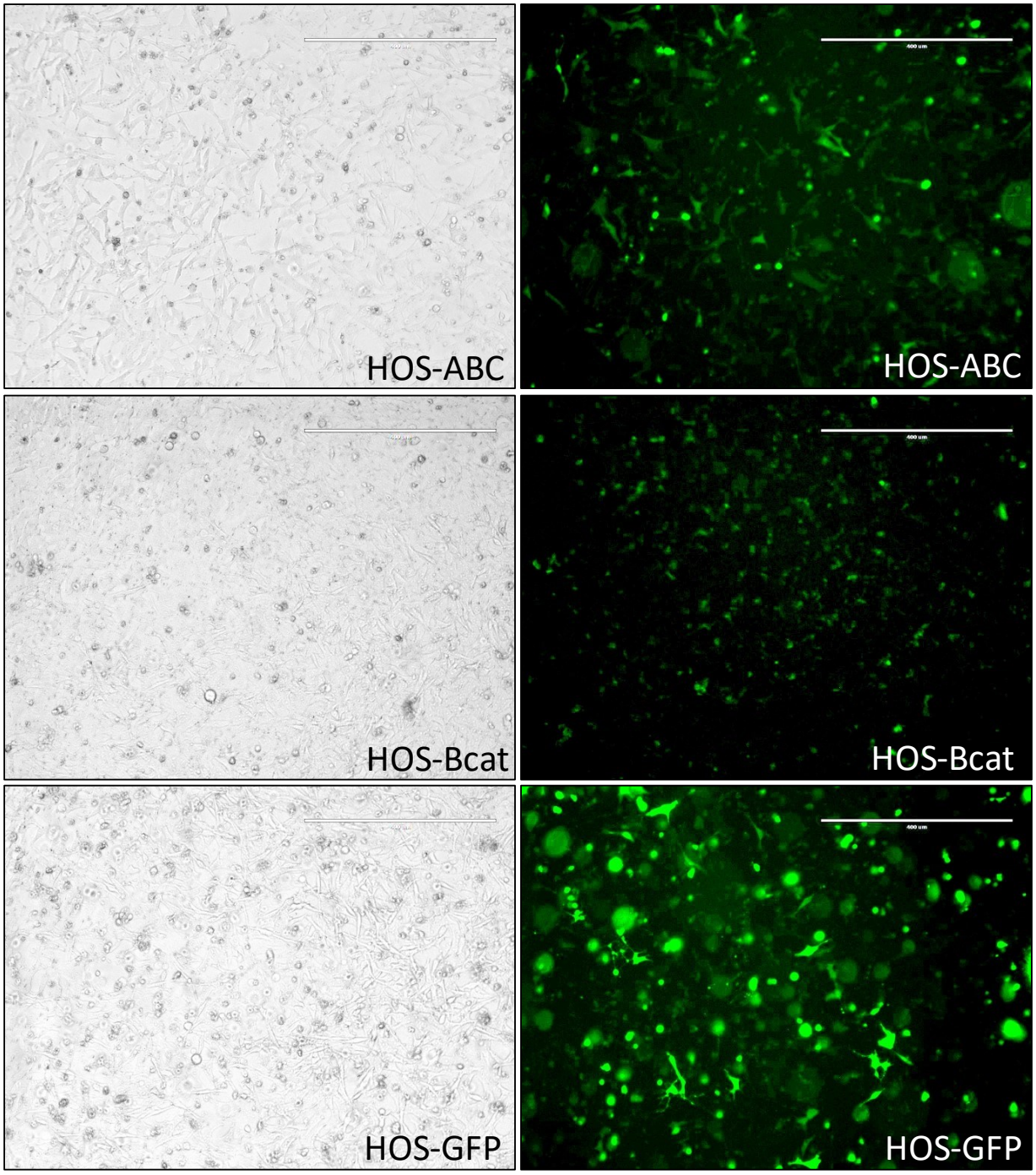

Figure 4.1 HOS cells were successfully transfected with ABC (HOS-ABC), β-catenin (HOS-βcat), and GFP (HOS-GFP). Images were taken at 10x and scale bars represent 400 μm.

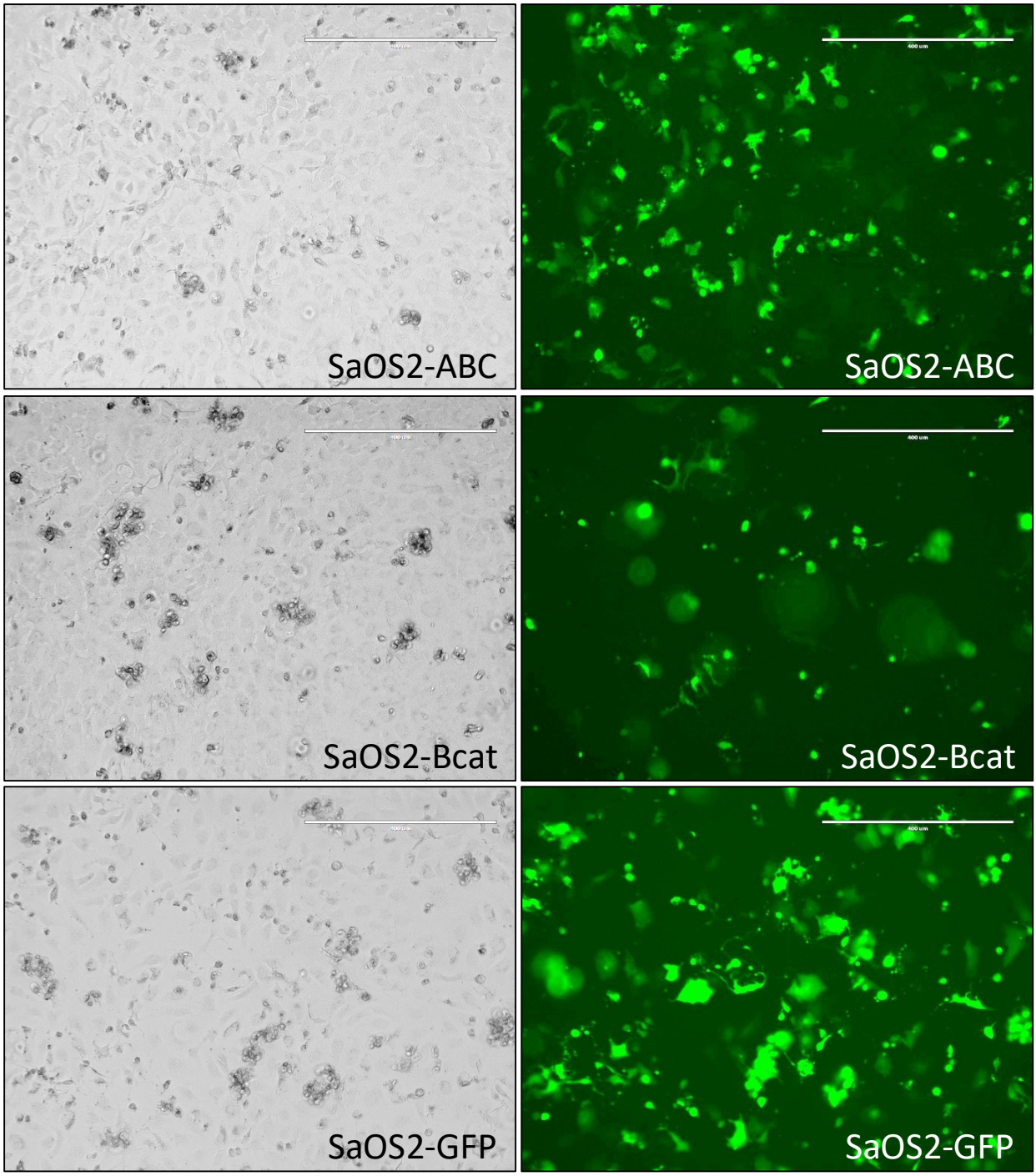

Figure 4.2 SaOS2 cells were successfully transfected with ABC (SaOS2-ABC), β-catenin (SaOS2-βcat), and GFP (SaOS2-GFP). Images were taken at 10x and scale bars represent 400 μm.

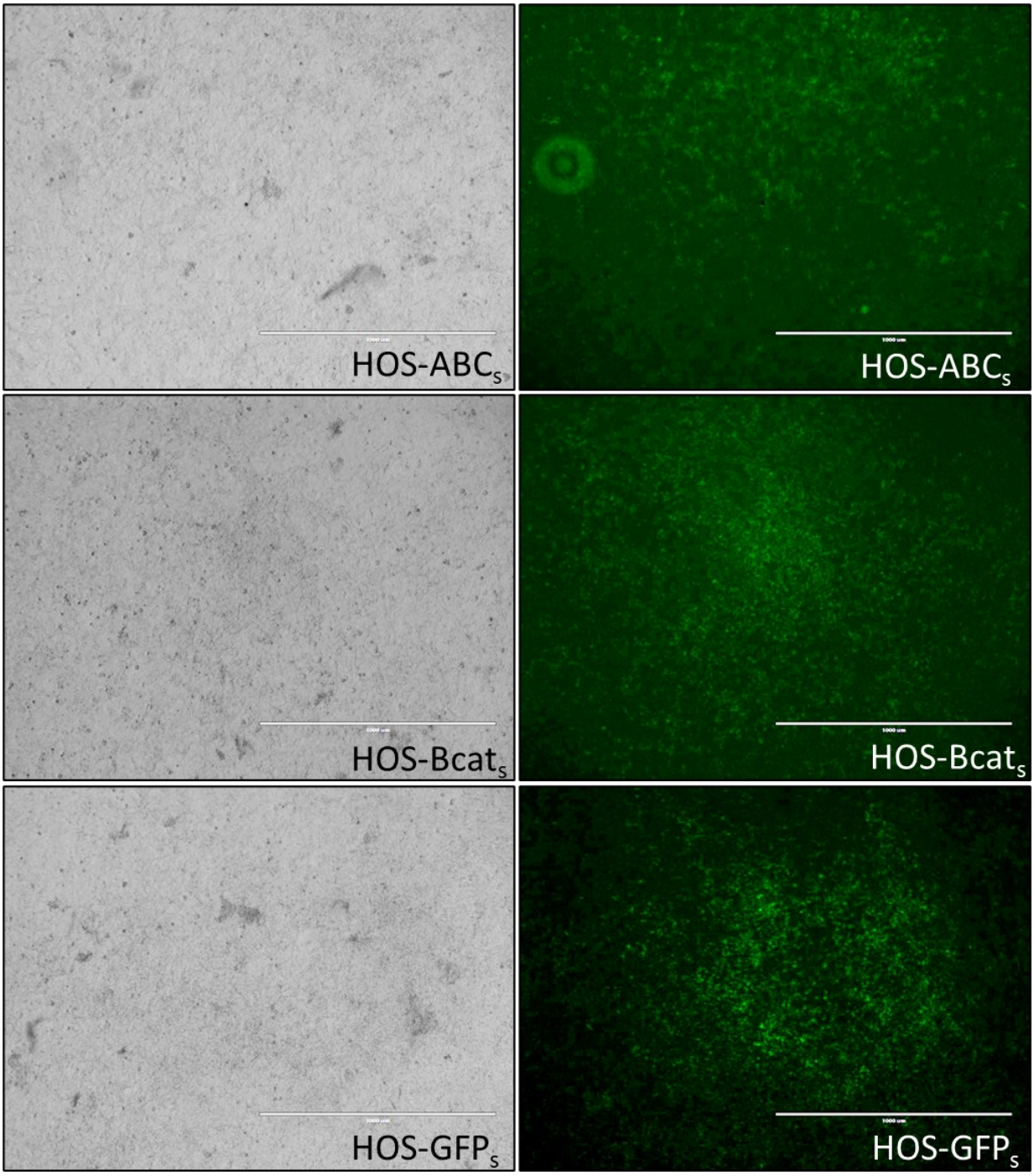

Figure 4.3 Stably transfected HOS cells with ABC (HOS-ABC_s), β-catenin (HOS-βcat_s), and GFP (HOS-GFP_s). Images were taken at 4x and scale bars represent 1000 μm.

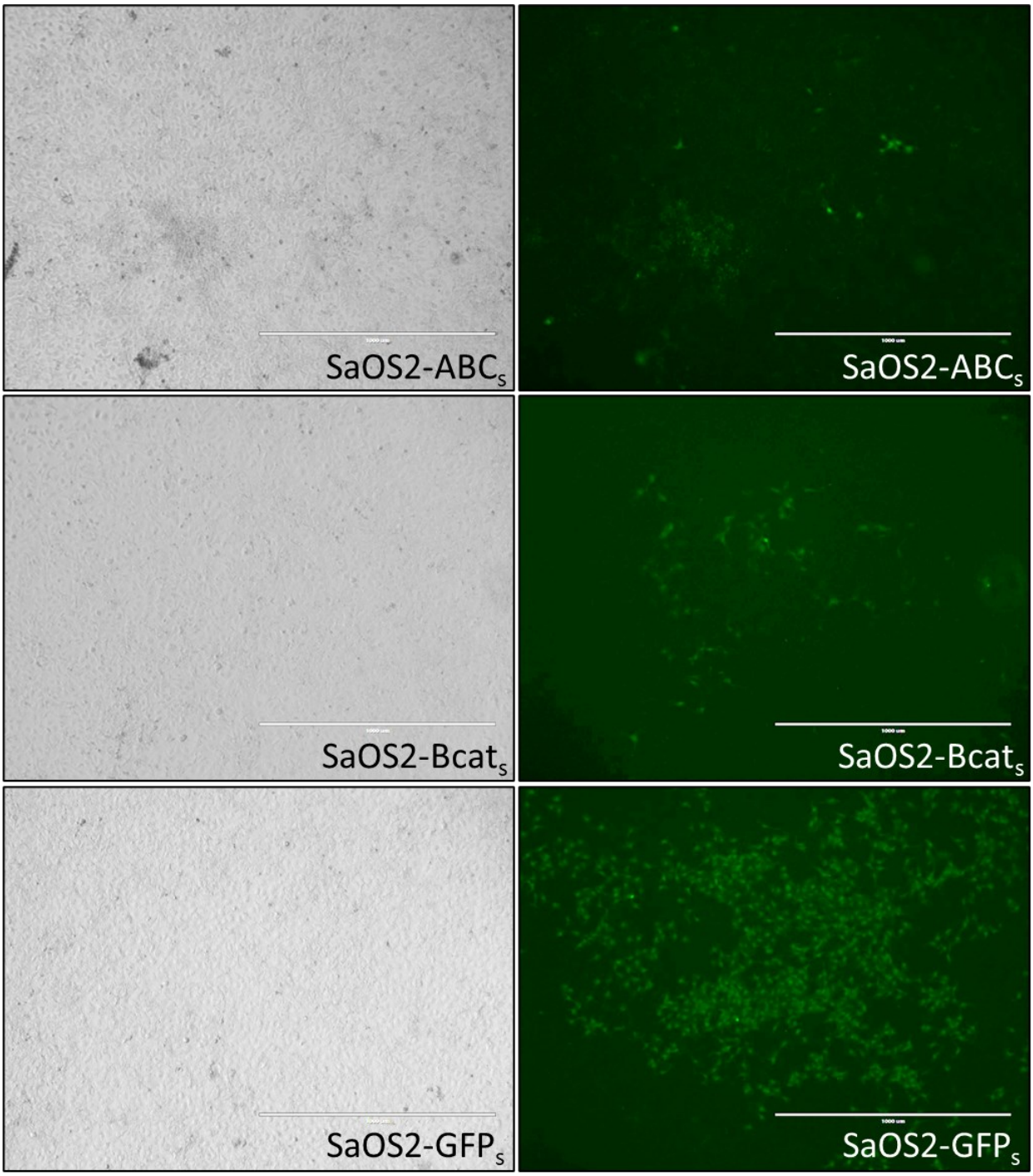

Figure 4.4 Stably transfected SaOS2 cells with ABC (SaOS2-ABC_s), β-catenin (SaOS2-βcat_s), and GFP (SaOS2-GFP_s). Images were taken at 4x and scale bars represent 1000 μm.

4.2 A 20% collagen in BMM mixture was superior for OS 3D culture scaffold

Initially, 3D cultures of the untransfected cell lines were successfully established in a pure BMM scaffold (Figure 4.5). Qualitatively, 143B cells established larger spheroids than HOS cells, and LM7 cells established larger spheroids than SaOS2. In contrast, both HOS and SaOS2 formed an interconnected network of tubules between spheroids that was not observed in the metastatic daughter lines. Unfortunately, the matrix scaffold dissolved during the fixation process and the orientation and interactions between spheroids was lost. No quantitative analysis was performed on these samples. This also occurred with the use of a 10% collagen in BMM mixture. As the percentage of collagen increased, the spheroids universally displayed a more invasive phenotype as demonstrated by increased projections (Figure 4.6). At 20% collagen in BMM, spheroids were successfully established, and the scaffold was maintained throughout the fixation process. This was selected for all subsequent experiments.

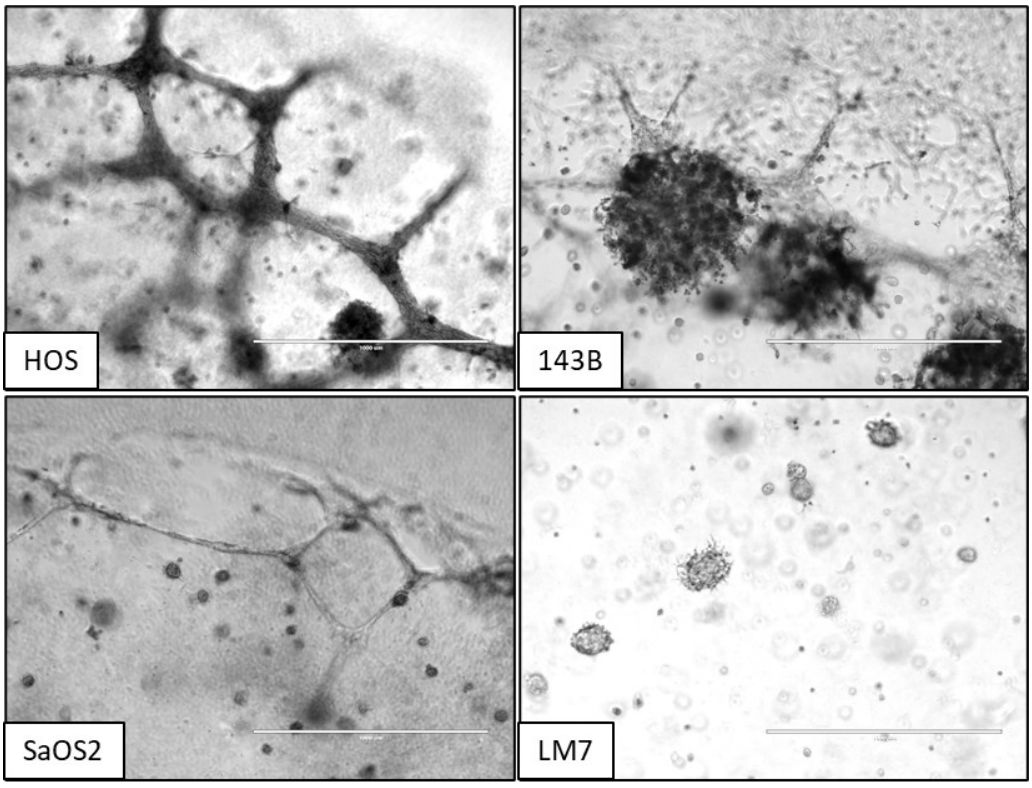

Figure 4.5 Preliminary spheroids of HOS, 143B, SaOS2, and LM7 cells established in a 100% BMM scaffold.

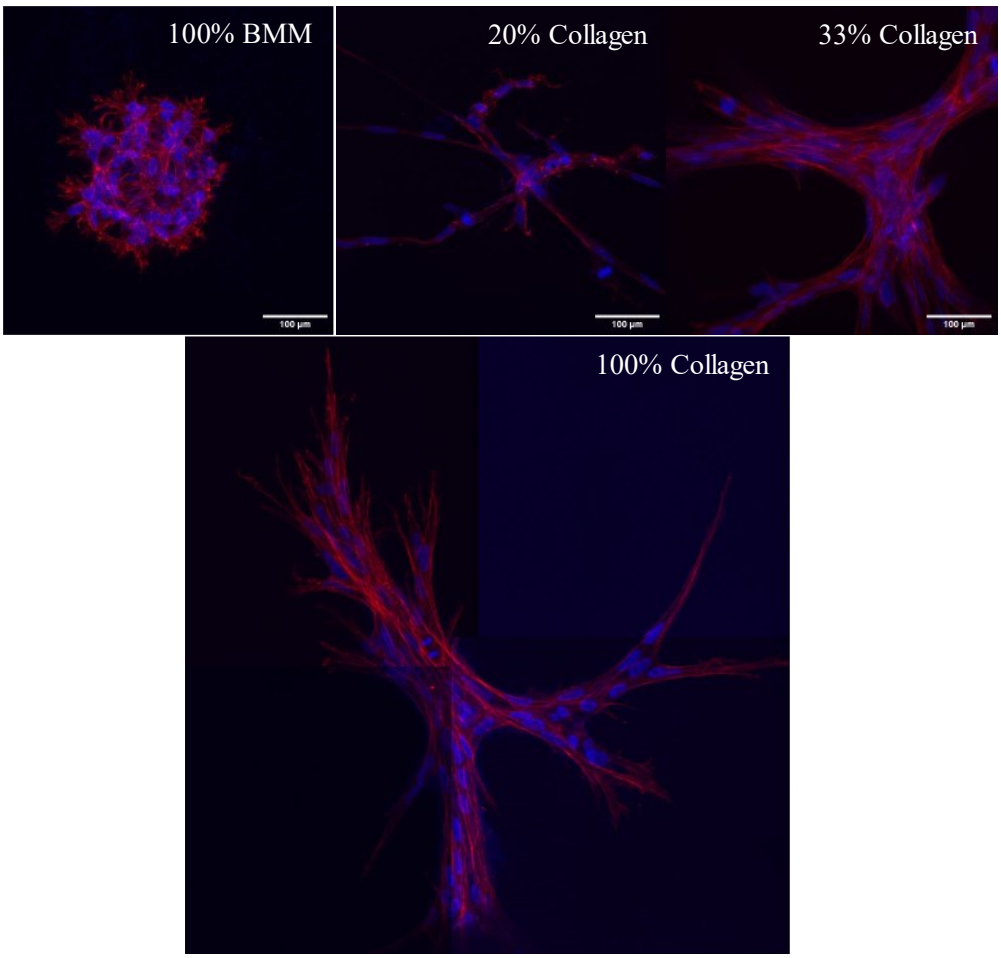

Figure 4.6 HOS spheroids grown for 7 days in different concentrations of collagen in BMM. As collagen percentage increased, size of the spheroids increased along with the number and size of projections. Images were acquired at 20x magnification, F-actin is stained red, and nuclei are stained blue.

4.3 Metastatic cell lines formed larger spheroids compared to non-metastatic cell lines

Figures 4.7 and 4.8 show representative images of 143B, HOS, LM7, and SaOS2 spheroids that were live-imaged at 2 weeks. Average IA, SA, and IL are given for each cell line in Table 4.1. The IA and SA of HOS cells were significantly smaller than the metastatic daughter line 143B ($p<0.05$); IL was also smaller in HOS compared to 143B but this did not reach statistical significance. Though not quantified, 143B spheroids were observed to be denser (i.e. appeared to contain more tightly-packed cells) than HOS spheroids. The IA, SA and IL were all significantly smaller in SaOS2 compared to its metastatic daughter line LM7 ($P<0.05$).

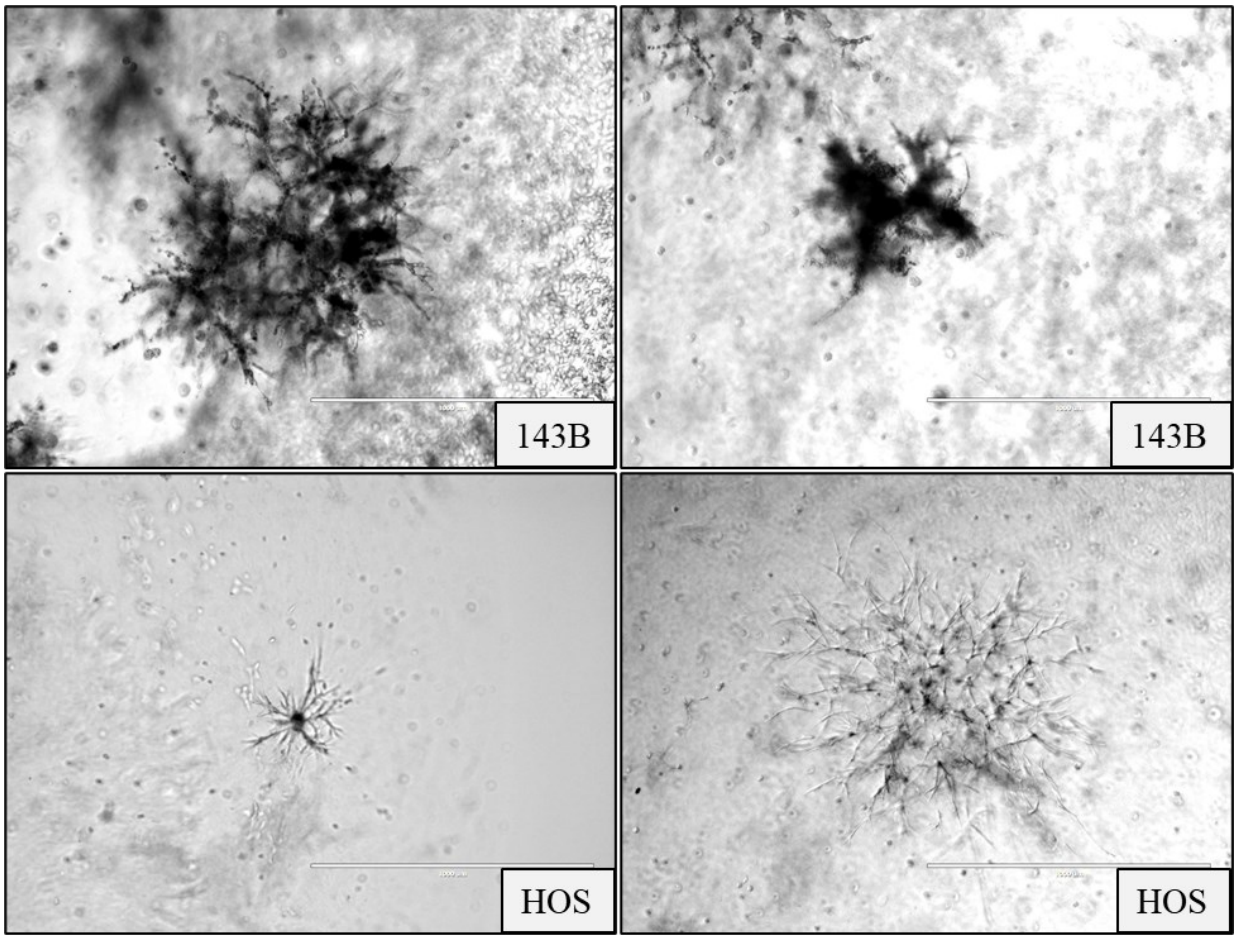

Figure 4.7 Representative images of 143B and HOS spheroids. Images were taken at 4x magnification and scale bars represent 1000 μm.

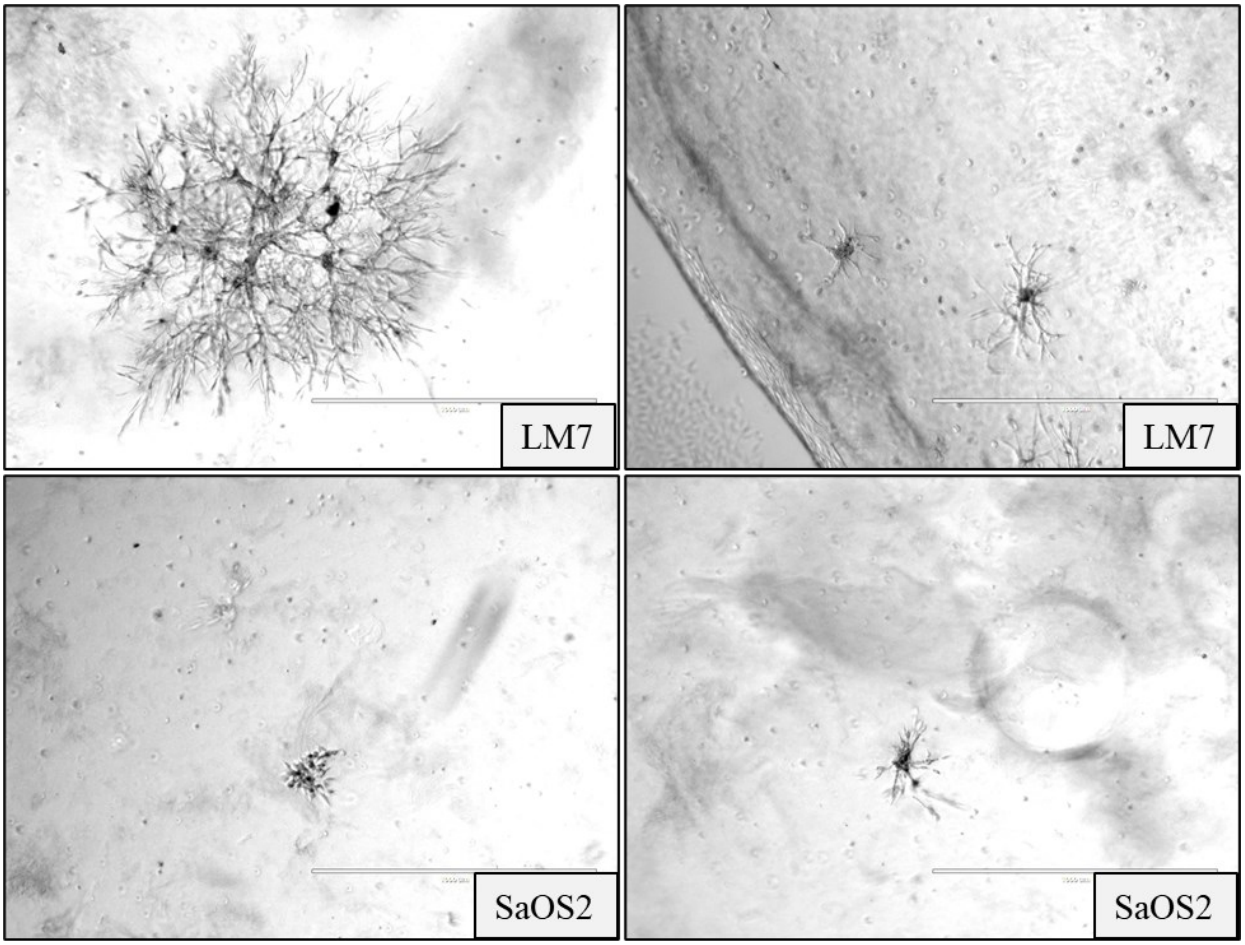

Figure 4.8 Representative images of LM7 and SaOS2 spheroids. Images were taken at 4x magnification and scale bars represent 1000 µm.

Table 4.1 Average invasion area, spheroid area, and Invasion length of HOS, 143B, SaOS2, and LM7.

Cell Line	Invasion Area ($x10^4 µm^2$)	Spheroid Area ($x10^4 µm^2$)	Invasion Length (µm)
HOS	47.8 ± 37.6	16.6 ± 16.7	160.2 ± 54.0
143B	88.6 ± 36.8	35.4 ± 25.1	200.6 ± 59.5
p	**<0.05**	**<0.05**	0.11
SaOS2	9.15 ± 5.20	1.21 ± 1.16	106.3 ± 39.1
LM7	66.2 ± 60.2	13.8 ± 14.8	239.6 ± 92.5
p	**<0.05**	**<0.05**	**<0.05**

4.4 Stable and transient transfections did not form equivalent spheroids

Figures 4.9, 4.10, and 4.11 show representative images of spheroids formed from transiently and stably transfected HOS cells, HOS-GFP, HOS-ABC, and HOS-βcat. Also shown are box-and-

whisker plots of the IA, SA, and IL for each cell line. While these values were all statistically similar for HOS-βcat, there were significant differences between transient and stable transfectants of HOS-ABC and HOS-GFP. Transiently transfected SaOS2 cells did not form any dectectable spheroids. Stably transfected SaOS2 cells formed very few spheroids, which are shown in Figure 4.12. There were insufficient spheroids generated from transfected SaOS2 cells for analysis.

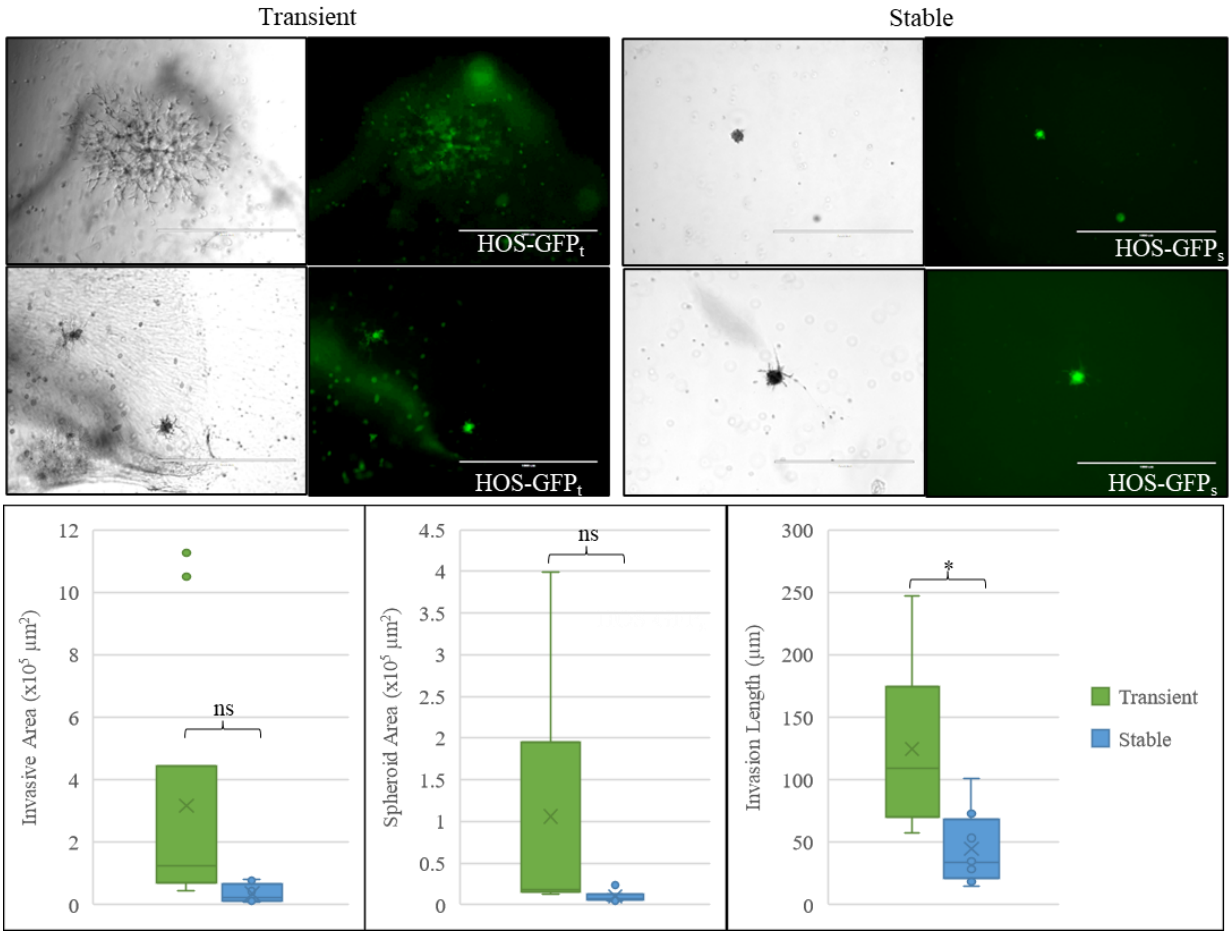

Figure 4.9 Representative brightfield and fluorescent images, IA, SA, and IL of transient and stable HOS-GFP transfections. Images were taken at 4x magnification and scale bars represent 1000 µm. Box and whisker plots representing invasive area, spheroid area, and invasion length. Invasion length was found to be significantly different difference transient and stably transfected spheroids ($p<0.05$). No significant difference was found in invasive area or spheroid area ($p>0.05$).

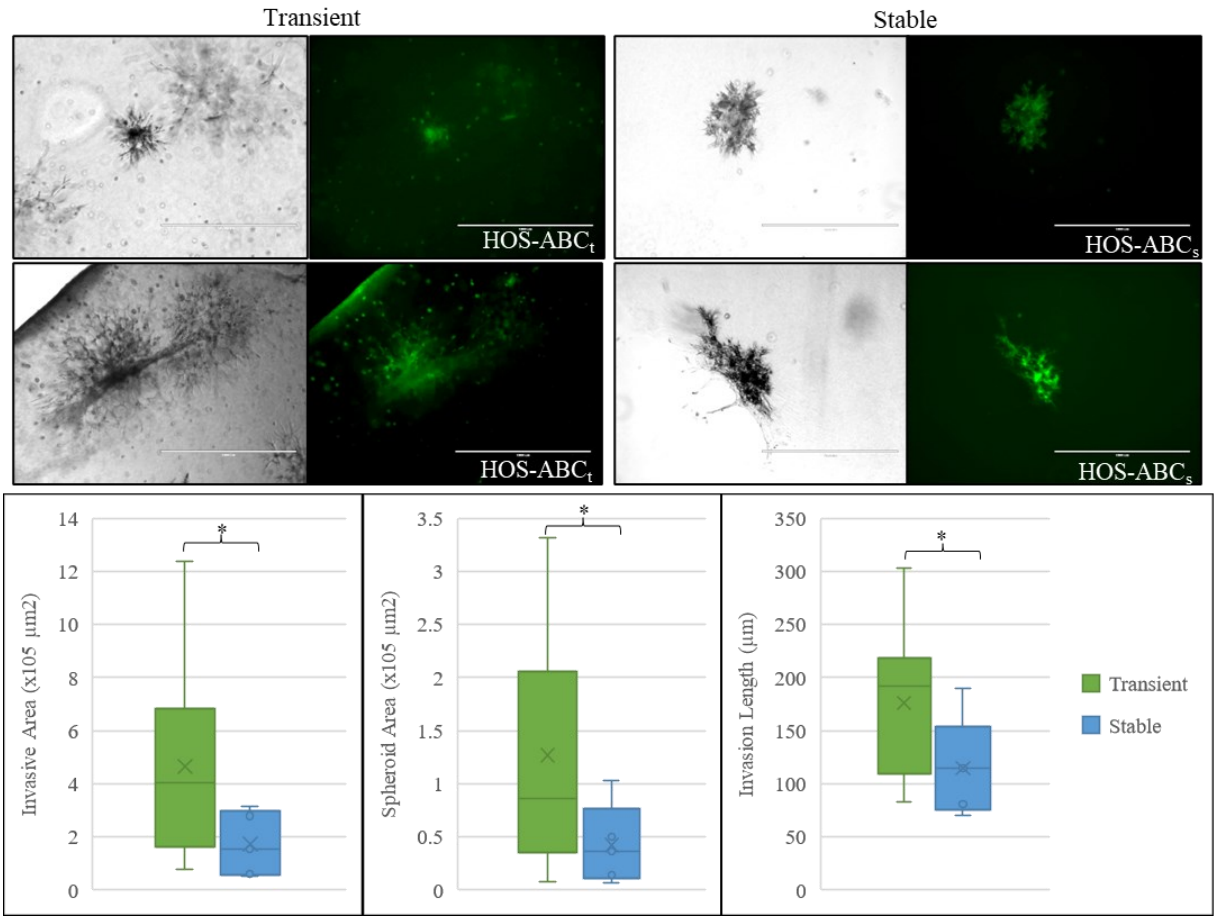

Figure 4.10 Representative brightfield and fluorescent images, IA, SA, and IL of transient and stable HOS-ABC transfections. Images were taken at 4x magnification and scale bars represent 1000 µm. Box and whisker plots representing invasive area, spheroid area, and invasion length. All parameters were found to be significantly different difference transient and stably transfected spheroids ($p<0.05$).

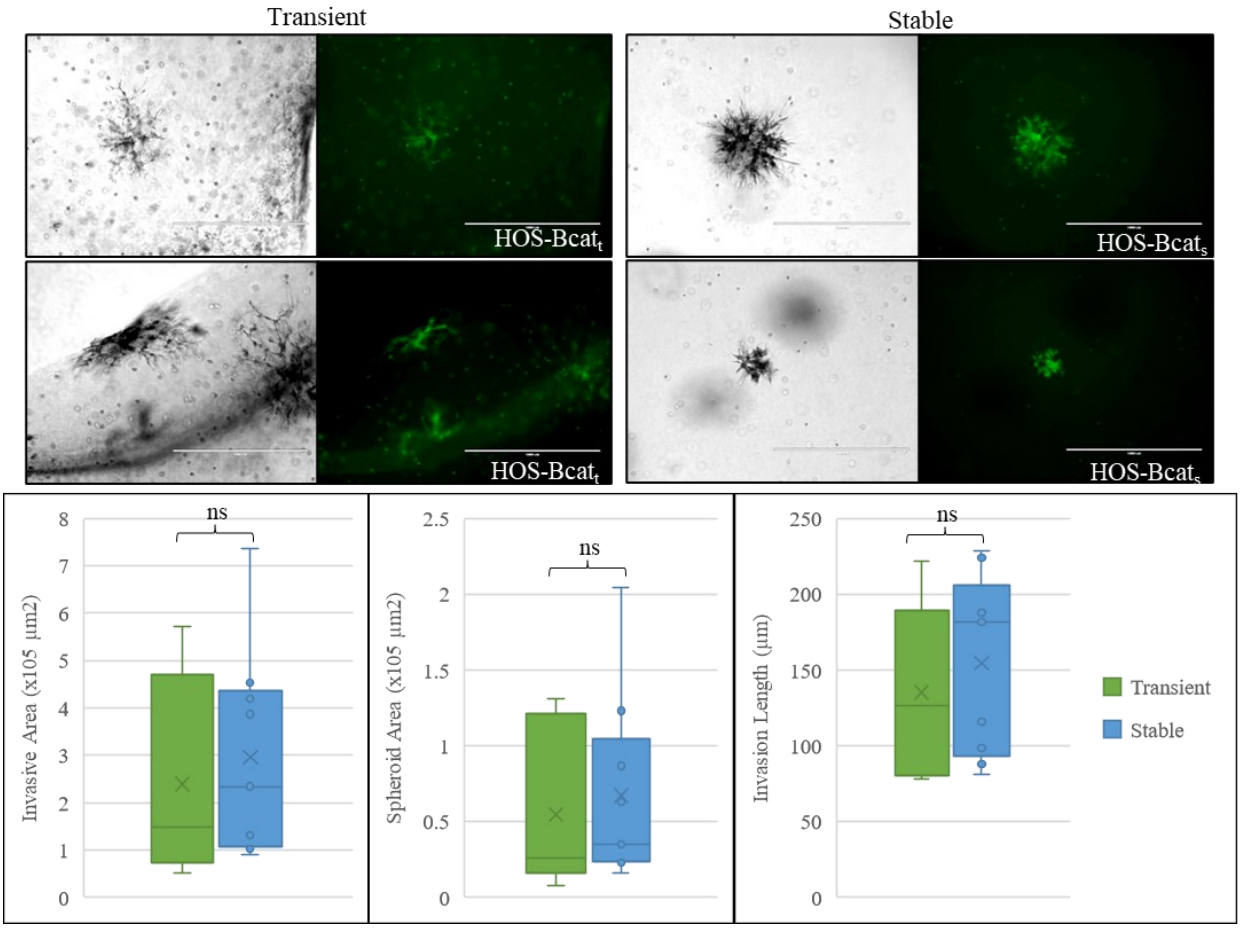

Figure 4.11 Representative brightfield and fluorescent images, IA, SA, and IL of transient and stable HOS-ABC transfections. Images were taken at 4x magnification and scale bars represent 1000 µm. Box and whisker plots representing invasive area, spheroid area, and invasion length. No significant difference was found in any parameters between transient and stably transfected spheroids ($p>0.05$).

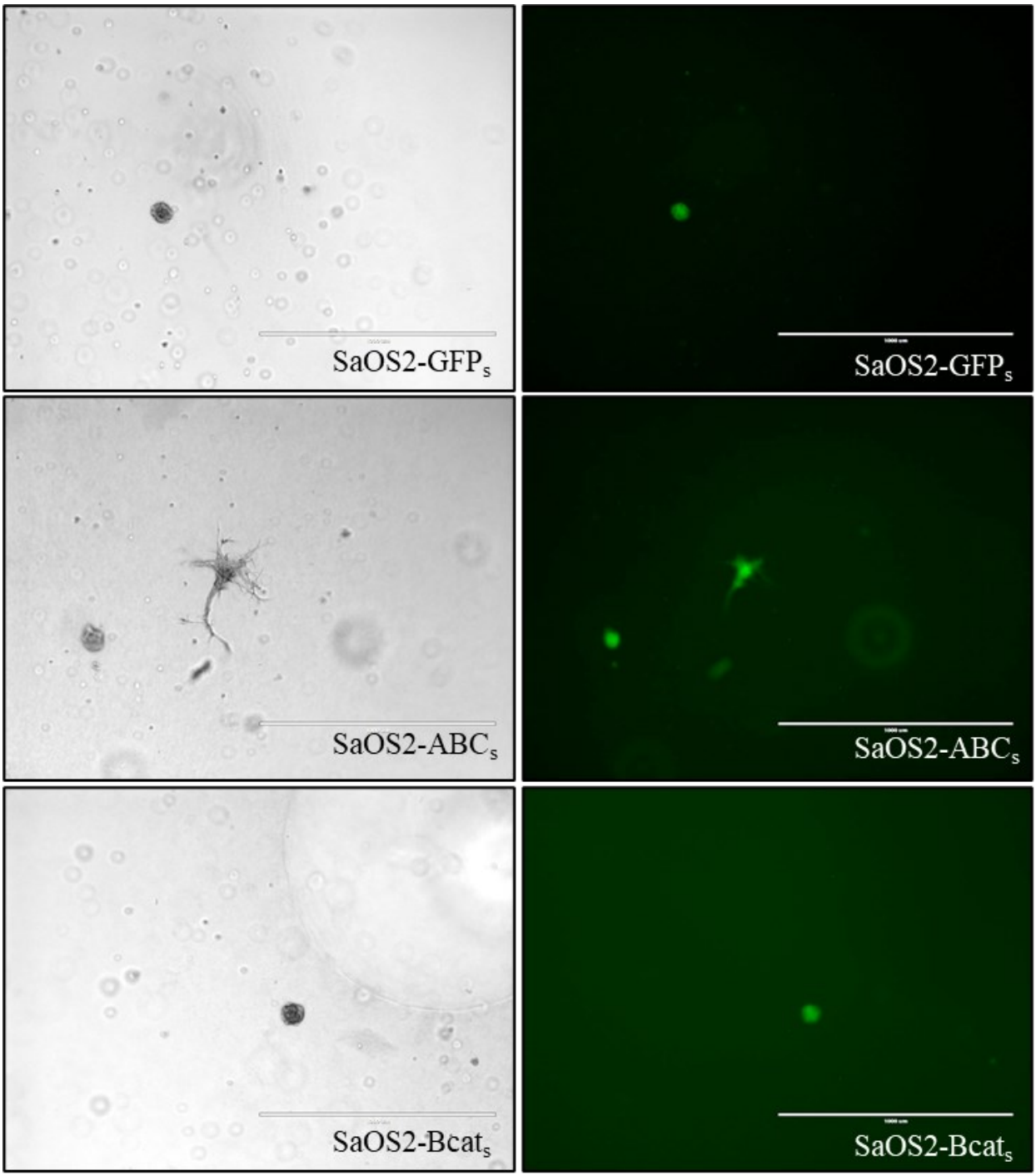

Figure 4.12 Representative brightfield and fluorescent images of spheroids generated from stably transfected SaOS-GFP, SaOS-ABC, and SaOS-βcat. Images were taken at 4x magnification and scale bars represent 1000 μm.

4.5 Spheroids generated from HOS cells overexpressing ABC or β- are similar in size and have a similar invasion length to negative controls

Given the significant differences in morphology between spheroids generated from stably transfected cells and those generated from transient transfections, values were not pooled for further analyses. To validate the use of HOS-GFP spheroids as a negative control, ANOVA testing was performed to detect any difference between the IA, SA and IL of spheroids generated from untransfected HOS, transiently transfected HOS-GFP, and stably transfected HOS-GFP. Table 4.2 demonstrates that the size and morphology of spheroids made from transiently transfected cells are similar to the untransfected parent cells whereas the stably tranfected spheroids had a significantly smaller invasion area and length ($p<0.05$) and trended toward a smaller SA ($p=0.06$). All further analysis was therefore performed only with the results of transient transfections for all cell lines.

Table 4.3 shows the effect of ABC and β-catenin transfection on the morphological characteristics of HOS spheroids. No significant difference was found in IA, SA, and IL of the different HOS transfectant lines (HOS-GFP, HOS-ABC, and HOS-βcat) compared to untransfected HOS.

Table 4.2 Mean invasion area, spheroid area, and invasion length of transient and stable GFP-transfected HOS cells (HOS-GFPt and HOS-GFPs, respectively) compared to untransfected HOS cells.

Cell Line	Invasion Area ($x10^4 \mu m^2$)	Spheroid Area ($x10^4 \mu m^2$)	Invasion Length (μm)
HOS	47.8 ± 37.6	16.6 ± 16.7	160.2 ± 54.0
$HOS\text{-}GFP_t$	31.7 ± 41.2	10.6 ± 15.6	124.6 ± 65.6
p	0.81	0.96	0.37
$HOS\text{-}GFP_s$	3.52 ± 2.84	0.99 ± 6.23	44.6 ± 29.7
p	**<0.05**	0.06	**<0.05**

Table 4.3 Mean invasion area, spheroid area, and invasion length of spheroids generated from untransfected HOS, HOS-GFP, HOS-ABC, and HOS βcat

Cell Line	Invasion Area ($x10^4 \mu m^2$)	Spheroid Area ($x10^4 \mu m^2$)	Invasion Length (μm)
HOS	47.8 ± 37.6	16.6 ± 16.7	160.2 ± 54.0
HOS-GFP	31.7 ± 41.2	10.6 ± 15.6	124.6 ± 65.6
HOS-ABC	46.4 ± 34.6	12.7 ± 11.0	175.9 ± 63.5
HOS-βcat	23.9 ± 21.3	54.8 ± 54.8	135.4 ± 56.1
p	0.44	0.41	0.20

Planned Western Blots for ABC, β-catenin, GFP, E-cadherin, and vimentin could not be performed on spheroids due to insufficient protein in the spheroid lysates.

4.6 Intratibial injection of SaOS2 and LM7 cells did not form primary or metastatic tumors

Technically successful intraosseous injection of cell suspension was achieved in 13 of 15 mice. One mouse died suddenly under anesthesia. Another underwent an apparently successful injection at the time of procedure but did not have any signs of knee trauma on microscopic examination after necropsy. The remainder of the mice had signs of successful intra-osseus injection on microscopic examination as demonstrated in Figure 4.13. However, no mouse in any group developed a primary tumor. There were no metastatic tumors in the lungs or liver tissues of the mice on gross and microscopic examination by a veterinary pathologist.

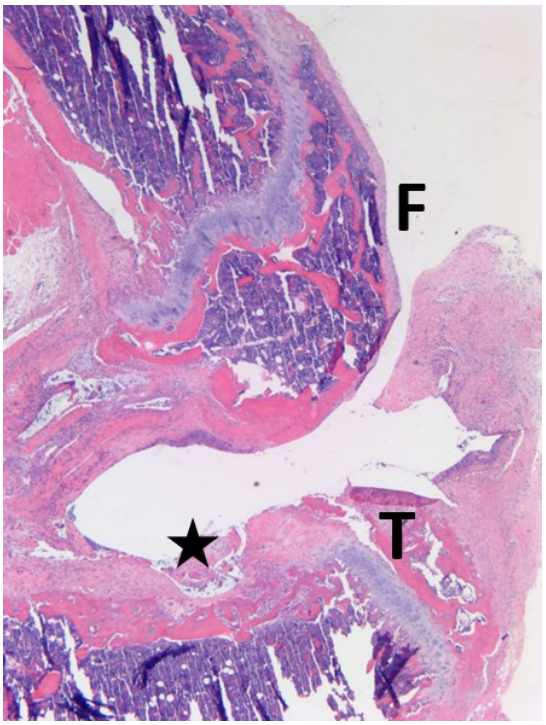

Figure 4.13 Sagittal cross-section of a mouse knee showing evidence of successful injection into the proximal tibia. F indicates the femur, T indicates the tibia, and the star marks focal cartilage damage consistent with a needle passing through the cartilage into the bone of the proximal tibia.

5 Discussion

This study explored the feasibility of 3D and *in vivo* modelling of OS to study the role of ABC in OS progression and metastasis. Previous work in our lab has demonstrated that higher levels of ABC correlate with clinical disease stage and that levels are higher in known metastatic cell lines compared to less aggressive parent lines[45]. We have further shown that the overexpression of ABC in HOS and SaOS2 increases colony formation and cellular invasion in 2D cell culture[297].

Consistent with these results, Fang *et al* identified elevated levels of ABC in multiple OS cell lines and found that *wnt* inhibition led to decreased OS proliferation, migration, and invasion *in vitro* in two OS cell lines, 143-B and SJSA-1[46]. While many investigators do not distinguish between ABC and β-catenin in their methods and results, multiple studies have found an increase in nuclear β-catenin in OS[44,45,298–301], which is most likely ABC. This supports the proposed role of ABC in OS that is distinct from β-catenin. In contrast, however, Cai *et al* examined 52 OS biopsy specimens via immunohistochemistry (IHC) and found that the majority of the samples lacked nuclear β-catenin[302], suggesting ABC levels and therefore *wnt* signalling patterns are not uniform across all OS tumors.

These previous results highlight a potential role for ABC as a prognostic factor in OS. Up to 28% of OS patients who have non-metastatic disease at diagnosis will develop metastases within 5 years[8], which significantly reduces overall survival[51]. The ability to identify individuals in this at-risk group could lead to changes in the approach to treatment or monitoring of these patients in order to minimize disease progression. ABC has also been identified as a potential therapeutic target in OS. ABC is the form of β-catenin that mediates signalling of the canonical *wnt* pathway[303]. This pathway is vital in the development and progression of many cancers including OS and is a popular target in the development of novel therapeutics[304]. Given the complex and ubiquitous role of *wnt* signalling throughout normal tissues, the safety of targeting this pathway has been called into question[305]. Despite this, multiple early phase clinical trials examining *wnt* inhibition have been undertaken or are currently underway[306]. This includes an investigation of the use of Tegavivint therapy for treatment-refractory solid tumors including osteosarcoma[307]. This medication blocks the association of β-catenin with transducing beta-like protein 1 (TBL1), an interaction necessary for the transcriptional regulation and tumorigenesis associated with this pathway[308].

One of the likely mechanisms by which increased ABC leads to OS progression and metastasis is via the epithelial to mesenchymal transition (EMT). EMT is a process by which cells with an epithelial phenotype take on the characteristics and cell-surface markers of mesenchymal cells, and is known to lead a greater migration, invasion, and metastasis[309]. The canonical *wnt* pathway is a well known and key activator of this process[310]. EMT is classically described for carcinomas—cancers originating from epithelial cells—and its relevance in sarcomas has been debated[83,84]. However, many studies have found that regulation of EMT in OS is associated with changes in cell behaviour consistent with a more invasive and metastatic phenotype[311]. Sannino *et al* have proposed that sarcoma tumors such as OS use the EMT pathways to acquire features of *both* epithelial and mesenchymal cells to promote both the initiation and establishment of metastases[83]. Activation of β-catenin is a key component of EMT regulation[312].

This study was the first to our knowledge that examined the role of ABC in OS in 3D cell culture, which allows the cells to organize and migrate in three dimensions rather than the traditional two-dimensional monolayer. This is a closer mimic to the cells' natural environment and is potentially vital for understanding the behaviours of mesenchymal cells such as those that form OS, which are less likely than epithelial cells to organize into discrete layers *in vivo*. 3D culture also allows for cancer cell organization into small tumoroids (spheroids). Depending on a cell's location within the spheroid, it may exhibit altered characteristics and may react differently to external stimuli. The complex interactions between cells within the spheroid play an important role in understanding cancer biology and studying therapeutic response or resistance. A benefit to our scaffold-based 3D culture model is that it provides extracellular proteins found in the tumor environment. Recent studies have also suggested adding hydroxyapatite to the scaffold for 3D OS models to mimic the unique environment found in bone tissue[313,314].

There are limitations to the 3D cell culture method. In addition to being more expensive, it is much more technically challenging and time consuming than 2D culture. The 3D cultures also lack associated cells and structures such as tumor-associated macrophages, blood vessels, and lymphatic vessels. While different co-culturing techniques have been developed in an attempt to replicate some of these conditions[48], *in vitro* techniques will never be a perfect mimic of the natural tumor environment.

Of all of the 3D scaffold solutions studied, growth in pure BMM resulted in the most discrete spheroids that would arguably be the easiest to study and to discern differences between conditions. However, the scaffold fully dissolved during fixation resulting in the loss of the majority of the spheroids in the washing solution as well as the loss of the orientation and any connections between cells of neighbouring spheroids. This issue has been previously reported with BMM scaffolds[315]. We therefore trialled different mixtures of BMM and neutralized collagen to develop a less fragile scaffold. Collagen scaffolds have been used to induce a more invasive spheroid phenotype than BMM[315], and this was supported by our observations that spheroids were larger and more branched as collagen concentration increased (Figure 4.6). To minimize this effect, we sought the lowest concentration of collagen in BMM that would withstand the fixation process at the appropriate time period, which was a 4:1 BMM-collagen mixture. This resulted in more reliable and reproducible experiments.

Despite this, there was a very wide range in the size and morphology of different spheroids within each cell line even when grown under the same conditions and contained within the same scaffold/well. This is exemplified by the wide standard deviations reported for the invasion areas and spheroid areas reported for every cell line. In the future, to improve the likelihood of finding significant results, this protocol would benefit from increased observances and potentially a size cut-off to determine which spheroids would qualify for analysis. For example, Tanaka *et al* classified OS spheroids grown for 7 days as having a diameter greater than or less than 300 μm and used this classification as an investigative tool[316].

Two recent reviews of 3D OS culture systems delineate dozens of different protocols including differing scaffolds, scaffold-free techniques, cell concentrations, culture conditions, and other technical considerations[48,317]. The ongoing investigations into such a wide variety of methods suggests there is still no method that has been identified as an ideal model that is economical, reliable, and reproducible.

In addition to the size variability of our spheroids, there were two other concerns with the 3D culture system. The first was that transfected SaOS2 cells did not form spheroids even after 10 days of incubation and regular media changes. SaOS2 is a more indolent cell line[318], and it is possible they were more susceptible than the HOS cells to the adverse effects of liposomal transfection, which includes cytotoxicity and slow growth in some cells even after transfection of

only an empty vector containing a fluoresce reporter[319], which was our negative control in this series of experiments. The second concern was the statistically smaller size of the spheroids formed from stably transfected HOS cells compared to transient transfections. Stably transfected cells and spheroids were maintained in culture containing geneticin, which is known to interfere with cellular growth and metabolism[319,320]. The spheroids formed for transiently transfected HOS cells in this study were persistently fluorescent at 2 weeks (Figures 4.10, 4.11, and 4.12), suggesting they continued to produce the target proteins despite being grown in our normal maintenance media rather than a selection media. The transient HOS-GFP cells formed spheroids similar in size to untransfected HOS, suggesting the transient transfection conditions did not alter the spheroid characteristics. Further investigations should therefore focus on spheroids generated from transient rather than stable HOS transfections.

Our study attempted to examine the role of ABC in OS metastasis *in vivo* in an orthotopic murine model via injection of a cell suspension in PBS into the proximal tibial metaphysis. This is a well-established method of studying OS[321–325]. Unfortunately, none of our mice developed primary or metastatic tumors, indicating there was likely a problem either with the mice, the technique, and/or the cell suspension.

We selected male adolescent mice with open physes as this represents the group most affected by OS[5]. However, we do note the cell lines used in our lab were originally derived from female patients. While we are not aware of any sex-specific characteristics of the cells, future use of female mice may optimize the tumour microenvironment. Given the deficiency of both innate and acquired immunity in NOD/SCID mice[326], they are unlikely to have mounted a host versus graft response to reject injected tumor cells. This could also be a potential drawback in a successful murine model as immune cells play a critical role in the OS tumor microenvironment[269,327].

The proximal tibia was selected as the injection site for multiple reasons. It is the second most common site for OS in humans[9], and the most common site for orthotopic OS xenograft reported in the literature[179,321–325,328–331]. PBS was similarly the most commonly reported cell vehicle. However, some authors have used cell suspensions in BMM or collagen[325,332]. The use of a protein-rich matrix such as these not only provide additional nutritive support for the cells while they are establishing a primary tumor, but the increased viscosity may help prevent extravasation of the cell suspension into the vasculature or surrounding soft tissues[325,332]. Conversely, higher

viscosity vehicles have also been associated with increased shear stress of injected cell solutions and decreased cell viability[333]. To reduce shear stress in our procedure, we utilized a low-viscosity vehicle (PBS) and a relatively large-bore 18-gauge needle.

With respect to the cells used for the *in vivo* experiments, SaOS2 was selected after careful consideration. While HOS is not as aggressive and metastatic as 143B, it is still a very locally aggressive cell line[318]. We felt that, compared to HOS/143B, the SaOS2/LM7 paired cell lines would have less potential for pain and disability caused to the animals. We also theorized that differences caused by the overexpression of ABC may be easier to detect from a more indolent baseline. The 3D cell culture and mouse studies were done simultaneously. At the time of cell injection, we were unaware that SaOS2 transfectants would not reliably form spheroids in 3D culture. Had we had these results at that time, we may have selected HOS cells for our orthotopic xenograft rather than SaOS2. However, the untransfected SaOS2 and LM7 cells also failed to form primary or metastatic tumors in our mice despite forming spheroids in 3D culture.

Many researchers have raised concerns about the effect of multiple passages on the reliability of results when working with cell lines[334–336]. LM7 cells had been recently thawed from a frozen low-passage vial. SaOS2 cells were purchased new and had been passaged fewer than four times prior to injection, which should reduce contamination and/or altered phenotype. Regardless, cells will be sent for characterization prior to performing any new animal experiments.

The aim of the mouse model is to study the effects of ABC overexpression on both primary tumor characteristics as well as the size and number of metastases. Some investigators contend that intra-osseous injection of tumor cells is not truly representative of spontaneous metastases as it could lead to the introduction of tumor cells directly into the circulatory system rather than from invasion of the primary tumor. This is based on the finding of pulmonary metastases that developed by 4 weeks following OS cell injection despite the injected limb being amputated within 30 minutes[337]. This time frame would not allow for the development of a primary tumor that then spontaneously metastasized to the lungs. However, this is disputed by the results of another group with a similar protocol whose mice only developed metastases if the limb was retained for more than 7 days[322]. We aimed to minimize the possible effect of this in our protocol by injecting a small volume of cells into the metaphyseal bone via a pre-drilled hole. Maloney *et al.* found the maximum volume that a mouse tibia could contain prior to extravasation into the soft tissues or

systemic circulation was 10 μL[337], which why we chose that volume for injection. However, we noted during the procedure that the 10 μL Hamilton syringe selected for precise injection in our protocol did not provide much tactile or visual feedback to confirm a successful injection. Future experiments would likely be done with a more traditional syringe and possibly a higher injection volume. While injection of more than 10 μL may provide direct seeding to the lungs, this is still a relevant model to study the establishment and growth of pulmonary metastases, especially considering the fact that some studies of OS metastases are done via direct vascular access through a tail vein injection[122,338,339]. The added advantage of the orthotopic model rather than tail vein injection is that it allows us to study both the primary and metastatic tumors and provides a more representative microenvironment for the primary tumor.

6 Conclusions and Future Directions

We were able to successfully culture spheroids of HOS cells overexpressing ABC and β-catenin. The continued overexpression of these proteins even after a week of culture was suggested by ongoing fluorescence but should be confirmed with Western Blot looking at ABC, β-catenin, and GFP levels and comparing these to freshly transfected cells. Unfortunately, we were unable to collect adequate protein from the spheroids in this study to carry out this confirmatory testing.

While our limited data did not show any differences in spheroids induced by the overexpression of ABC, the present investigations were focused on optimizing the 3D model. Now that the culture conditions have been established, further investigations are needed to explore the potential differences between cell lines. Specifically, we would like to acquire more accurate information on the effects of ABC and β-catenin overexpression on morphology via confocal microscopy of fixed spheroids. Cytoskeletal morphology and 3D architecture can be characterized through the staining of F-actin with phalloidin as seen in Figure 4.6. We would also like to visualize the EMT transformation by incubating fixed spheroids with immunofluorescent antibodies to key EMT markers such as E-cadherin, N-cadherin, and Vimentin.

Our *in vivo* model of OS was unsuccessful. Our next steps will be to perform a new pilot study using low-passage HOS cell lines, which we will first characterize to ensure they have not been contaminated or altered in some way from their baseline. We will continue to use an orthotopic model via intra-osseus injection but may explore the effects of distal femur injection, performing the procedure on both male and female mice, and using a BMM or collagen matrix for cell suspension. After ensuring the procedure is successful with all cell lines (including transfected cells), we will complete a full series of six animals per group to study the effects of ABC overexpression on OS tumorigenesis and metastasis *in vivo.*

To further validate the role of ABC in OS progression and metastasis, it will be important to elucidate the exact downstream targets of ABC transcriptional regulation that result in phenotypic changes, local invasion, and metastasis. We are currently in discussions with another group regarding a proteomic analysis to identify the most likely candidates.

To identify whether ABC or the *wnt* pathway are viable therapeutic targets, both *in vitro* (2D and 3D) and *in vivo* experiments would ideally be repeated with ABC knockdown and/or wnt inhibition. Additionally, human studies will need to be undertaken to evaluate whether our results are generalizable to multiple presentations of OS and whether ABC inhibition could be an effective treatment to prevent OS progression without causing overwhelming systemic side effects.

With respect to the role of ABC as a potential biomarker for OS metastasis, we are currently pursuing a study of paired biopsy and tumor specimens to validate a clinical role for ABC testing. A pilot study in our lab examining 30 specimens with immunohistochemistry targeting ABC has yielded promising results (not yet published), and we are set to receive additional samples to complete the study. This could eventually lead to the development of a test for tumor ABC levels at the time of OS diagnosis to identify patients at risk for metastasis and potentially modify treatment or surveillance for this group.

References

1. Mirabello, L., Troisi, R. J. & Savage, S. A. International osteosarcoma incidence patterns in children and adolescents, middle ages and elderly persons. *Int J Cancer* **125**, 229–234 (2009).

2. Rojas, G. A., Hubbard, A. K., Diessner, B. J., Ribeiro, K. B. & Spector, L. G. International trends in incidence of osteosarcoma (1988-2012). *Int J Cancer* **149**, 1044–1053 (2021).

3. Mirabello, L., Troisi, R. J. & Savage, S. A. Osteosarcoma incidence and survival rates from 1973 to 2004: Data from the surveillance, epidemiology, and end results program. *Cancer* **115**, 1531–1543 (2009).

4. Sadykova, L. R. *et al.* Epidemiology and Risk Factors of Osteosarcoma. *Cancer Invest* **38**, 259–269 (2020).

5. American Cancer Society. Key Statistics for Osteosarcoma. https://www.cancer.org/cancer/osteosarcoma/about/key-statistics.html (2020).

6. Smeland, S. *et al.* Survival and prognosis with osteosarcoma: outcomes in more than 2000 patients in the EURAMOS-1 (European and American Osteosarcoma Study) cohort. *Eur J Cancer* **109**, 36–50 (2019).

7. Marko, T. A., Diessner, B. J. & Spector, L. G. Prevalence of Metastasis at Diagnosis of Osteosarcoma: An International Comparison. *Pediatr Blood Cancer* **63**, 1006–1011 (2016).

8. Aljubran, A. H., Griffin, A., Pintilie, M. & Blackstein, M. Osteosarcoma in adolescents and adults: Survival analysis with and without lung metastases. *Annals of Oncology* **20**, 1136–1141 (2009).

9. Bielack, S. *et al.* Prognostic factors in high-grade osteosarcoma of the extremities of trunk: An analysis of 1,702 patients treated on neoadjuvant coperative osteosarcoma study group protocols. *Journal of Clinical Oncology* **20**, 776–790 (2002).

10. Beird, H. C. *et al.* Osteosarcoma. *Nat Rev Dis Primers* **8**, 77 (2022).

11. Alexander, J. H., Binitie, O. T., Letson, G. D. & Joyce, D. M. Osteosarcoma: An Evolving Understanding of a Complex Disease. *Journal of the American Academy of Orthopaedic Surgeons* **29**, e993–e1004 (2021).

12. Strauss, S. J. *et al.* Bone sarcomas: ESMO–EURACAN–GENTURIS–ERN PaedCan Clinical Practice Guideline for diagnosis, treatment and follow-up. *Annals of Oncology* **32**, 1520–1536 (2021).

13. Edge, S. B. & American Joint Committee on Cancer. *AJCC cancer staging manual.* (Springer, 2010).

14. Enneking, W. F. A System of Staging Musculoskeletal Neoplasms. *Clin Orthop Relat Res* **204**, 9–24 (1985).

15. Allison, D. C. *et al.* A meta-analysis of osteosarcoma outcomes in the modern medical era. *Sarcoma* vol. 2012 Preprint at https://doi.org/10.1155/2012/704872 (2012).

16. de Azevedo, J. W. V. *et al.* Biology and pathogenesis of human osteosarcoma (Review). *Oncology Letters* vol. 19 1099–1116 Preprint at https://doi.org/10.3892/ol.2019.11229 (2020).

17. Czarnecka, A. M. *et al.* Molecular biology of osteosarcoma. *Cancers* vol. 12 1–27 Preprint at https://doi.org/10.3390/cancers12082130 (2020).

18. Hameed, M. & Mandelker, D. Tumor Syndromes Predisposing to Osteosarcoma. *Advances in Anatomic Pathology* vol. 25 217–222 Preprint at https://doi.org/10.1097/PAP.0000000000000190 (2018).

19. Hansen, M. F., Seton, M. & Merchant, A. Osteosarcoma in Paget's disease of bone. *Journal of Bone and Mineral Research* **22**, (2007).

20. Sheng, G., Gao, Y., Yang, Y. & Wu, H. Osteosarcoma and Metastasis. *Frontiers in Oncology* vol. 11 Preprint at https://doi.org/10.3389/fonc.2021.780264 (2021).

21. Cui, J., Dean, D., Hornicek, F. J., Chen, Z. & Duan, Z. The role of extracelluar matrix in osteosarcoma progression and metastasis. *Journal of Experimental and Clinical Cancer Research* vol. 39 Preprint at https://doi.org/10.1186/s13046-020-01685-w (2020).

22. Felx, M. *et al.* Endothelin-1 (ET-1) promotes MMP-2 and MMP-9 induction involving the transcription factor NF-κB in human osteosarcoma. *Clin Sci* **110**, 645–654 (2006).

23. Frisch, S. & Francis, H. Disruption of epithelial cell-matrix interactions induces apoptosis. *Journal of Cell Biology* **124**, 619–626 (1994).

24. Broadhead, M. L., Clark, J. C. M., Myers, D. E., Dass, C. R. & Choong, P. F. M. The molecular pathogenesis of osteosarcoma: A review. *Sarcoma* vol. 2011 Preprint at https://doi.org/10.1155/2011/959248 (2011).

25. Berner, K. & Bruland, Ø. S. Prognostic impact of proximal versus distal localization in extremity long bone osteosarcomas. *Anticancer Res* **39**, 2459–2466 (2019).

26. Limmahakhun, S. *et al.* Relationships between serum biomarker levels and clinical presentation of human osteosarcomas. *Asian Pacific Journal of Cancer Prevention* **12**, 1717–1722 (2011).

27. Bacci, G. *et al.* Prognostic Significance of Serum Alkaline Phosphatase Measurements in Patients with Osteosarcoma Treated with Adjuvant or Neoadjuvant Chemotherapy. *Cancer* **71**, 1224–1230 (1993).

28. Han, J. *et al.* High serum alkaline phosphatase cooperating with MMP-9 predicts metastasis and poor prognosis in patients with primary osteosarcoma in Southern China. *World J Surg Oncol* **10**, (2012).

29. Bramer, J. A. M., van Linge, J. H., Grimer, R. J. & Scholten, R. J. P. M. Prognostic factors in localized extremity osteosarcoma: A systematic review. *European Journal of Surgical Oncology* vol. 35 1030–1036 Preprint at https://doi.org/10.1016/j.ejso.2009.01.011 (2009).

30. Chen, J., Sun, M. X., Hua, Y. Q. & Cai, Z. D. Prognostic significance of serum lactate dehydrogenase level in osteosarcoma: A meta-analysis. *J Cancer Res Clin Oncol* **140**, 1205–1210 (2014).

31. Liu, J. *et al.* Pretreatment Prediction of Relapse Risk in Patients with Osteosarcoma Using Radiomics Nomogram Based on CT: A Retrospective Multicenter Study. *Biomed Res Int* **2021**, (2021).

32. Zheng, J., Yuan, X. & Guo, W. Relationship between red cell distribution width and prognosis of patients with osteosarcoma. *Biosci Rep* **39**, (2019).

33. Yapar, A. *et al.* Diagnostic and Prognostic Role of Neutrophil/Lymphocyte Ratio, Platelet/Lymphocyte Ratio, and Lymphocyte/Monocyte Ratio in Patients with Osteosarcoma. *Jt Dis Relat Surg* **32**, 489–496 (2021).

34. Li, Y., Li, M., Wei, R. & Wu, J. Identification and Functional Analysis of EPOR+Tumor-Associated Macrophages in Human Osteosarcoma Lung Metastasis. *J Immunol Res* **2020**, (2020).

35. Chen, Y., Zhao, B. & Wang, X. Tumor infiltrating immune cells (TIICs) as a biomarker for prognosis benefits in patients with osteosarcoma. *BMC Cancer* **20**, (2020).

36. Liu, P., Xiao, Q., Zhou, B., Dai, Z. & Kang, Y. Prognostic Significance of Programmed Death Ligand 1 Expression and Tumor-Infiltrating Lymphocytes in Axial Osteosarcoma. *World Neurosurg* **129**, e240–e254 (2019).

37. Zhang, C. *et al.* Profiles of immune cell infiltration and immune-related genes in the tumor microenvironment of osteosarcoma. *Aging* **12**, 3486–3501 (2020).

38. Gusho, C. A. *et al.* The prognostic significance of lymphovascular tumor invasion in localized high-grade osteosarcoma: Outcomes of a single institution over 10 years. *J Surg Oncol* **123**, 1624–1632 (2021).

39. Tsuda, Y. *et al.* Is Microscopic Vascular Invasion in Tumor Specimens Associated with Worse Prognosis in Patients with High-grade Localized Osteosarcoma? *Clin Orthop Relat Res* **478**, 1190–1198 (2020).

40. MacDonald, B. T., Tamai, K. & He, X. Wnt/β-Catenin Signaling: Components, Mechanisms, and Diseases. *Developmental Cell* vol. 17 9–26 Preprint at https://doi.org/10.1016/j.devcel.2009.06.016 (2009).

41. Persad, A. *et al.* Active β-catenin is regulated by the PTEN/PI3 kinase pathway: a role for protein phosphatase PP2A. *Genes Cancer* **7**, 368–382 (2016).

42. Aoki, M., Sobek, V., Maslyar, D. J., Hecht, A. & Vogt, P. K. Oncogenic transformation by b-catenin: deletion analysis and characterization of selected target genes. *Oncogene* **21**, 6983–6991 (2002).

43. Haydon, R. C. *et al.* Cytoplasmic and/or nuclear accumulation of the β-catenin protein is a frequent event in human osteosarcoma. *Int J Cancer* **102**, 338–342 (2002).

44. Iwaya, K. *et al. Cytoplasmic and/or nuclear staining of beta-catenin is associated with lung metastasis*. *Clinical & Experimental Metastasis* vol. 20 (2003).

45. Ali, N. *et al.* Osteosarcoma progression is associated with increased nuclear levels and transcriptional activity of activated β-Catenin. *Genes Cancer* **10**, 63–79 (2019).

46. Fang, F. *et al. Targeting the Wnt/β-catenin pathway in human osteosarcoma cells*. *Oncotarget* vol. 9 www.oncotarget.comwww.oncotarget.com (2018).

47. Monteiro, C. F., Custódio, C. A. & Mano, J. F. Three-Dimensional Osteosarcoma Models for Advancing Drug Discovery and Development. *Advanced Therapeutics* vol. 2 Preprint at https://doi.org/10.1002/adtp.201800108 (2019).

48. De Luca, A. *et al.* Relevance of 3d culture systems to study osteosarcoma environment. *Journal of Experimental and Clinical Cancer Research* vol. 37 Preprint at https://doi.org/10.1186/s13046-017-0663-5 (2018).

49. Bassi, G. *et al.* Scaffold-based 3D cellular models mimicking the heterogeneity of osteosarcoma stem cell niche. *Sci Rep* **10**, (2020).

50. Uluçkan, Ö., Segaliny, A., Botter, S., Santiago, J. M. & Mutsaers, A. J. Preclinical mouse models of osteosarcoma. *Bonekey Rep* **4**, (2015).

51. American Cancer Society. Survival rates for osteosarcoma. https://www.cancer.org/cancer/osteosarcoma/detection-diagnosis-staging/survival-rates.html (2021).

52. Cole, S., Gianferante, D. M., Zhu, B. & Mirabello, L. Osteosarcoma: A Surveillance, Epidemiology, and End Results program-based analysis from 1975 to 2017. *Cancer* **128**, 2107–2118 (2022).

53. Brabletz, S., Schuhwerk, H., Brabletz, T. & Stemmler, M. P. Dynamic EMT: a multi-tool for tumor progression. *EMBO J* **40**, (2021).

54. Dongre, A. & Weinberg, R. A. New insights into the mechanisms of epithelial–mesenchymal transition and implications for cancer. *Nat Rev Mol Cell Biol* **20**, 69–84 (2019).

55. Zheng, X. *et al.* Epithelial-to-mesenchymal transition is dispensable for metastasis but induces chemoresistance in pancreatic cancer. *Nature* **527**, 525–530 (2015).

56. Fischer, K. R. *et al.* Epithelial-to-mesenchymal transition is not required for lung metastasis but contributes to chemoresistance. *Nature* **527**, 472–476 (2015).

57. Lourenco, A. R. *et al.* Differential contributions of pre- And post-EMT tumor cells in breast cancer metastasis. *Cancer Res* **80**, 163–169 (2020).

58. Morikawa, M., Derynck, R. & Miyazono, K. TGF- β and the TGF-β family: Context-dependent roles in cell and tissue physiology. *Cold Spring Harbor Perspectives in Biology* vol. 8 Preprint at https://doi.org/10.1101/cshperspect.a021873 (2016).

59. Grande, M. T. *et al.* Snail1-induced partial epithelial-to-mesenchymal transition drives renal fibrosis in mice and can be targeted to reverse established disease. *Nat Med* **21**, 989–97 (2015).

60. Dhasarathy, A., Phadke, D., Mav, D., Shah, R. R. & Wade, P. A. The Transcription Factors Snail and Slug Activate the Transforming Growth Factor-Beta Signaling Pathway in Breast Cancer. *PLoS One* **6**, e26514 (2011).

61. Lamouille, S., Xu, J. & Derynck, R. Molecular mechanisms of epithelial–mesenchymal transition. *Nat Rev Mol Cell Biol* **15**, 178–196 (2014).

62. Clevers, H. Wnt/β-Catenin Signaling in Development and Disease. *Cell* **127**, 469–480 (2006).

63. Wu, Y. *et al.* Expression of Wnt3 Activates Wnt/β-Catenin Pathway and Promotes EMT-like Phenotype in Trastuzumab-Resistant HER2-Overexpressing Breast Cancer Cells. *Molecular Cancer Research* **10**, 1597–1606 (2012).

64. Stemmer, V., De Craene, B., Berx, G. & Behrens, J. Snail promotes Wnt target gene expression and interacts with β-catenin. *Oncogene* **27**, 5075–5080 (2008).

65. Gauger, K. J., Chenausky, K. L., Murray, M. E. & Schneider, S. S. SFRP1 reduction results in an increased sensitivity to TGF-β signaling. *BMC Cancer* **11**, 59 (2011).

66. Balsamo, J., Arregui, C., Leung, T. & Lilien, J. The Nonreceptor Protein Tyrosine Phosphatase PTP1B Binds to the Cytoplasmic Domain of N-Cadherin and Regulates the Cadherin–Actin Linkage. *Journal of Cell Biology* **143**, 523–532 (1998).

67. Misiorek, J. O. *et al.* Context matters: Notch signatures and pathway in cancer progression and metastasis. *Cells* vol. 10 1–32 Preprint at https://doi.org/10.3390/cells10010094 (2021).

68. Natsuizaka, M. *et al.* Interplay between Notch1 and Notch3 promotes EMT and tumor initiation in squamous cell carcinoma. *Nat Commun* **8**, (2017).

69. Timmerman, L. A. *et al.* Notch promotes epithelial-mesenchymal transition during cardiac development and oncogenic transformation. *Genes Dev* **18**, 99–115 (2004).

70. Matsuno, Y., Coelho, A. L., Jarai, G., Westwick, J. & Hogaboam, C. M. Notch signaling mediates TGF-β1-induced epithelial-mesenchymal transition through the induction of Snai1. *International Journal of Biochemistry and Cell Biology* **44**, 776–789 (2012).

71. Zavadil, J., Cermak, L., Soto-Nieves, N. & Böttinger, E. P. Integration of TGF-β/Smad and Jagged1/Notch signalling in epithelial-to-mesenchymal transition. *EMBO J* **23**, 1155–1165 (2004).

72. Di Domenico, M. & Giordano, A. Signal transduction growth factors: the effective governance of transcription and cellular adhesion in cancer invasion. *Oncotarget* **8**, 36869–36884 (2017).

73. Pottier, C. *et al.* Tyrosine kinase inhibitors in cancer: Breakthrough and challenges of targeted therapy. *Cancers* vol. 12 Preprint at https://doi.org/10.3390/cancers12030731 (2020).

74. Maehara, O. *et al.* Fibroblast growth factor-2-mediated FGFR/Erk signaling supports maintenance of cancer stem-like cells in esophageal squamous cell carcinoma. *Carcinogenesis* **38**, 1073–1083 (2017).

75. Tashiro, E., Henmi, S., Odake, H., Ino, S. & Imoto, M. Involvement of the MEK/ERK pathway in EGF-induced E-cadherin down-regulation. *Biochem Biophys Res Commun* **477**, 801–806 (2016).

76. Lo, H.-W. *et al.* Epidermal Growth Factor Receptor Cooperates with Signal Transducer and Activator of Transcription 3 to Induce Epithelial-Mesenchymal Transition in Cancer Cells via Up-regulation of *TWIST* Gene Expression. *Cancer Res* **67**, 9066–9076 (2007).

77. Uttamsingh, S. *et al.* Synergistic effect between EGF and TGF-β1 in inducing oncogenic properties of intestinal epithelial cells. *Oncogene* **27**, 2626–2634 (2008).

78. Kim, J., Kong, J., Chang, H., Kim, H. & Kim, A. EGF induces epithelial-mesenchymal transition through phospho-Smad2/3-Snail signaling pathway in breast cancer cells. *Oncotarget* **7**, 85021–85032 (2016).

79. Vichalkovski, A., Gresko, E., Hess, D., Restuccia, D. F. & Hemmings, B. A. PKB/AKT phosphorylation of the transcription factor Twist-1 at Ser42 inhibits p53 activity in response to DNA damage. *Oncogene* **29**, 3554–3565 (2010).

80. Hong, K. O. *et al.* Inhibition of Akt activity induces the mesenchymal-to-epithelial reverting transition with restoring E-cadherin expression in KB and KOSCC-25B oral squamous cell carcinoma cells. *Journal of Experimental and Clinical Cancer Research* **28**, (2009).

81. Grotegut, S., von Schweinitz, D., Christofori, G. & Lehembre, F. Hepatocyte growth factor induces cell scattering through MAPK/Egr-1-mediated upregulation of Snail. *EMBO J* **25**, 3534–3545 (2006).

82. Ogunwobi, O. O., Puszyk, W., Dong, H.-J. & Liu, C. Epigenetic Upregulation of HGF and c-Met Drives Metastasis in Hepatocellular Carcinoma. *PLoS One* **8**, e63765 (2013).

83. Sannino, G., Marchetto, A., Kirchner, T. & Grünewald, T. G. P. Epithelial-to-Mesenchymal and Mesenchymal-to-Epithelial Transition in Mesenchymal Tumors: A Paradox in Sarcomas? *Cancer Res* **77**, 4556–4561 (2017).

84. Kahlert, U. D., Joseph, J. V. & Kruyt, F. A. E. EMT- and MET-related processes in nonepithelial tumors: importance for disease progression, prognosis, and therapeutic opportunities. *Molecular Oncology* vol. 11 860–877 Preprint at https://doi.org/10.1002/1878-0261.12085 (2017).

85. Sato, H., Hasegawa, T., Abe, Y., Sakai, H. & Hirohashi, S. Expression of E-Cadherin in Bone and Soft Tissue Sarcomas: A Possible Role in Epithelial Differentiation. *Hum Pathol* **30**, 1344–1349 (1999).

86. Yin, K., Liao, Q., He, H. & Zhong, D. Prognostic value of Twist and E-cadherin in patients with osteosarcoma. *Medical Oncology* **29**, 3449–3455 (2012).

87. Sung, J. Y. *et al.* Interferon consensus sequence-binding protein (ICSBP) promotes epithelial-to-mesenchymal transition (EMT)-like phenomena, cell-motility, and invasion via TGF-β signaling in U2OS cells. *Cell Death Dis* **5**, (2014).

88. Cheng, G. *et al.* Visfatin promotes osteosarcoma cell migration and invasion via induction of epithelial-mesenchymal transition. *Oncol Rep* **34**, 987–994 (2015).

89. Cheng, Z. *et al.* Nitidine chloride suppresses epithelial-to-mesenchymal transition in osteosarcoma cell migration and invasion through Akt/GSK-3β/Snail signaling pathway. *Oncol Rep* **36**, 1023–1029 (2016).

90. Ru, N. *et al.* SPRY4 Intronic Transcript 1 Promotes Epithelial-Mesenchymal Transition Through Association with Snail1 in Osteosarcoma. *DNA Cell Biol* **35**, 290–295 (2016).

91. Feng, Z. M. & Guo, S. M. Tim-3 facilitates osteosarcoma proliferation and metastasis through the NF-κB pathway and epithelial-mesenchymal transition. *Genetics and Molecular Research* **15**, (2016).

92. Lv, Y. fan *et al.* Downregulation of tumor suppressing STF cDNA 3 promotes epithelial-mesenchymal transition and tumor metastasis of osteosarcoma by the Wnt/GSK-3β/β-catenin/Snail signaling pathway. *Cancer Lett* **373**, 164–173 (2016).

93. Chen, Y., Zhang, K., Li, Y. & He, Q. Estrogen-related receptor α participates transforming growth factor-β (TGF-β) induced epithelial-mesenchymal transition of osteosarcoma cells. *Cell Adh Migr* **11**, 338–346 (2017).

94. Zhang, Z., Zhang, M., Chen, Q. & Zhang, Q. Downregulation of microRNA-145 promotes epithelial-mesenchymal transition via regulating Snail in osteosarcoma. *Cancer Gene Ther* **24**, 83–88 (2017).

95. Kong, G. *et al.* Irisin reverses the IL-6 induced epithelial-mesenchymal transition in osteosarcoma cell migration and invasion through the STAT3/Snail signaling pathway. *Oncol Rep* **38**, 2647–2656 (2017).

96. Qiu, M. *et al.* Sex-determining region Y-box protein 3 induces epithelial-mesenchymal transition in osteosarcoma cells via transcriptional activation of Snail1. *J Exp Clin Cancer Res* **36**, 46 (2017).

97. Zhang, D. & Liu, S. SOX5 promotes epithelial-mesenchymal transition in osteosarcoma via regulation of Snail. *Journal of the Balkan Union of Oncology* **22**, 258–264 (2017).

98. Wang, Z., Chen, X., Zhao, Y., Jin, Y. & Zheng, J. G-protein-coupled estrogen receptor suppresses the migration of osteosarcoma cells via post-translational regulation of Snail. *J Cancer Res Clin Oncol* **145**, 87–96 (2019).

99. Chen, Y. *et al.* Melatonin suppresses epithelial-to-mesenchymal transition in the MG-63 cell line. *Mol Med Rep* **21**, 1356–1364 (2020).

100. Wen, J. F. *et al.* LncRNA-XIST promotes the oxidative stress-induced migration, invasion, and epithelial-to-mesenchymal transition of osteosarcoma cancer cells through miR-153-SNAI1 axis. *Cell Biol Int* **44**, 1991–2001 (2020).

101. Sun, Y. *et al.* Oridonin prevents epithelial-mesenchymal transition and TGF-β1-induced epithelial-mesenchymal transition by inhibiting TGF-β1/Smad2/3 in osteosarcoma. *Chem Biol Interact* **296**, 57–64 (2018).

102. Sharili, A. S., Allen, S., Smith, K., Price, J. & McGonnell, I. M. Snail2 promotes osteosarcoma cell motility through remodelling of the actin cytoskeleton and regulates tumor development. *Cancer Lett* **333**, 170–179 (2013).

103. Ishikawa, T. *et al.* Twist2 functions as a tumor suppressor in murine osteosarcoma cells. *Cancer Sci* **104**, 880–888 (2013).

104. Hou, C. H., Lin, F. L., Hou, S. M. & Liu, J. F. Cyr61 promotes epithelial-mesenchymal transition and tumor metastasis of osteosarcoma by Raf-1/MEK/ERK/Elk-1/TWIST-1 signaling pathway. *Mol Cancer* **13**, (2014).

105. Wang, Z., Li, J., Li, K. & Xu, J. SOX6 is downregulated in osteosarcoma and suppresses the migration, invasion and epithelial-mesenchymal transition via TWIST1 regulation. *Mol Med Rep* **17**, 6803–6811 (2018).

106. Shi, D. *et al.* LncRNA AFAP1-AS1 promotes tumorigenesis and epithelial-mesenchymal transition of osteosarcoma through RhoC/ROCK1/p38MAPK/Twist1 signaling pathway. *Journal of Experimental and Clinical Cancer Research* **38**, (2019).

107. Yu, X. J. *et al.* SIRT1-ZEB1-positive feedback promotes epithelial-mesenchymal transition process and metastasis of osteosarcoma. *J Cell Biochem* **120**, 3727–3735 (2019).

108. Feng, T. *et al.* The microRNA-708-5p/ZEB1/EMT axis mediates the metastatic potential of osteosarcoma. *Oncol Rep* **43**, 491–502 (2020).

109. Yao, H. *et al.* LncRNA SPRY4-IT1 promotes progression of osteosarcoma by regulating ZEB1 and ZEB2 expression through sponging of miR-101 activity. *Int J Oncol* **56**, 85–100 (2020).

110. Shen, A., Zhang, Y., Yang, H., Xu, R. & Huang, G. Overexpression of ZEB1 relates to metastasis and invasion in osteosarcoma. *J Surg Oncol* **105**, 830–834 (2012).

111. Verrecchia, F. & Rédini, F. Transforming growth factor-β signaling plays a pivotal role in the interplay between osteosarcoma cells and their microenvironment. *Frontiers in Oncology* vol. 8 Preprint at https://doi.org/10.3389/fonc.2018.00133 (2018).

112. Lin, C. Y. *et al.* Reduction of invasion and cell stemness and induction of apoptotic cell death by Cinnamomum cassia extracts on human osteosarcoma cells. *Environ Toxicol* **37**, 1261–1274 (2022).

113. He, D. *et al.* TGF-β inhibitor RepSox suppresses osteosarcoma via the JNK/Smad3 signaling pathway. *Int J Oncol* **59**, (2021).

114. Ma, K., Zhang, C. & Li, W. Gamabufotalin suppressed osteosarcoma stem cells through the TGF-β/periostin/PI3K/AKT pathway. *Chem Biol Interact* **331**, (2020).

115. Jiang, X. *et al.* Glaucocalyxin A reverses EMT and TGF-β1-induced EMT by inhibiting TGF-β1/Smad2/3 signaling pathway in osteosarcoma. *Chem Biol Interact* **307**, 158–166 (2019).

116. Dong, F., Liu, T., Jin, H. & Wang, W. Chimaphilin inhibits human osteosarcoma cell invasion and metastasis through suppressing the TGF-β1-induced epithelial-to-mesenchymal transition markers via PI-3K/Akt, ERK1/2, and Smad signaling pathways. *Can J Physiol Pharmacol* **96**, 1–7 (2018).

117. Wang, Y. *et al.* Baicalin inhibits human osteosarcoma cells invasion, metastasis, and anoikis resistance by suppressing the transforming growth factor-β1-induced epithelial-to-mesenchymal transition. *Anticancer Drugs* **28**, 581–587 (2017).

118. Kang, H. M. *et al.* Delphinidin induces apoptosis and inhibits epithelial-to-mesenchymal transition via the ERK/p38 MAPK-signaling pathway in human osteosarcoma cell lines. *Environ Toxicol* **33**, 640–649 (2018).

119. Xie, C. *et al.* miR-19 Promotes Cell Proliferation, Invasion, Migration, and EMT by Inhibiting SPRED2-mediated Autophagy in Osteosarcoma Cells. *Cell Transplant* **29**, (2020).

120. Raimondi, L. *et al.* Potential Anti-Metastatic Role of the Novel miR-CT3 in Tumor Angiogenesis and Osteosarcoma Invasion. *Int J Mol Sci* **23**, (2022).

121. Wang, Z. *et al.* E2F1 silencing inhibits migration and invasion of osteosarcoma cells via regulating DDR1 expression. *Int J Oncol* **51**, 1639–1650 (2017).

122. Zheng, B. *et al.* VEGFR2 Promotes Metastasis and PD-L2 Expression of Human Osteosarcoma Cells by Activating the STAT3 and RhoA-ROCK-LIMK2 Pathways. *Front Oncol* **10**, (2020).

123. Han, Y. *et al.* Tumor-associated macrophages promote lung metastasis and induce epithelial-mesenchymal transition in osteosarcoma by activating the COX-2/STAT3 axis. *Cancer Lett* **440–441**, 116–125 (2019).

124. Huang, H. *et al.* ML264 inhibits osteosarcoma growth and metastasis via inhibition of JAK2/STAT3 and WNT/β-catenin signalling pathways. *J Cell Mol Med* **24**, 5652–5664 (2020).

125. Hu, Y. *et al.* Piperlongumine inhibits the progression of osteosarcoma by downregulating the SOCS3/JAK2/STAT3 pathway via miR-30d-5p. *Life Sci* **277**, (2021).

126. Zhang, J. *et al.* The role of Notch ligand Jagged1 in osteosarcoma proliferation, metastasis, and recurrence. *J Orthop Surg Res* **16**, (2021).

127. Yu, L. *et al.* The notch pathway promotes osteosarcoma progression through activation of ephrin reverse signaling. *Molecular Cancer Research* **17**, 2383–2394 (2019).

128. Li, Z., Tang, Y., Xing, W., Dong, W. & Wang, Z. LncRNA, CRNDE promotes osteosarcoma cell proliferation, invasion and migration by regulating Notch1 signaling and epithelial-mesenchymal transition. *Exp Mol Pathol* **104**, 19–25 (2018).

129. Deng, Y., Zhao, F., Zhang, Z., Sun, F. & Wang, M. Long Noncoding RNA SNHG7 Promotes the Tumor Growth and Epithelial-to-Mesenchymal Transition via Regulation of miR-34a Signals in Osteosarcoma. *Cancer Biother Radiopharm* **33**, 365–372 (2018).

130. Dai, G., Liu, G., Zheng, D. & Song, Q. Inhibition of the Notch signaling pathway attenuates progression of cell motility, metastasis, and epithelial-to-mesenchymal transition-like phenomena induced by low concentrations of cisplatin in osteosarcoma. *Eur J Pharmacol* **899**, (2021).

131. Wang, S. *et al.* Fibulin-3 promotes osteosarcoma invasion and metastasis by inducing epithelial to mesenchymal transition and activating the Wnt/β-catenin signaling pathway. *Sci Rep* **7**, (2017).

132. Cao, J., Han, X., Qi, X., Jin, X. & Li, X. TUG1 promotes osteosarcoma tumorigenesis by upregulating EZH2 expression via MIR-144-3p. *Int J Oncol* **51**, 1115–1123 (2017).

133. Zhang, M., Wang, D., Zhu, T. & Yin, R. RASSF4 overexpression inhibits the proliferation, invasion, EMT, and wnt signaling pathway in osteosarcoma cells. *Oncol Res* **25**, 83–91 (2017).

134. Yu, M., Guo, D., Cao, Z., Xiao, L. & Wang, G. Inhibitory Effect of MicroRNA-107 on Osteosarcoma Malignancy Through Regulation of Wnt/β-catenin Signaling in Vitro. *Cancer Invest* **36**, 175–184 (2018).

135. Tian, H. *et al.* Bone morphogenetic protein-2 promotes osteosarcoma growth by promoting epithelial-mesenchymal transition (EMT) through the Wnt/β-catenin signaling pathway. *Journal of Orthopaedic Research* **37**, 1638–1648 (2019).

136. Fan, S., Gao, X., Chen, P. & Li, X. Carboxypeptidase E-ΔN promotes migration, invasiveness, and epithelial-mesenchymal transition of human osteosarcoma cells via the Wnt-β-catenin pathway. *Biochemistry and Cell Biology* **97**, 446–453 (2019).

137. Chen, X. *et al.* Down-regulation of microRNA-31-5p inhibits proliferation and invasion of osteosarcoma cells through Wnt/β-catenin signaling pathway by enhancing AXIN1. *Exp Mol Pathol* **108**, 32–41 (2019).

138. Liu, Q. *et al.* miR-342-5p inhibits osteosarcoma cell growth, migration, invasion, and sensitivity to Doxorubicin through targeting Wnt7b. *Cell Cycle* **18**, 3325–3336 (2019).

139. Zeng, Q. *et al.* Ubiquitin-specific protease 7 promotes osteosarcoma cell metastasis by inducing epithelial-mesenchymal transition. *Oncol Rep* **41**, 543–551 (2019).

140. Ding, Q. *et al.* LncRNA CRNDE is activated by SP1 and promotes osteosarcoma proliferation, invasion, and epithelial-mesenchymal transition via Wnt/β-catenin signaling pathway. *J Cell Biochem* **121**, 3358–3371 (2020).

141. Chen, X., Zhao, W. & Fan, W. Long non-coding RNA GHET1 promotes osteosarcoma development and progression via Wnt/β-catenin signaling pathway. *Oncol Rep* **44**, 349–359 (2020).

142. Yi, Z. *et al.* Silencing of RIPK4 inhibits epithelial-mesenchymal transition by inactivating the Wnt/β-catenin signaling pathway in osteosarcoma. *Mol Med Rep* **21**, 1154–1162 (2020).

143. Wang, H. & Zhang, P. lncRNA-CASC15 promotes osteosarcoma proliferation and metastasis by regulating epithelial-mesenchymal transition via the Wnt/β-catenin signaling pathway. *Oncol Rep* **45**, (2021).

144. Liang, K. *et al.* microRNA-377-3p inhibits osteosarcoma progression by targeting CUL1 and regulating Wnt/β-catenin signaling pathway. *Clinical and Translational Oncology* **23**, 2350–2357 (2021).

145. Zhang, H., Zhou, Q. & Shen, W. Circ-FOXM1 promotes the proliferation, migration and EMT process of osteosarcoma cells through FOXM1-mediated Wnt pathway activation. *J Orthop Surg Res* **17**, 344 (2022).

146. Bi, W., Yang, M., Xing, P. & Huang, T. MicroRNA miR-331-3p suppresses osteosarcoma progression via the Bcl-2/Bax and Wnt/β-Catenin signaling pathways and the epithelial-mesenchymal transition by targeting N-acetylglucosaminyltransferase I (MGAT1). *Bioengineered* **13**, 14159–14174 (2022).

147. Singla, A. *et al.* Wnt Signaling in Osteosarcoma. in *Current Advances in Osteosarcoma* (ed. Kleinerman, E. S.) 125–139 (Springer, 2020).

148. Zhang, D. *et al.* Fibulin-4 promotes osteosarcoma invasion and metastasis by inducing epithelial to mesenchymal transition via the PI3K/Akt/mTOR pathway. *Int J Oncol* **50**, 1513–1530 (2017).

149. Zhang, X., Qu, P., Zhao, H., Zhao, T. & Cao, N. COX-2 promotes epithelial-mesenchymal transition and migration in osteosarcoma MG-63 cells via PI3K/AKT/NF-κB signaling. *Mol Med Rep* **20**, 3811–3819 (2019).

150. Zhang, Y., Cheng, H., Li, W., Wu, H. & Yang, Y. Highly-expressed P2X7 receptor promotes growth and metastasis of human HOS/MNNG osteosarcoma cells via PI3K/Akt/GSK3β/β-catenin and mTOR/HIF1α/VEGF signaling. *Int J Cancer* **145**, 1068–1082 (2019).

151. Wang, S., Zhao, G., Zhao, S., Qiao, Y. & Yang, H. The effects of interleukin-33 (IL-33) on osteosarcoma cell viability, apoptosis, and epithelial-mesenchymal transition are mediated through the PI3K/AKT pathway. *Medical Science Monitor* **26**, (2020).

152. Liu, W. *et al.* miR-210-5p promotes epithelial–mesenchymal transition by inhibiting PIK3R5 thereby activating oncogenic autophagy in osteosarcoma cells. *Cell Death Dis* **11**, (2020).

153. Lu, D.-G. *et al.* Targeting EZH2 by microRNA-449a inhibits osteosarcoma cell proliferation, invasion and migration via regulation of PI3K/AKT signaling pathway and epithelial-mesenchymal transition. *Eur Rev Med Pharmacol Sci* **24**, 1656–1665 (2020).

154. Xing, S. *et al.* Down-regulation of PDGFRβ suppresses invasion and migration in osteosarcoma cells by influencing epithelial–mesenchymal transition. *FEBS Open Bio* **10**, 1748–1757 (2020).

155. Wang, X. *et al.* Neuropilin and tolloid-like 2 regulates the progression of osteosarcoma. *Gene* **768**, (2021).

156. Zheng, J., Liu, C., Shi, J., Wen, K. & Wang, X. AIM2 inhibits the proliferation, invasion and migration, and promotes the apoptosis of osteosarcoma cells by inactivating the PI3K/AKT/mTOR signaling pathway. *Mol Med Rep* **25**, (2022).

157. Lu, K. H. *et al.* 3-Hydroxyflavone inhibits human osteosarcoma U2OS and 143B cells metastasis by affecting EMT and repressing u-PA/MMP-2 via FAK-Src to MEK/ERK and RhoA/MLC2 pathways and reduces 143B tumor growth in vivo. *Food and Chemical Toxicology* **97**, 177–186 (2016).

158. Zhang, F. *et al.* Novel oncogene COPS3 interacts with Beclin1 and Raf-1 to regulate metastasis of osteosarcoma through autophagy. *Journal of Experimental and Clinical Cancer Research* **37**, (2018).

159. Lv, D.-B. *et al.* MicroRNA-765 targets MTUS1 to promote the progression of osteosarcoma via mediating ERK/EMT pathway. *Eur Rev Med Pharmacol Sci* **23**, 4618–4628 (2019).

160. Lin, H., Hao, Y., Wan, X., He, J. & Tong, Y. Baicalein inhibits cell development, metastasis and EMT and induces apoptosis by regulating ERK signaling pathway in osteosarcoma. *Journal of Receptors and Signal Transduction* **40**, 49–57 (2020).

161. Greenfield, E. M., Collier, C. D. & Getty, P. J. Receptor tyrosine kinases in osteosarcoma: 2019 update. in *Advances in Experimental Medicine and Biology* vol. 1258 141–155 (Springer, 2020).

162. U.S. National Library of Medicine. List of clinical trials studying tyrosine kinase inhibition in osteosarcoma. *ClinicalTrials.gov* https://clinicaltrials.gov/ct2/results?cond=osteosarcoma&term=tyrosine+kinase (2023).

163. Sun, W., Wang, W., Lei, J., Li, H. & Wu, Y. Actin-like protein 6A is a novel prognostic indicator promoting invasion and metastasis in osteosarcoma. *Oncol Rep* **37**, 2405–2417 (2017).

164. Dai, F. *et al.* Calponin 3 is associated with poor prognosis and regulates proliferation and metastasis in osteosarcoma. *Aging* **12**, 14037–14049 (2020).

165. Wu, Y., Zhou, W., Yang, Z., Li, J. & Jin, Y. miR-185-5p Represses Cells Growth and Metastasis of Osteosarcoma via Targeting Cathepsin E. *Int J Toxicol* **41**, 115–125 (2022).

166. Pang, X. *et al.* cPLA2a correlates with metastasis and poor prognosis of osteosarcoma by facilitating epithelial-mesenchymal transition. *Pathol Res Pract* **215**, (2019).

167. Zhao, X., Li, R., Wang, Q., Wu, M. & Wang, Y. Overexpression of carboxypeptidase X M14 family member 2 predicts an unfavorable prognosis and promotes proliferation and migration of osteosarcoma. *Diagn Pathol* **14**, (2019).

168. Li, X., Xu, R., Liu, H. & Fang, K. CUL4A expression in pediatric osteosarcoma tissues and its effect on cell growth in osteosarcoma cells. *Tumor Biology* **37**, 8139–8144 (2016).

169. Ma, Y., Xu, X. & Luo, M. CXCR6 promotes tumor cell proliferation and metastasis in osteosarcoma through the Akt pathway. *Cell Immunol* **311**, 80–85 (2017).

170. Habel, N. *et al.* CYR61 triggers osteosarcoma metastatic spreading via an IGF1Rβ-dependent EMT-like process. *BMC Cancer* **19**, (2019).

171. Yuan, X. *et al.* Erythrocyte membrane protein band 4.1-like 3 inhibits osteosarcoma cell invasion through regulation of Snai1-induced epithelial-to-mesenchymal transition. *Aging* **13**, 1947–1961 (2020).

172. Yang, Y., Chen, J. & Chen, Q. Upregulation of HOXB7 promotes proliferation and metastasis of osteosarcoma cells. *Mol Med Rep* **16**, 2773–2778 (2017).

173. Xu, W. *et al.* Knockdown of HuR represses osteosarcoma cells migration, invasion and stemness through inhibition of YAP activation and increases susceptibility to chemotherapeutic agents. *Biomedicine and Pharmacotherapy* **102**, 587–593 (2018).

174. Gong, X. *et al.* Monoacylglycerol Lipase (MAGL) Inhibition Impedes the Osteosarcoma Progression by Regulating Epithelial Mesenchymal Transition. *Tohoku Journal of Experimental Medicine* **256**, 19–26 (2022).

175. Tang, J., Shen, L., Yang, Q. & Zhang, C. Overexpression of metadherin mediates metastasis of osteosarcoma by regulating epithelial-mesenchymal transition. *Cell Prolif* **47**, 427–434 (2014).

176. Jiang, L. *et al.* Oxidized low density lipoprotein receptor 1 promotes lung metastases of osteosarcomas through regulating the epithelial-mesenchymal transition. *J Transl Med* **17**, (2019).

177. Zhai, Q. *et al.* PADI4 modulates the invasion and migration of osteosarcoma cells by down-regulation of epithelial-mesenchymal transition. *Life Sci* **256**, (2020).

178. Niinaka, Y. *et al.* Silencing of autocrine motility factor induces mesenchymal-to-epithelial transition and suppression of osteosarcoma pulmonary metastasis. *Cancer Res* **70**, 9483–9493 (2010).

179. Ren, T. *et al.* Osteosarcoma cell intrinsic PD-L2 signals promote invasion and metastasis via the RhoA-ROCK-LIMK2 and autophagy pathways. *Cell Death Dis* **10**, 1–14 (2019).

180. Wang, X., Liang, X., Liang, H. & Wang, B. SENP1/HIF-1α feedback loop modulates hypoxia-induced cell proliferation, invasion, and EMT in human osteosarcoma cells. *J Cell Biochem* **119**, 1819–1826 (2018).

181. Yang, P., Liu, Y., Qi, Y. C. & Lian, Z. H. High SENP3 Expression Promotes Cell Migration, Invasion, and Proliferation by Modulating DNA Methylation of E-Cadherin in Osteosarcoma. *Technol Cancer Res Treat* **19**, (2020).

182. Meng, Q., Ren, C., Wang, L., Zhao, Y. & Wang, S. Knockdown of ST6Gal-I inhibits the growth and invasion of osteosarcoma MG-63 cells. *Biomedicine and Pharmacotherapy* **72**, 172–178 (2015).

183. Zhou, Y., Jin, Q., Xiao, W. & Sun, C. Tankyrase1 antisense oligodeoxynucleotides suppress the proliferation, migration and invasion through Hippo/YAP pathway in human osteosarcoma cells. *Pathol Res Pract* **215**, (2019).

184. Zeng, S. X. *et al.* High expression of TRIM29 (ATDC) contributes to poor prognosis and tumor metastasis by inducing epithelial-mesenchymal transition in osteosarcoma. *Oncol Rep* **38**, 1645–1654 (2017).

185. Chen, Y. *et al.* TRIM66 overexpresssion contributes to osteosarcoma carcin ogenesis and indicates poor survival outcome. *Oncotarget* **6**, (2015).

186. Liu, W. *et al.* UHRF1 promotes human osteosarcoma cell invasion by downregulating the expression of E-cadherin in an Rb1-dependent manner. *Mol Med Rep* **13**, 315–320 (2016).

187. Song, C., Liu, W. & Li, J. USP17 is upregulated in osteosarcoma and promotes cell proliferation, metastasis, and epithelial-mesenchymal transition through stabilizing SMAD4. *Tumor Biology* **39**, 1–10 (2017).

188. Zhang, D., Jiang, F., Wang, X. & Li, G. Downregulation of ubiquitin-specific protease 22 inhibits proliferation, invasion, and epithelial-mesenchymal transition in osteosarcoma cells. *Oncol Res* **25**, 743–751 (2017).

189. Xu, N. *et al.* Low Arid1a Expression Correlates with Poor Prognosis and Promotes Cell Proliferation and Metastasis in Osteosarcoma. *Pathology and Oncology Research* **25**, 875–881 (2019).

190. Liu, P., Yang, P., Zhang, Z., Liu, M. & Hu, S. Ezrin/NF-κB pathway regulates EGF-induced epithelial-mesenchymal transition (EMT), metastasis, and progression of osteosarcoma. *Medical Science Monitor* **24**, 2098–2108 (2018).

191. Yu, G.-H., Fu, L., Chen, J., Wei, F. & Shi, W.-X. Decreased expression of ferritin light chain in osteosarcoma and its correlation with epithelial-mesenchymal transition. *Eur Rev Med Pharmacol Sci* **22**, 2580–2587 (2018).

192. Zhang, J. *et al.* LAIR-1 overexpression inhibits epithelial-mesenchymal transition in osteosarcoma via GLUT1-related energy metabolism. *World J Surg Oncol* **18**, (2020).

193. Gao, K., Yin, J. & Dong, J. Deregulated WWOX is involved in a negative feedback loop with microRNA-214-3p in osteosarcoma. *Int J Mol Med* **38**, 1850–1856 (2016).

194. Hanahan, D. & Weinberg, R. A. Hallmarks of cancer: The next generation. *Cell* vol. 144 646–674 Preprint at https://doi.org/10.1016/j.cell.2011.02.013 (2011).

195. Fedele, V. & Melisi, D. Permissive State of EMT: The Role of Immune Cell Compartment. *Frontiers in Oncology* vol. 10 Preprint at https://doi.org/10.3389/fonc.2020.00587 (2020).

196. Alsaab, H. O. *et al.* PD-1 and PD-L1 checkpoint signaling inhibition for cancer immunotherapy: mechanism, combinations, and clinical outcome. *Frontiers in Pharmacology* vol. 8 Preprint at https://doi.org/10.3389/fphar.2017.00561 (2017).

197. Cano, A. *et al. The transcription factor Snail controls epithelial-mesenchymal transitions by repressing E-cadherin expression*. *NATURE CELL BIOLOGY* vol. 2 (2000).

198. Cech, T. R. & Steitz, J. A. The noncoding RNA revolution - Trashing old rules to forge new ones. *Cell* vol. 157 77–94 Preprint at https://doi.org/10.1016/j.cell.2014.03.008 (2014).

199. Xu, S., Gong, Y., Yin, Y., Xing, H. & Zhang, N. The multiple function of long noncoding RNAs in osteosarcoma progression, drug resistance and prognosis. *Biomedicine and Pharmacotherapy* vol. 127 Preprint at https://doi.org/10.1016/j.biopha.2020.110141 (2020).

200. Lietz, C. E. *et al.* MicroRNA-mRNA networks define translatable molecular outcome phenotypes in osteosarcoma. *Sci Rep* **10**, (2020).

201. Xiong, W., Zhang, Y. & Yu, H. Comprehensive characterization of circular RNAs in osteosarcoma cell lines. *Cell Signal* **71**, (2020).

202. Zhang, Y., Li, J., Wang, Y., Jing, J. & Li, J. The roles of circular RNAs in osteosarcoma. *Medical Science Monitor* **25**, 6378–6382 (2019).

203. Liu, F., Xing, L., Zhang, X. & Zhang, X. A four-pseudogene classifier identified by machine learning serves as a novel prognostic marker for survival of osteosarcoma. *Genes (Basel)* **10**, (2019).

204. Yiqi, Z., Ziyun, L., Qin, F., Xingli, W. & Liyu, Y. Identification of 9-Gene Epithelial-Mesenchymal Transition Related Signature of Osteosarcoma by Integrating Multi Cohorts. *Technol Cancer Res Treat* **19**, (2020).

205. Feng, Z. hua *et al.* EIF4A3-induced circular RNA PRKAR1B promotes osteosarcoma progression by miR-361-3p-mediated induction of FZD4 expression. *Cell Death Dis* **12**, (2021).

206. Sun, F., Yu, Z., Wu, B., Zhang, H. & Ruan, J. LINC00319 promotes osteosarcoma progression by regulating the miR-455-3p/NFIB axis. *Journal of Gene Medicine* **22**, (2020).

207. Wu, S. *et al.* LINC00324 accelerates the proliferation and migration of osteosarcoma through regulating WDR66. *J Cell Physiol* **235**, 339–348 (2020).

208. Lian, H. *et al.* Linc00460 promotes osteosarcoma progression via miR-1224-5p/FADS1 axis. *Life Sci* **233**, (2019).

209. Bian, X., Sun, Y. M., Wang, L. M. & Shang, Y. L. ELK1-induced upregulation lncRNA LINC02381 accelerates the osteosarcoma tumorigenesis through targeting CDCA4 via sponging miR-503–5p. *Biochem Biophys Res Commun* **548**, 112–119 (2021).

210. Han, G. *et al.* LncRNA BCRT1 facilitates osteosarcoma progression via regulating miR-1303/FGF7 axis. *Aging* **13**, 15501–15510 (2021).

211. Yan, L. *et al.* LncRNA CCAT2 promoted osteosarcoma cell proliferation and invasion. *J Cell Mol Med* **22**, 2592–2599 (2018).

212. Zhang, H. *et al.* DDX11-AS1 contributes to osteosarcoma progression via stabilizing DDX11. *Life Sci* **254**, (2020).

213. Wang, Y. *et al.* LncRNA FAL1 is a negative prognostic biomarker and exhibits pro-oncogenic function in osteosarcoma. *J Cell Biochem* **119**, 8481–8489 (2018).

214. Yang, W. *et al.* Knockdown of lncRNA GHET1 inhibits osteosarcoma cells proliferation, invasion, migration and EMT in vitro and in vivo. *Cancer Biomarkers* **23**, 589–601 (2018).

215. Zhao, W. & Li, L. SP1-induced upregulation of long non-coding RNA HCP5 promotes the development of osteosarcoma. *Pathol Res Pract* **215**, 439–445 (2019).

216. Cai, L. *et al.* The lncRNA HNF1A-AS1 is a negative prognostic factor and promotes tumorigenesis in osteosarcoma. *J Cell Mol Med* **21**, 2654–2662 (2017).

217. Lin, H., Zhao, Z., Hao, Y., He, J. & He, J. Long noncoding RNA HIF1A-AS2 facilitates cell survival and migration by sponging miR-33b-5p to modulate SIRT6 expression in osteosarcoma. *Biochemistry and Cell Biology* **98**, 284–292 (2020).

218. Wang, Y., Zhang, R., Cheng, G., Xu, R. & Han, X. Long non-coding RNA HOXA-AS2 promotes migration and invasion by acting as a ceRNA of miR-520c-3p in osteosarcoma cells. *Cell Cycle* **17**, 1637–1648 (2018).

219. He, J. wen, Li, D. jian, Zhou, J. hua, Zhu, Y. long & Yu, B. qing. SP1-mediated upregulation of lncRNA LMCD1-AS1 functions a ceRNA for miR-106b-5p to facilitate osteosarcoma progression. *Biochem Biophys Res Commun* **526**, 670–677 (2020).

220. Li, J., Wu, Q. M., Wang, X. Q. & Zhang, C. Q. Long noncoding RNA miR210HG sponges miR-503 to facilitate osteosarcoma cell invasion and metastasis. *DNA Cell Biol* **36**, 1117–1125 (2017).

221. Wu, F., Zhong, Y., Lang, X.-B., Tu, Y.-L. & Sun, S.-F. MNX1-AS1 accelerates the epithelial-mesenchymal transition in osteosarcoma cells by activating MNX1 as a functional oncogene. *Eur Rev Med Pharmacol Sci* **23**, 8194–8202 (2019).

222. Zhang, L., Zhao, G., Ji, S., Yuan, Q. & Zhou, H. Downregulated Long Non-Coding RNA MSC-AS1 Inhibits Osteosarcoma Progression and Increases Sensitivity to Cisplatin by Binding to MicroRNA-142. *Medical Science Monitor* **26**, (2020).

223. Tan, H. & Zhao, L. lncRNA nuclear-enriched abundant transcript 1 promotes cell proliferation and invasion by targeting miR-186-5p/HIF-1α in osteosarcoma. *J Cell Biochem* **120**, 6502–6514 (2019).

224. Liu, W., Liu, P., Gao, H., Wang, X. & Yan, M. Long non-coding RNA PGM5-AS1 promotes epithelial-mesenchymal transition, invasion and metastasis of osteosarcoma cells by impairing miR-140-5p-mediated FBN1 inhibition. *Mol Oncol* **14**, 2660–2677 (2020).

225. Xun, C., Jiang, D., Tian, Z., Yunus, A. & Chen, J. Long noncoding RNA plasmacytoma variant translocation gene 1 promotes epithelial-mesenchymal transition in osteosarcoma. *J Clin Lab Anal* **35**, (2021).

226. Tong, C.-J. *et al.* LncRNA RUSC1-AS1 promotes osteosarcoma progression through regulating the miR-340-5p and PI3K/AKT pathway. *Aging* **13**, 20116–20130 (2021).

227. Deng, R., Zhang, J. & Chen, J. LncRNA SNHG1 negatively regulates miRNA-101-3p to enhance the expression of ROCK1 and promote cell proliferation, migration and invasion in osteosarcoma. *Int J Mol Med* **43**, 1157–1166 (2019).

228. Huang, Y. F., Lu, L., Shen, H. L. & Lu, X. X. LncRNA SNHG4 promotes osteosarcoma proliferation and migration by sponging miR-377-3p. *Mol Genet Genomic Med* **8**, (2020).

229. Zhang, J., Ju, C., Zhang, W. & Xie, L. LncRNA SNHG20 is associated with clinical progression and enhances cell migration and invasion in osteosarcoma. *IUBMB Life* **70**, 1115–1121 (2018).

230. Yu, X. *et al.* Long non-coding RNA Taurine upregulated gene 1 promotes osteosarcoma cell metastasis by mediating HIF-1α via miR-143-5p. *Cell Death Dis* **10**, (2019).

231. Zhao, X. *et al.* miR-17-5p promotes proliferation and epithelial-mesenchymal transition in human osteosarcoma cells by targeting SRC kinase signaling inhibitor 1. *J Cell Biochem* **120**, 5495–5504 (2019).

232. Zhang, H. *et al.* MicroRNA-93 promotes the tumorigenesis of osteosarcoma by targeting TIMP2. *Biosci Rep* **39**, (2019).

233. Chen, J. *et al.* Micro RNA-130a promotes the metastasis and epithelialmesenchymal transition of osteosarcoma by targeting PTEN. *Oncol Rep* **35**, 3285–3292 (2016).

234. Shen, S. *et al.* A miR-135b-TAZ positive feedback loop promotes epithelial–mesenchymal transition (EMT) and tumorigenesis in osteosarcoma. *Cancer Lett* **407**, 32–44 (2017).

235. Yao, J., Lin, J., He, L., Huang, J. & Liu, Q. TNF-α/miR-155 axis induces the transformation of osteosarcoma cancer stem cells independent of TP53INP1. *Gene* **726**, (2020).

236. Wang, X. *et al.* MiR-196a promoted cell migration, invasion and the epithelial-mesenchymal transition by targeting HOXA5 in osteosarcoma. *Cancer Biomarkers* **29**, 291–298 (2020).

237. Chen, Z. *et al.* MiR-199b-5p promotes malignant progression of osteosarcoma by regulating HER2. *J BUON* **23**, 1816–1824 (2018).

238. Shi, C. *et al.* Pseudogene MSTO2P enhances hypoxia-induced osteosarcoma malignancy by upregulating PD-L1. *Biochem Biophys Res Commun* **530**, 673–679 (2020).

239. Ma, L. *et al.* Overexpression of FER1L4 promotes the apoptosis and suppresses epithelial-mesenchymal transition and stemness markers via activating PI3K/AKT signaling pathway in osteosarcoma cells. *Pathol Res Pract* **215**, (2019).

240. Ye, F., Tian, L., Zhou, Q. & Feng, D. LncRNA FER1L4 induces apoptosis and suppresses EMT and the activation of PI3K/AKT pathway in osteosarcoma cells via inhibiting miR-18a-5p to promote SOCS5. *Gene* **721**, (2019).

241. Shen, B. *et al.* LncRNA MEG3 negatively modified osteosarcoma development through regulation of miR-361-5p and FoxM1. *J Cell Physiol* **234**, 13464–13480 (2019).

242. Zhang, G., Li, Y., Liao, G. & Qiu, H. LncRNA NKILA inhibits invasion and migration of osteosarcoma cells via NF-κB/Snail signaling pathway. *Eur Rev Med Pharmacol Sci* **23**, 4118–4125 (2019).

243. Fan, H., Liu, T., Tian, H. & Zhang, S. Tusc8 inhibits the development of osteosarcoma by sponging mir-197-3p and targeting ehd2. *Int J Mol Med* **46**, 1311–1320 (2020).

244. Zhang, Z., Zhao, M. & Wang, G. Upregulation of microRNA-7 contributes to inhibition of the growth and metastasis of osteosarcoma cells through the inhibition of IGF1R. *J Cell Physiol* **234**, 22195–22206 (2019).

245. Jiao, Z.-H., Wang, J.-D. & Wang, X.-J. MicroRNA-16 suppressed the invasion and migration of osteosarcoma by directly inhibiting RAB23. *Eur Rev Med Pharmacol Sci* **22**, 2598–2605 (2018).

246. Chen, B. *et al.* MicroRNA-25 suppresses proliferation, migration, and invasion of osteosarcoma by targeting SOX4. *Tumor Biology* **39**, (2017).

247. Gong, H. L. *et al.* MicroRNA-29a suppresses the invasion and migration of osteosarcoma cells by regulating the SOCS1/NF-κB signalling pathway through negatively targeting DNMT3B. *Int J Mol Med* **44**, 1219–1232 (2019).

248. Waresijiang, N. *et al.* The downregulation of MIR-125a-5p functions as a tumor suppressor by directly targeting MMP-11 in osteosarcoma. *Mol Med Rep* **13**, 4859–4864 (2016).

249. Liu, X. *et al.* MicroRNA-128 inhibits EMT of human osteosarcoma cells by directly targeting integrin α2. *Tumor Biology* **37**, 7951–7957 (2016).

250. Liu, Y., Li, Y., Liu, J., Wu, Y. & Zhu, Q. MicroRNA-132 inhibits cell growth and metastasis in osteosarcoma cell lines possibly by targeting Sox4. *Int J Oncol* **47**, 1672–1684 (2015).

251. Shi, Y. K. & Guo, Y. H. MiR-139-5p suppresses osteosarcoma cell growth and invasion through regulating DNMT1. *Biochem Biophys Res Commun* **503**, 459–466 (2018).

252. Guo, Q., Zhang, N., Liu, S., Pang, Z. & Chen, Z. By targeting TRAF6, miR-140-3p inhibits TGF-β1-induced human osteosarcoma epithelial-to-mesenchymal transition, migration, and invasion. *Biotechnol Lett* **42**, 2123–2133 (2020).

253. Fu, Y., Tang, Y., Wang, J. & Guo, Z. MicroRNA-181c suppresses the biological progression of osteosarcoma via targeting smad7 and regulating transforming growth factor-β (TGF-β) signaling pathway. *Medical Science Monitor* **25**, 4801–4810 (2019).

254. Yang, D., Liu, G. & Wang, K. MiR-203 Acts as a tumor suppressor gene in Osteosarcoma by regulating RAB22A. *PLoS One* **10**, (2015).

255. He, F., Fang, L. & Yin, Q. MiR-363 acts as a tumor suppressor in osteosarcoma cells by inhibiting PDZD2. *Oncol Rep* **41**, 2729–2738 (2019).

256. Zhang, Y., Wang, F., Wang, L. & Zhang, Q. MiR-363 suppresses cell migration, invasion, and epithelial-mesenchymal transition of osteosarcoma by binding to NOB1. *World J Surg Oncol* **18**, (2020).

257. Xu, M. *et al.* MiR-382 inhibits osteosarcoma metastasis and relapse by targeting y box-binding protein 1. *Molecular Therapy* **23**, 89–98 (2015).

258. Tan, Y., Chen, L., Li, S., Hao, H. & Zhang, D. MiR-384 Inhibits Malignant Biological Behavior Such as Proliferation and Invasion of Osteosarcoma by Regulating IGFBP3. *Technol Cancer Res Treat* **19**, (2020).

259. Liu, Y. *et al.* MiR-486 inhibited osteosarcoma cells invasion and epithelial-mesenchymal transition by targeting PIM1. *Cancer Biomarkers* **23**, 269–277 (2018).

260. Qiu, J., Zhang, Y., Chen, H. & Guo, Z. MicroRNA-488 inhibits proliferation, invasion and EMT in osteosarcoma cell lines by targeting aquaporin 3. *Int J Oncol* **53**, 1493–1504 (2018).

261. Wang, Y., Lin, S., Chen, L., Qiu, H. & Wang, J. MicroRNA-489 suppresses osteosarcoma invasion, migration and epithelial-to-mesenchymal transition by directly targeting NAA10. *Minerva Endocrinol* **45**, 150–153 (2020).

262. Wang, T. *et al.* The TGFβ-miR-499a-SHKBP1 pathway induces resistance to EGFR inhibitors in osteosarcoma cancer stem cell-like cells. *Journal of Experimental and Clinical Cancer Research* **38**, (2019).

263. Guo, X. *et al.* MicroRNA-503 represses epithelial–mesenchymal transition and inhibits metastasis of osteosarcoma by targeting c-myb. *Tumor Biology* **37**, 9181–9187 (2016).

264. Wang, D., Bao, F., Teng, Y., Li, Q. & Li, J. MicroRNA-506-3p initiates mesenchymal-to-epithelial transition and suppresses autophagy in osteosarcoma cells by directly targeting SPHK1. *Biosci Biotechnol Biochem* **83**, 836–844 (2019).

265. Wang, X. *et al.* MicroRNA-761 suppresses tumor progression in osteosarcoma via negatively regulating ALDH1B1. *Life Sci* **262**, (2020).

266. Di Fiore, R. *et al.* Let-7d miRNA Shows Both Antioncogenic and Oncogenic Functions in Osteosarcoma-Derived 3AB-OS Cancer Stem Cells. *J Cell Physiol* **231**, 1832–1841 (2016).

267. Yan, M. *et al.* Circular RNA PVT1 promotes metastasis via regulating of miR-526b/FOXC2 signals in OS cells. *J Cell Mol Med* **24**, 5593–5604 (2020).

268. Ye, K. *et al.* Long Noncoding RNA GAS5 Suppresses Cell Growth and Epithelial–Mesenchymal Transition in Osteosarcoma by Regulating the miR-221/ARHI Pathway. *J Cell Biochem* **118**, 4772–4781 (2017).

269. Yang, H., Zhao, L., Zhang, Y. & Li, F. F. A comprehensive analysis of immune infiltration in the tumor microenvironment of osteosarcoma. *Cancer Med* **10**, 5696–5711 (2021).

270. Ling, J. *et al.* Feedback modulation of endothelial cells promotes epithelial-mesenchymal transition and metastasis of osteosarcoma cells by Von Willebrand Factor release. *J Cell Biochem* **120**, 15971–15979 (2019).

271. Dai, J. *et al.* Matrix stiffness regulates epithelial-mesenchymal transition via cytoskeletal remodeling and MRTF-A translocation in osteosarcoma cells. *J Mech Behav Biomed Mater* **90**, 226–238 (2019).

272. De Las Rivas, J. *et al.* Cancer drug resistance induced by EMT: novel therapeutic strategies. *Archives of Toxicology* vol. 95 2279–2297 Preprint at https://doi.org/10.1007/s00204-021-03063-7 (2021).

273. Ding, L. *et al.* S-phase kinase-Associated protein 2 is involved in epithelial-mesenchymal transition in methotrexate-resistant osteosarcoma cells. *Int J Oncol* **52**, 1841–1852 (2018).

274. Huang, Y. *et al.* MiR-33a mediates the anti-tumor effect of lovastatin in osteosarcoma by targeting CYR61. *Cellular Physiology and Biochemistry* **51**, 938–948 (2018).

275. Cheng, H.-L. *et al.* Zoledronate blocks geranylgeranylation not farnesylation to suppress human osteosarcoma U2OS cells metastasis by EMT via Rho A activation and FAK-inhibited JNK and p38 pathways. *Oncotarget* **7**, 9742–9758 (2016).

276. Kim, E. H. *et al.* Zoledronic acid is an effective radiosensitizer in the treatment of osteosarcoma. *Oncotarget* **7**, 70869–70880 (2016).

277. Fang, D. *et al.* 17β-Estradiol regulates cell proliferation, colony formation, migration, invasion and promotes apoptosis by upregulating miR-9 and thus degrades MALAT-1 in osteosarcoma cell MG-63 in an estrogen receptor-independent manner. *Biochem Biophys Res Commun* **457**, 500–506 (2015).

278. Sánchez-Sánchez, A. M. *et al.* Calcium acts as a central player in melatonin antitumor activity in sarcoma cells. *Cellular Oncology* 1–14 (2022) doi:10.1007/s13402-022-00674-9.

279. Qu, H. *et al.* Melatonin inhibits osteosarcoma stem cells by suppressing SOX9-mediated signaling. *Life Sci* **207**, 253–264 (2018).

280. Fontanella, R. *et al.* A novel antagonist of CXCR4 prevents bone marrow-derived mesenchymal stem cell-mediated osteosarcoma and hepatocellular carcinoma cell migration and invasion. *Cancer Lett* **370**, 100–107 (2016).

281. Zheng, B., Ren, T., Huang, Y. & Guo, W. Apatinib inhibits migration and invasion as well as PD-L1 expression in osteosarcoma by targeting STAT3. *Biochem Biophys Res Commun* **495**, 1695–1701 (2018).

282. Seba, V. *et al.* Chalcone derivatives 4′-amino-1-naphthyl-chalcone (D14) and 4′-amino-4-methyl-1-naphthyl-chalcone (D15) suppress migration and invasion of osteosarcoma cells mediated by p53 regulating emt-related genes. *Int J Mol Sci* **19**, (2018).

283. Mishra, R., Nathani, S., Varshney, R., Sircar, D. & Roy, P. Berberine reverses epithelial-mesenchymal transition and modulates histone methylation in osteosarcoma cells. *Mol Biol Rep* **47**, 8499–8511 (2020).

284. Wang, D., Zhang, K., Du, G., Wang, J. & Zhao, J. Berberine enhances the radiosensitivity of osteosarcoma by targeting Rad51 and epithelial-mesenchymal transition. *J Cancer Res Ther* **16**, 215–221 (2020).

285. Liu, X. *et al.* Dehydroandrographolide Inhibits Osteosarcoma Cell Growth and Metastasis by Targeting SATB2-mediated EMT. *Anticancer Agents Med Chem* **19**, 1728–1736 (2019).

286. Wang, Y. *et al.* Magnoflorine inhibits the malignant phenotypes and increases cisplatin sensitivity of osteosarcoma cells via regulating miR-410-3p/HMGB1/NF-κB pathway. *Life Sci* **256**, (2020).

287. Chang, J. *et al.* Molecular mechanisms of Polyphyllin I-induced apoptosis and reversal of the epithelial-mesenchymal transition in human osteosarcoma cells. *J Ethnopharmacol* **170**, 117–127 (2015).

288. Ma, Z. *et al.* Rosmarinic acid exerts an anticancer effect on osteosarcoma cells by inhibiting DJ-1 via regulation of the PTEN-PI3K-Akt signaling pathway. *Phytomedicine* **68**, (2020).

289. Muscella, A. *et al.* Antitumor and antimigration effects of Salvia clandestina L. extract on osteosarcoma cells. *Ann N Y Acad Sci* **1500**, 34–47 (2021).

290. Zhou, D. & He, L. Sauchinone inhibits hypoxia-induced invasion and epithelial–mesenchymal transition in osteosarcoma cells via inactivation of the sonic hedgehog pathway. *Journal of Receptors and Signal Transduction* **42**, 173–179 (2022).

291. Jiang, C. *et al.* Triptolide inhibits the growth of osteosarcoma by regulating microRNA-181a via targeting PTEN gene in vivo and vitro. *Tumor Biology* **39**, (2017).

292. Chang, J. *et al.* Polyphyllin I suppresses human osteosarcoma growth by inactivation of Wnt/β-catenin pathway in vitro and in vivo. *Sci Rep* **7**, (2017).

293. Oh, J. Y., Lee, Y. J. & Kim, E. H. Tumor-Treating Fields Inhibit the Metastatic Potential of Osteosarcoma Cells. *Technol Cancer Res Treat* **19**, (2020).

294. Botter, S. M., Arlt, M. J. E., Born, W. & Fuchs, B. Mammalian models of bone sarcomas. in *Bone Cancer* 349–363 (Elsevier, 2015). doi:10.1016/B978-0-12-416721-6.00030-3.

295. Jia, S.-F., Worth, L. L. & Kleinerman, E. S. *A nude mouse model of human osteosarcoma lung metastases for evaluating new therapeutic strategies*. *Clinical & Experimental Metastasis* vol. 17 (1999).

296. Monteiro, C. F., Custódio, C. A. & Mano, J. F. Bioengineering a humanized 3D tri-culture osteosarcoma model to assess tumor invasiveness and therapy response. *Acta Biomater* **134**, 204–214 (2021).

297. Landry, T. Active-β-catenin (ABC) transcriptional activity is associated with an may promote invasive phenotype in osteosarcoma (OS). (University of Alberta, 2021).

298. Haydon, R. C. *et al.* Cytoplasmic and/or nuclear accumulation of the β-catenin protein is a frequent event in human osteosarcoma. *Int J Cancer* **102**, 338–342 (2002).

299. Kansara, M. *et al.* Wnt inhibitory factor 1 is epigenetically silenced in human osteosarcoma, and targeted disruption accelerates osteosarcomagenesis in mice. *Journal of Clinical Investigation* **119**, 837–851 (2009).

300. Chen, K. *et al.* Wnt10b induces chemotaxis of osteosarcoma and correlates with reduced survival. *Pediatr Blood Cancer* **51**, 349–355 (2008).

301. Hoang, B. H. *et al.* Expression of LDL receptor-related protein 5 (LRP5) as a novel marker for disease progression in high-grade osteosarcoma. *Int J Cancer* **109**, 106–111 (2004).

302. Cai, Y. *et al.* Inactive Wnt/β-catenin pathway in conventional high-grade osteosarcoma. *Journal of Pathology* **220**, 24–33 (2010).

303. Staal, F. J. T., Van Noort, M., Strous, G. J. & Clevers, H. C. *Wnt signals are transmitted through N-terminally dephosphorylated β-catenin*. *EMBO reports* vol. 3 (2002).

304. Zhang, Y. & Wang, X. Targeting the Wnt/β-catenin signaling pathway in cancer. *Journal of Hematology and Oncology* vol. 13 Preprint at https://doi.org/10.1186/s13045-020-00990-3 (2020).

305. Kahn, M. Can we safely target the WNT pathway? *Nature Reviews Drug Discovery* vol. 13 513–532 Preprint at https://doi.org/10.1038/nrd4233 (2014).

306. Neiheisel, A., Kaur, M., Ma, N., Havard, P. & Shenoy, A. K. Wnt pathway modulators in cancer therapeutics: An update on completed and ongoing clinical trials. *International Journal of Cancer* vol. 150 727–740 Preprint at https://doi.org/10.1002/ijc.33811 (2022).

307. Whittle, S. B., Children's Oncology Group & National Cancer Institute. Tegavivint for the treatment of recurrent or refractory solid tumors, including lymphomas and desmoid tumors. NCT04851119. https://clinicaltrials.gov/ct2/show/NCT04851119 (2023).

308. Li, J. & Wang, C. Y. TBL1-TBLR1 and β-catenin recruit each other to Wnt target-gene promoter for transcription activation and oncogenesis. *Nat Cell Biol* **10**, 160–169 (2008).

309. Luu, T. Epithelial-Mesenchymal Transition and Its Regulation Mechanisms in Pancreatic Cancer. *Front Oncol* **11**, (2021).

310. Zhang, J., Tian, X. J. & Xing, J. Signal transduction pathways of EMT induced by TGF-β, SHH, and WNT and their crosstalks. *Journal of Clinical Medicine* vol. 5 Preprint at https://doi.org/10.3390/jcm5040041 (2016).

311. Hinton, K., Kirk, A., Paul, P. & Persad, S. Regulation of the epithelial to mesenchymal transition in osteosarcoma. *Submitted manuscript under review* Preprint at (2023).

312. Li, J. & Zhou, B. P. Activation of β-catenin and Akt pathways by Twist are critical for the maintenance of EMT associated cancer stem cell-like characters. *BMC Cancer* **11**, 49 (2011).

313. Bassi, G. *et al.* Scaffold-based 3D cellular models mimicking the heterogeneity of osteosarcoma stem cell niche. *Sci Rep* **10**, (2020).

314. González Díaz, E. C. *et al.* A 3D Osteosarcoma Model with Bone-Mimicking Cues Reveals a Critical Role of Bone Mineral and Informs Drug Discovery. *Adv Healthc Mater* **11**, (2022).

315. Nguyen-Ngoc, K.-V. *et al.* 3D Culture Assays of Murine Mammary Branching Morphogenesis and Epithelial Invasion. in *Tissue orphogenesis: Methods and Protocols* (ed. Nelson, C. M.) vol. 1189 135–162 (Springer Science + Business Media, 2015).

316. Tanaka, T. *et al.* Dynamic analysis of lung metastasis by mouse osteosarcoma LM8: VEGF is a candidate for anti-metastasis therapy. *Clin Exp Metastasis* **30**, 369–379 (2013).

317. Munoz-Garcia, J. *et al.* In vitro three-dimensional cell cultures for bone sarcomas. *Journal of Bone Oncology* vol. 30 Preprint at https://doi.org/10.1016/j.jbo.2021.100379 (2021).

318. Lauvrak, S. U. *et al.* Functional characterisation of osteosarcoma cell lines and identification of mRNAs and miRNAs associated with aggressive cancer phenotypes. *Br J Cancer* **109**, 2228–2236 (2013).

319. Stepanenko, A. A. & Heng, H. H. Transient and stable vector transfection: Pitfalls, off-target effects, artifacts. *Mutation Research - Reviews in Mutation Research* vol. 773 91–103 Preprint at https://doi.org/10.1016/j.mrrev.2017.05.002 (2017).

320. Yallop, C. A. & Svendsen, I. *The effects of G418 on the growth and metabolism of recombinant mammalian cell lines*. *Cytotechnology* vol. 35 (2001).

321. Luu, H. H. *et al.* An orthotopic model of human osteosarcoma growth and spontaneous pulmonary metastasis. *Clin Exp Metastasis* **22**, 319–329 (2005).

322. Sottnik, J. L., Duval, D. L., J. Ehrhart, E. & Thamm, D. H. An orthotopic, postsurgical model of luciferase transfected murine osteosarcoma with spontaneous metastasis. *Clin Exp Metastasis* **27**, 151–160 (2010).

323. Tang, T. T. *et al.* Tumorigenesis and spontaneous metastasis by luciferase-labeled human xenograft osteosarcoma cells in nude mice. *Chin Med J (Engl)* **125**, 4022–4030 (2012).

324. Grisez, B. T., Ray, J. J., Bostian, P. A., Markel, J. E. & Lindsey, B. A. Highly metastatic K7M2 cell line: A novel murine model capable of in vivo imaging via luciferase vector transfection. *Journal of Orthopaedic Research* **36**, 2296–2304 (2018).

325. Talbot, L. J. *et al.* A Novel Orthotopic Implantation Technique for Osteosarcoma Produces Spontaneous Metastases and Illustrates Dose-Dependent Efficacy of B7-H3-CAR T Cells. *Front Immunol* **12**, (2021).

326. Shultz, L. D. *et al.* Multiple defects in innate and adaptive immunologic function in NOD/LtSz-scid mice. *J Immunol* **154**, 180–91 (1995).

327. Corre, I., Verrecchia, F., Crenn, V., Redini, F. & Trichet, V. The Osteosarcoma Microenvironment: A Complex But Targetable Ecosystem. *Cells* vol. 9 Preprint at https://doi.org/10.3390/cells9040976 (2020).

328. Jiang, Y. *et al.* KDM6B-mediated histone demethylation of LDHA promotes lung metastasis of osteosarcoma. *Theranostics* **11**, 3868–3881 (2021).

329. Zhang, H. *et al.* Downregulation of the long non-coding RNA FOXD2-AS1 inhibits cell proliferation, migration and invasion in osteosarcoma. *Mol Med Rep* **20**, 292–302 (2019).

330. Zhang, J. *et al.* Targeting Super-Enhancer–Associated Oncogenes in Osteosarcoma with THZ2, a Covalent CDK7 Inhibitor. *Clinical Cancer Research* **26**, 2681–2692 (2020).

331. Blattmann, C. *et al.* Establishment of a patient-derived orthotopic osteosarcoma mouse model. *J Transl Med* **13**, (2015).

332. Sasaki, H., Iyer, S. V., Sasaki, K., Tawfik, O. W. & Iwakuma, T. An improved intrafemoral injection with minimized leakage as an orthotopic mouse model of osteosarcoma. *Anal Biochem* **486**, 70–74 (2015).

333. Wahlberg, B., Ghuman, H., Liu, J. R. & Modo, M. Ex vivo biomechanical characterization of syringe-needle ejections for intracerebral cell delivery. *Sci Rep* **8**, (2018).

334. Chatterjee, R. Cases of Mistaken Identity. *Science (1979)* **315**, 928–931 (2007).

335. Hughes, P., Marshall, D., Reid, Y., Parkes, H. & Gelber, C. The costs of using unauthenticated, over-passaged cell lines: How much more data do we need? *BioTechniques* vol. 43 575–586 Preprint at https://doi.org/10.2144/000112598 (2007).

336. Muff, R. *et al.* Genomic instability of osteosarcoma cell lines in culture: Impact on the prediction of metastasis relevant genes. *PLoS One* **10**, (2015).

337. Maloney, C. *et al.* Intratibial injection causes direct pulmonary seeding of osteosarcoma cells and is not a spontaneous model of metastasis: A mouse osteosarcoma model. *Clin Orthop Relat Res* **476**, 1514–1522 (2018).

338. Chen, X. *et al.* Mislocalized cytoplasmic p27 activates PAK1-mediated metastasis and is a prognostic factor in osteosarcoma. *Mol Oncol* **14**, 846–864 (2020).

339. Liu, J. F., Chen, P. C., Chang, T. M. & Hou, C. H. Monocyte Chemoattractant Protein-1 promotes cancer cell migration via c-Raf/MAPK/AP-1 pathway and MMP-9 production in osteosarcoma. *Journal of Experimental and Clinical Cancer Research* **39**, (2020).